AMPLITUDE SCINTILLATIONS ON EARTH-SPACE PROPAGATION PATHS AT 2 AND 30 GHz

D. M. J. Devasirvatham and D. B. Hodge

The Ohio State University

ElectroScience Laboratory

Department of Electrical Engineering
Columbus, Ohio 43212

Technical Report 4299-4

March 1977

Prepared for
National Aeronautics and Space Administration
GODDARD SPACE FLIGHT CENTER
Greenbelt, Maryland 20771

NOTICES

When Government drawings, specifications, or other data are used for any purpose other than in connection with a definitely related Government procurement operation, the United States Government thereby incurs no responsibility nor any obligation whatsoever, and the fact that the Government may have formulated, furnished, or in any way supplied the said drawings, specifications, or other data, is not to be regarded by implication or otherwise as in any manner licensing the holder or any other person or corporation, or conveying any rights or permission to manufacture, use, or sell any patented invention that may in any way be related thereto.

TECHNICAL REPORT STANDARD TITLE PAGE

1 Report No	2 Government Accession No	3 Recipient's Catalog No

4 Title and Subtitle
AMPLITUDE SCINTILLATIONS ON EARTH-SPACE PROPAGATION PATHS AT 2 AND 30 GHz

5 Report Date
March 1977

6 Performing Organization Code

7 Author(s)
D.M.J. Devasirvatham and D.B. Hodge

8 Performing Organization Report No
ESL 4299-4

9 Performing Organization Name and Address
The Ohio State University ElectroScience Laboratory, Department of Electrical Engineering, Columbus, Ohio 43212

10 Work Unit No

11 Contract or Grant No
NAS5-22575

12 Sponsoring Agency Name and Address
NASA, GSFC
Greenbelt, Maryland 20771
E. Hirschmann, Code 951, Technical Officer

13 Type of Report and Period Covered
Type II
Technical Report

14 Sponsoring Agency Code

15 Supplementary Notes
The material contained in this report is also used as a thesis submitted to the Department of Electrical Engineering, The Ohio State University as partial fulfillment for the degree Master of Science.

16 Abstract

Amplitude scintillation measurements were made simultaneously at 2.075 and 30 GHz on earth-space propagation paths over elevation angles in the range 0.4° to 44°. The experiment was performed as the Applications Technology Satellite (ATS-6) was moved slowly from a synchronous position over Africa to a new synchronous position over the United States. The received signal, variance, level, covariance, spectra and fade distributions are discussed as functions of the path elevation angle. These results are also compared wherever possible with similar measurements made earlier at 20 and 30 GHz.

17 Key Words (Selected by Author(s))		18 Distribution Statement
ATS-6	Millimeter wave	
Earth-Space	Propagation	
Low elevation angle	Scintillation	
Microwave		

19 Security Classif (of this report)	20 Security Classif (of this page)	21 No of Pages	22 Price*
U	U	98	

*For sale by the Clearinghouse for Federal Scientific and Technical Information, Springfield, Virginia 22151

TABLE OF CONTENTS

CHAPTER I
INTRODUCTION

Chapter 1 presents an overview of the current microwave scene and the rationale behind this study. The ATS-6 satellite and its role in this experiment are described. The equipment and facilities used and the data processing format are shown.

A. Overview

Microwaves are an indispensable component of modern living. Their use made the communications explosion possible and this in turn has fostered their continued growth. The wide bandwidths possible have made microwave systems a very viable and, in many instances, the only proposition for high data rate links.

The advent of the communications satellite marked the maturing of this technology. It has added literally another dimension to international and domestic communications. Small earth terminals together with high powered, space qualified transmitters are a giant step forward in the quest for instantaneous global communications.

Clearly, their potential has not gone unnoticed. The world, which until a few years ago was making do with a channel capacity of just the thirty megahertz in the high frequency (h.f.)-band, now uses almost as many gigahertz, an increase by a factor of 1000. Many of the traditional users of the h.f. bands, such as point-to-point and telex links, are moving into the microwave region. Further, totally new satellite techniques for services such as television, high speed computer-to-computer links, weather, survey and navigation have developed.

The consequent pressure for spectrum allocations has gradually pushed the working frequencies ever higher. The next series of INTELSAT commercial communication satellites will operate at 11/14 GHz [1]. The Communications Technology Satellite (CTS) is currently operating at 11.7 to 14.3 GHz [2]. Links are already being planned at 30 GHz [2]. Even higher frequencies are being explored.

However, the use of microwave and millimeter frequencies poses new problems to the systems engineer. Their wavelengths are comparable in size to inhomogeneities in the atmosphere or smaller; this, in turn, leads to enhanced scattering. These inhomogeneities are a result of the spatial and temporal variation of meteorological parameters such as temperature, pressure and water vapor content

along the propagation path. At millimeter wavelengths raindrops become comparable in size to the wavelength or larger and interact very strongly with the propagating signal. These small wavelengths also lie in the region of molecular absorption lines of the atmospheric gases [3,4,5,6,7]. To complicate matters further, ionospheric effects are found even at decimetric wavelengths.

The degree to which these factors affect a signal propagating through the troposphere depends strongly on the length of the propagation path through the troposphere. On earth-space links this length depends directly on the elevation angle of the path. At low elevation angles, the satellite-to-ground terminal path length is greater, and, as a result, there is a significant increase in signal fluctuations (scintillations) analogous to the twinkling of stars. Since the dynamic range of signal levels is of vital importance in system design and has a direct bearing on the cost and sophistication of the equipment, study of propagation at low elevation angles is of special interest [8].

The effect of the ionosphere on radio wave propagation, down to metric wavelengths, have been studied for several decades and a considerable body of literature exists [9,10]. Tropospheric effects have been studied by optical and radio astronomers at frequencies including and well above those of current interest [11,12]. However, these studies have necessarily used the sun and other stars which are themselves, incoherent, fluctuating, extended sources, requiring very large antennas. The artificial satellite, with fixed, coherent, accurately calibrated transmitters, is a significant new tool in this field; but space-qualified millimeter wave sources are a recent development. Consequently, present research is directed towards increasing the data at these frequencies [13,14].

This report is oriented toward the systems designer. The results presented herein establish numerical values for parameters describing microwave and millimeter wave scintillation at very low to medium elevation angles. These results are also related to existing theoretical results in order to establish the validity of the assumed models useful to the practicing engineer.

B. The ATS-6 Satellite

The ATS-6 is a geosynchronous satellite with facilities for several types of propagation experiments. The spacecraft is a fifth generation product embodying state-of-the-art high power transmitters and antennas for space applications. These include beacons at 30 GHz (Ka band) and 20 GHz (Ku band) for millimeter wave propagation experiments and one at 360.144 MHz for u.h.f. propagation studies. The L-band (860 MHz) transmitter for the Satellite Instructional Television Experiment (SITE) project and S-band (2.075 GHz) transmitter used in the Tracking and Data Relay (T & DRE)experiment

were designed for direct transmission to small earth or mobile terminals. The largest antenna deployed in space to date - a 30 foot (9.1m) diameter paraboloid - was used in conjunction with many experiments. For details of the satellite's capabilities used in this experiment, see Table 1 [8,15].

Table 1

TRANSMITTER			ANTENNA		
XMIT FREQ. (MHz)	POWER (WATTS)	ERP (dBW)	TYPE & POLARIZATION	BEAMWIDTH (DEGREES)	GAIN (dB)
30000	2	42	0.46m Paraboloid Linear	1.6	39
20000	2	30	Horn Linear	5x7	27
2075	20	50.5	9.1m Paraboloid RCP	1.2	39.4
360.144	0.48	3	Vee Beam Array Linear	35	4.3

Through an agreement with the Government of India, the satellite was moved to an orbital position over Lake Tanganika ($\approx$ 35°E) from its position over the United States ($\approx$ 94°W) to participate in the SITE program in June 1975. This provided an excellent opportunity to study microwave propagation characteristics at elevation angles varying from 40° to almost 0°. During the movement of the spacecraft, propagation characteristics at 20 and 30 GHz were studied at the Ohio State University ElectroScience Laboratory (ESL) and were reported earlier [16,17]. The results of these measurements indicated that severe system limitations would be imposed at these frequencies and at low elevation angles due to scintillation. Thus, further studies and measurements were desired to provide systems designers with a more detailed characterization of these effects.

C. The Experiment

The experiment discussed in this report was conducted during the return of the ATS-6 in August - September 1976 to its position over the United States after the conclusion of the SITE program with India. This provided once again an excellent opportunity to study microwave propagation characteristics at elevation angles from 0°-44° (Figure 1) and to compare these results with the earlier observations. The movement of the spacecraft was at a rate of about one degree per day in elevation. Plans were developed to utilize four frequencies (30 GHz, 20 GHz, 2.075 GHz and 360 MHz) spanning the microwave spectrum of current interest for this experiment.

Unfortunately, the 20 GHz beacon failed just before the experiment was scheduled to commence. The three remaining frequencies were monitored by Ohio State University, however, the 360 MHz signal was rendered virtually useless by radio frequency interference from other sources. Therefore the remainder of this study will be concerned with the 2 GHz and 30 GHz data only.

Records of the received signal will be presented and useful statistical parameters will be obtained The variance and the spectra of the received signals as well as the correlation between the signals will be examined. Agreement with available theoretical results will be checked. Whenever possible the analysis will be made using both the amplitude of the signal and the log amplitude; and the corresponding results will be compared. The results of the amplitude analysis are more amenable to direct physical interpretation, whereas the results of the log amplitude analysis permit direct comparison with theoretical results based on log amplitude analysis [18]. Both results should be identical for the case of small scintillations.

D. Equipment and Facilities

The ground terminal for this experiment was located at the Satellite Communications Facility of the ElectroScience Laboratory, Columbus, Ohio (Figure 2). The 30 GHz receiving system consisted of a 4.6m Cassegrainian, linearly polarized, horn-fed parabolic reflector antenna (r.m.s. tolerance 0.64mm or 0 064λ at 30 GHz) with a beamwidth of 0.2 degrees.

A low noise front-end containing a solid state first mixer and local oscillator producing the first intermediate frequency (IF) of 1.05 GHz was used. The 30 GHz radiometer Dicke switch in this module, which was used for earlier experiments was removed to reduce signal loss. Further amplification at 1.05 GHz using a tunnel-diode amplifier was followed by a manually controlled step attenuator. The signal was then fed into a Martin Marietta phase-locked-loop (PLL) receiver. This was slightly modified to increase the dynamic range. The measured system margin was approximately 52 dB with a receiver bandwidth of 55 Hz. See Figures 3 and 4 for block diagram and calibration characteristics of this receiving system.

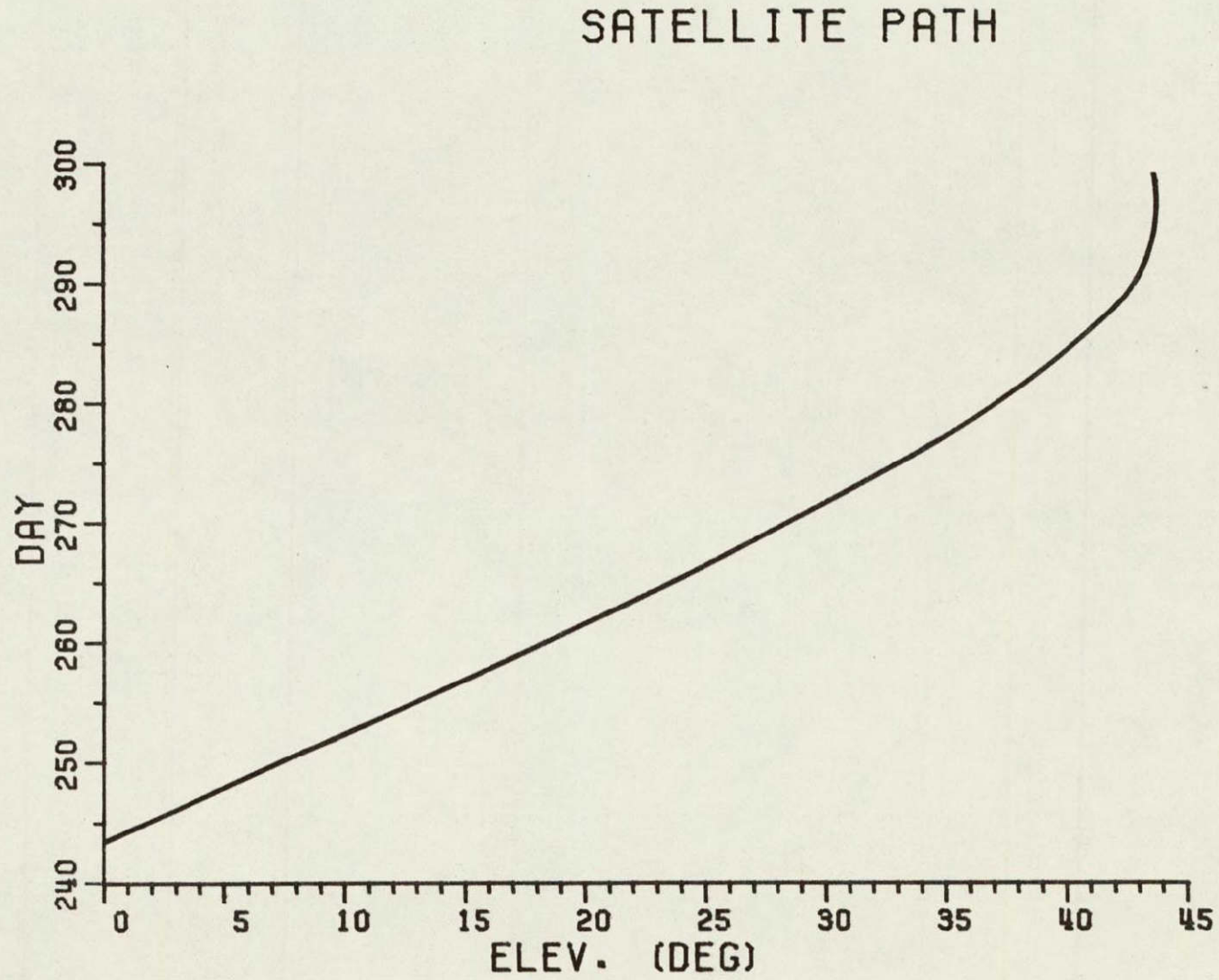

Figure 1--Satellite path. Day with elevation angle.

Figure 2. Satellite Communications Facility at Ohio State University.

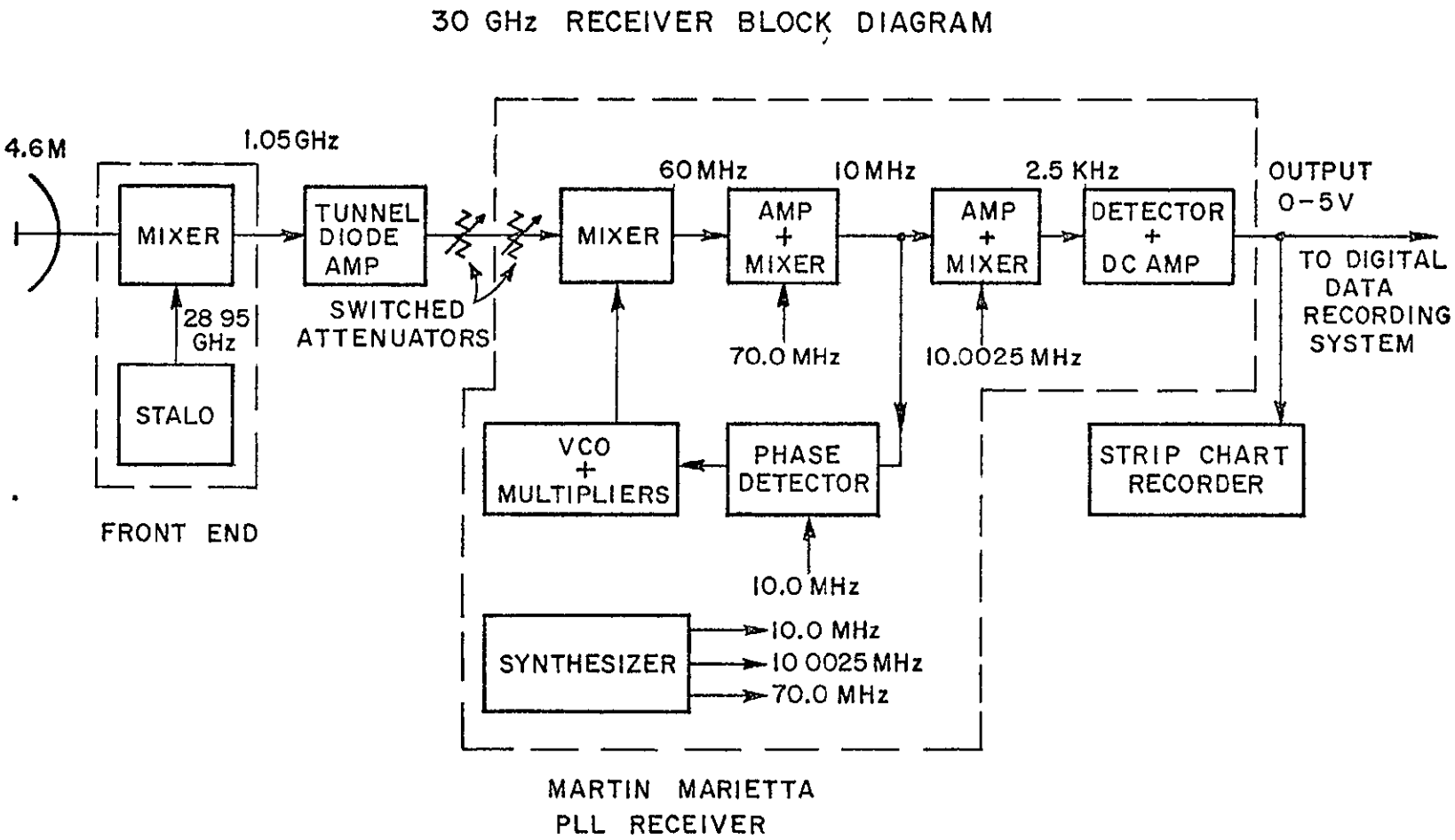

Figure 3--30 GHz receiver. Block diagram.

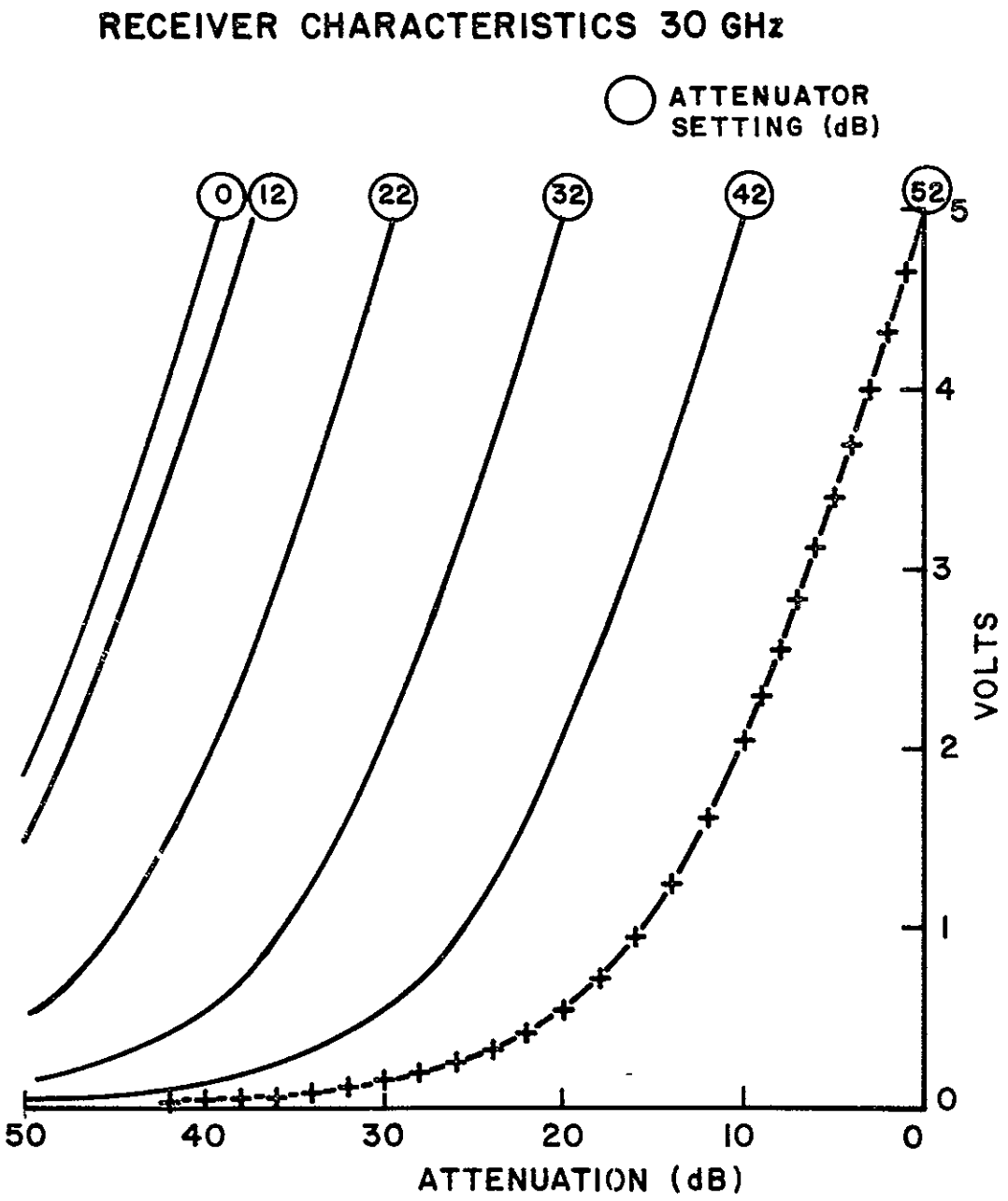

Figure 4--30 GHz receiver calibration curves.

2 GHz RECEIVER BLOCK DIAGRAM

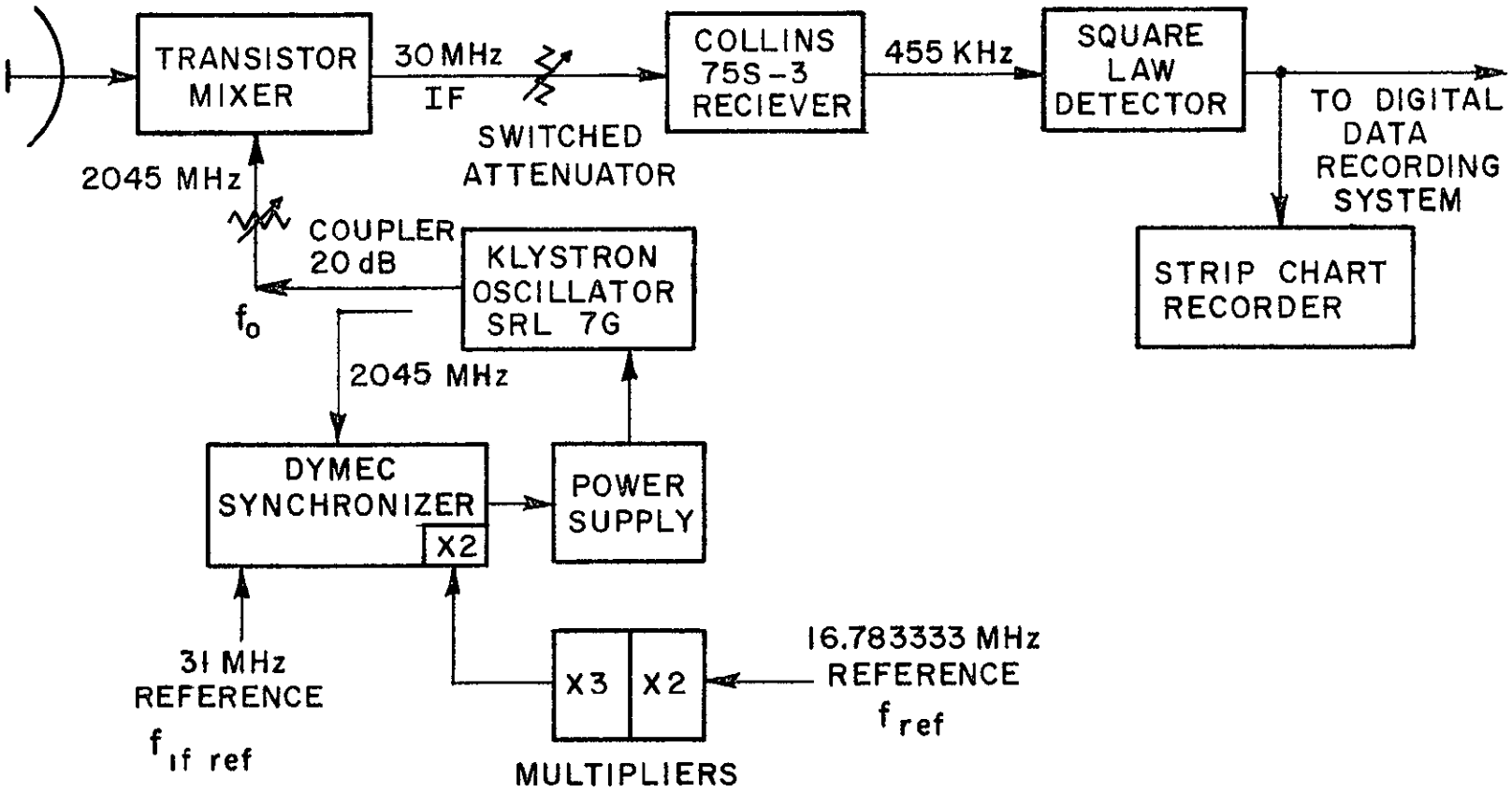

$f_o = 12 N f_{ref} + f_{if\ ref}$

N = HARMONIC NUMBER = 10

Figure 5--2 GHz receiver. Block diagram.

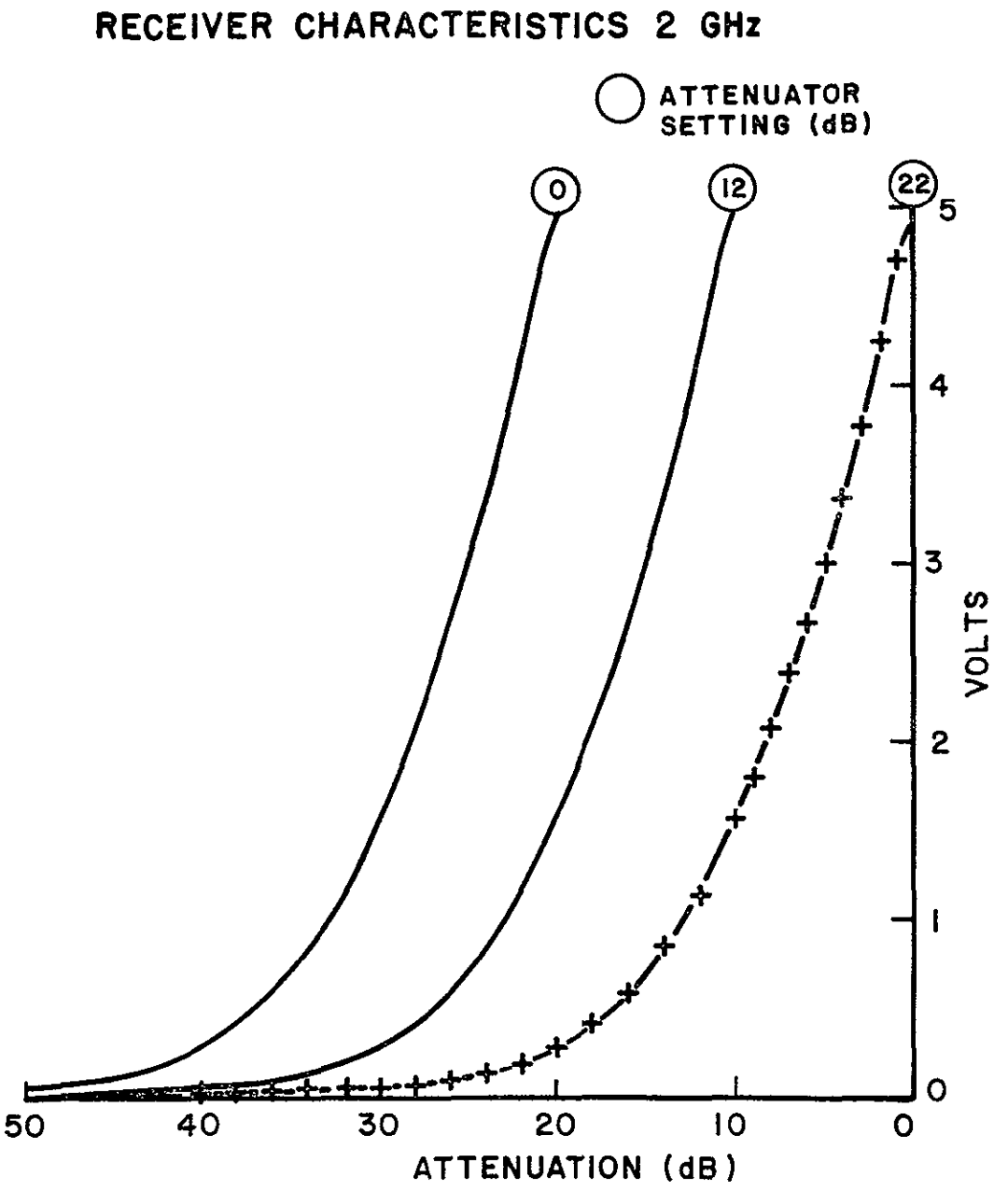

Figure 6--2 GHz receiver. Calibration curves.

The calibration curves (Figures 4,6) show the receiver output level for a given input signal level, expressed as an attenuation (dB) below the selected reference for that receiver. These are plotted for selected values of switched signal attenuators required to bring the levels within the working range of the receiver.

The 2 GHz receiving system used a 9.1m (30 foot) front-fed, linearly polarized, parabolic reflector antenna with horn feed. The surface tolerance was 1.2mm (.008 wavelengths) r.m.s. and the beamwidth was 1.3°. The block diagram of the Ohio State University-built receiver is shown in Figure 5. The local oscillator for the transistorized front-end was derived from a klystron oscillator. This was phase locked via a Dymec synchronizer to a reference signal obtained from a highly stable 16.783333 MHz synthesized source and multiplied by 6. An IF reference of 31 MHz was also supplied. The resulting 30 MHz IF was amplified using a modified Collins 75S-3 receiver. A laboratory built square-law detector was used for final detection. This approach, as opposed to phase-locking to the signal was possible due to the 4.5 KHz receiver bandwidth which could accommodate the Doppler shift resulting from satellite motion. The measured system margin was approximately 52 dB. The receiver calibration characteristics are shown in Figure 6

The link calculations for both of these receiving systems are shown in Table 2 [19,20].

Table 2

LINK CALCULATIONS

Elevation = 44°

		2 GHz	30 GHz
Transmitter power	(dBm)	43.0	33.0
Spacecraft system loss	(dB)	- 1.9	- 1.0
Spacecraft antenna gain	(dB)	39.4	39.0
Free space loss	(dB)	-190.2	-213.4
Clear air (H_2O, O_2) losses	(dB)	- 0.5	- 1.1
Ground antenna gain	(dB)	40.0	57.8
Polarization loss	(dB)	- 3.0	0
Ground waveguide loss	(dB)	-	- 1.5
Signal into mixer	(dBm)	- 73.2	- 87.2
Receiver noise temperature at mixer	(°K)	3500	18000
Receiver bandwidth	(Hz)	4500	55
Receiver noise level	(dBm)	-126.6	-138.7
S/N (max)	(dB)	53.4	51.5

The analog outputs of both receivers were in the range of 0-5 volts. These were sampled and digitally recorded in real time by a laboratory built, computer controlled data acquisition system at the rate of 10 samples per second at all times and 200 samples per second on demand. Record header information including time, receiver status and attenuator settings were combined with the sampled data before recording [21]. Strip chart recordings were also made at all times.

The data were subsequently edited by eliminating periods of equipment adjustment, antenna peaking or adjustment and data corrupted by ground reflections at elevation angles below 0.38°. After calibration to compensate for receiver characteristics, the edited data were rewritten onto a working tape in records of 2048 samples from each receiver, i.e., a data period of 204.8 seconds or 3.4 minutes. Header information including elevation and azimuth angle data, receiver status and time was also written for each record. For details of the data format see Appendix A. A table of the acceptable edited data periods is given in Appendix B.

Sky photographs were also taken regularly, and a log of wind conditions was kept. The experiment commenced on August 28, 1976 and continued through October 25, 1976.

CHAPTER II
THE DATA

The conversion of the recorded receiver output voltages into relative received signal power levels will be discussed in this chapter. Segments of the received signal records will be presented and the more significant features will be noted.

A. Recovering The Received Signals

The 2 and 30 GHz receivers were calibrated with respect to arbitrary levels somewhat above the maximum signal levels encountered during the experiment. All received signal levels were then expressed as attentuation levels in decibels (dB) with respect to these corresponding reference levels for each receiver by means of the receiver characteristic curves (Figures 4 and 6). This process also corrected the recorded voltages for receiver non-linearities. Thus if

$$V_{recorded} = f_1(P^{incident}, \text{Attenuators}), \tag{2-1}$$

then

$$P^{incident} = f_2\ (V_{recorded}, \text{Attenuators})\ . \tag{2-2}$$

The data recorder's analog to digital (A/D) converter was of the 8 bit, modified two's-complement type, measuring -5 to +5 volts in 256 levels. Since the receiver outputs ranged from 0-5 volts only, useful output of 128 levels was obtained.

The function f_2 was evaluated for each receiver from experimental calibration data for one attenuator setting only, by Lagrangian interpolation at 128 discrete steps. It was found that the complete family of characteristic curves (Figures 4 and 6) could be approximated by this master curve and shifted appropriately to represent the other attenuator settings.

A table of usable data periods was also generated and stored in the computer. This included a status word indicating whether the data from a particular receiver was usable or not (Appendix B).

The final working tape was written under the control of the data status table, using the receiver characteristics file, the quantity recorded being the signal levels below the respective references. The resolution on this tape was 0.1 dB. Overall accuracy of the data was estimated to be ± 1 dB, considering such factors as antenna pointing error, long term receiver drift and calibration errors.

B. Data Characteristics

A total of 75 hours of data was collected, including 28 hours when both the 2 and 30 GHz beacons were recorded simultaneously. Due to spacecraft power constraints during orbit transfer, the 2 GHz beacon could not be operated for continuous periods exceeding one hour.

In this section 30 minute segments of the received signal records are presented. Interesting 6 minute portions taken from these are also shown on expanded scales. In each case the data are plotted relative to the mean signal level for the period shown. Further, the 0.1 second samples are averaged over 10 samples (i.e., 1 second intervals) for ease of plotting. Consequently, components above 1 Hz will be smoothed out in these plots. All elevation angles recorded are predicted values based on the satellite orbital elements and are not corrected for refraction, though the antenna itself was pointed at the observed position of the spacecraft.

The satellite was first acquired at a nominal elevation angle of -0.79°; however, the data below 0.38°, i.e., until the 30 GHz receiving antenna had cleared the ground by a few beamwidths, were not considered reliable due to possible ground reflection effects.

Data were collected almost continuously during the first 3 days. As the elevation angle increased and the signals quieted, observations were reduced to one or two hourly periods at different times of the days. In the last few days of the experiment, these were further reduced to an hour's observation every 3 or 4 days.

It is recognized that due to the relatively short duration of the experiment the data collected would be insufficient to average out the day to day variation in weather conditions. Therefore, care should be exercised in interpreting the data.

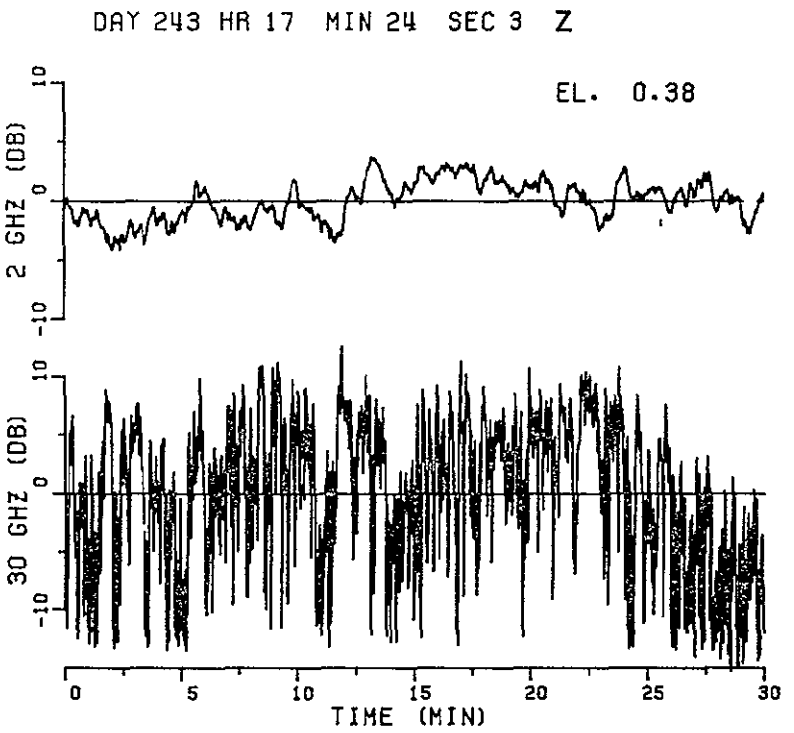

(a)

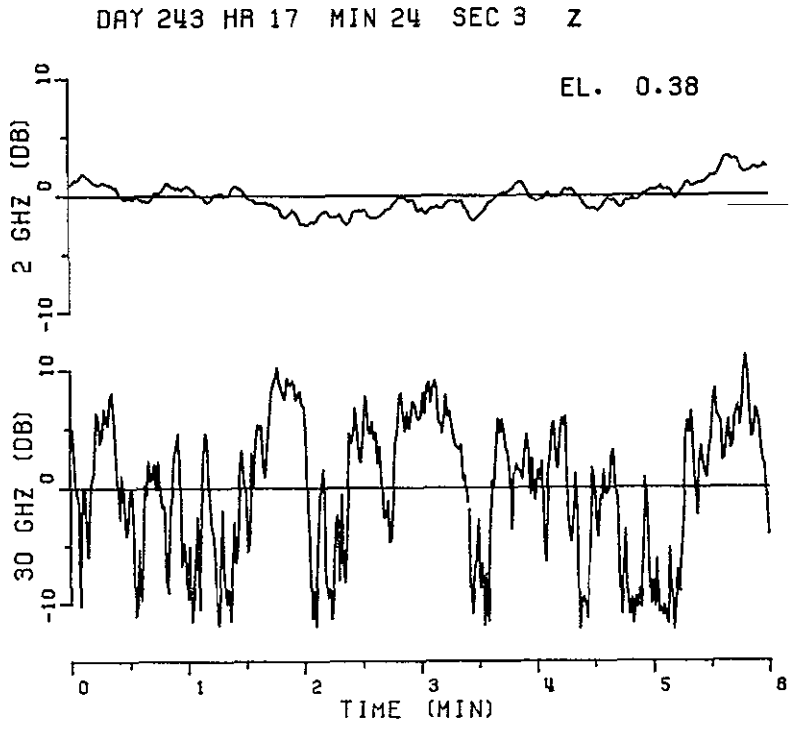

(b)

Figure 7. Received signals on day 243. Elevation angle 0.38°.

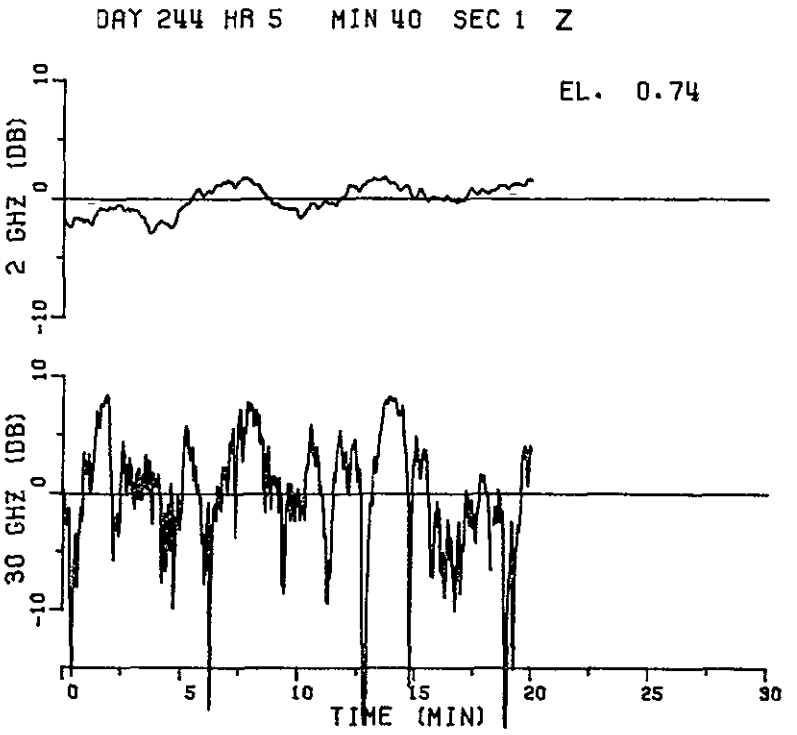

(a)

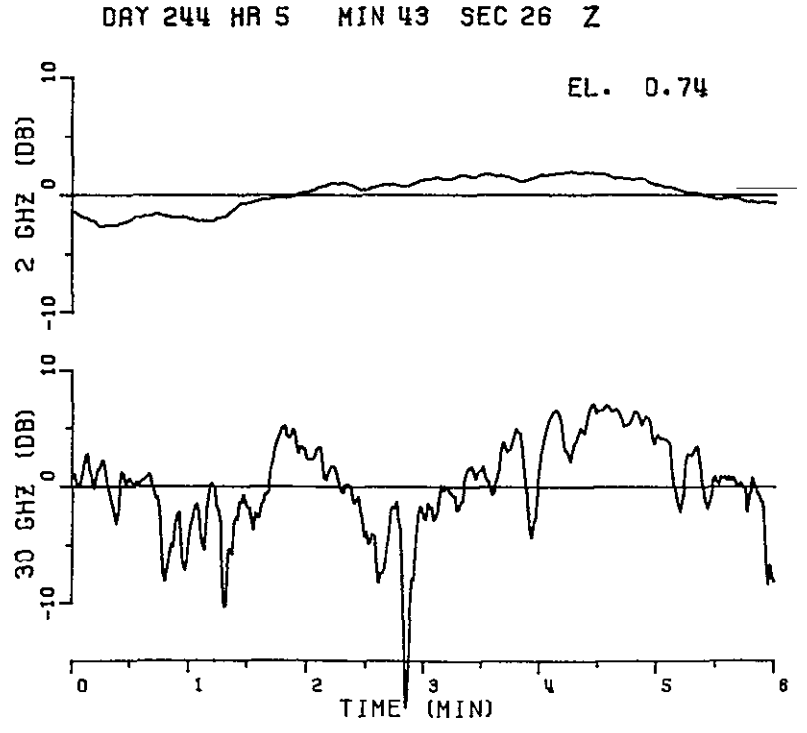

(b)

Figure 8. Received signals on day 244. Elevation angle 0.74°

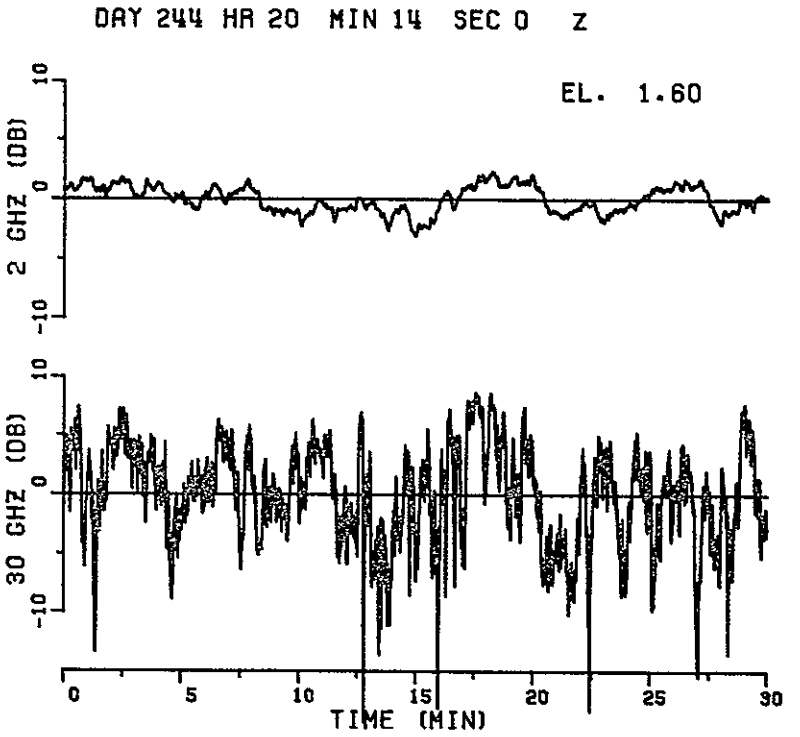

(a)

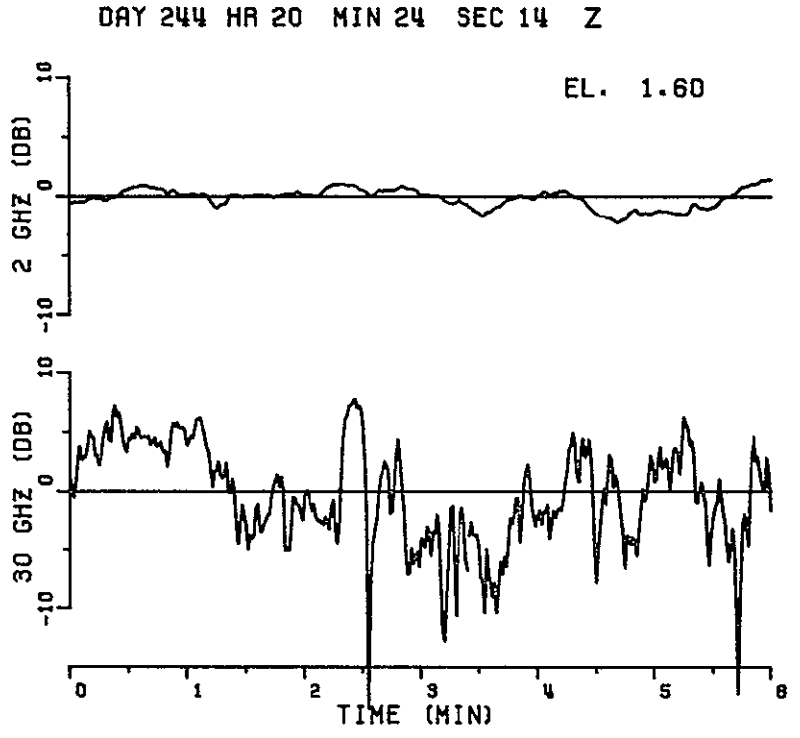

(b)

Figure 9. Received signals on day 244. Elevation angle 1 60°

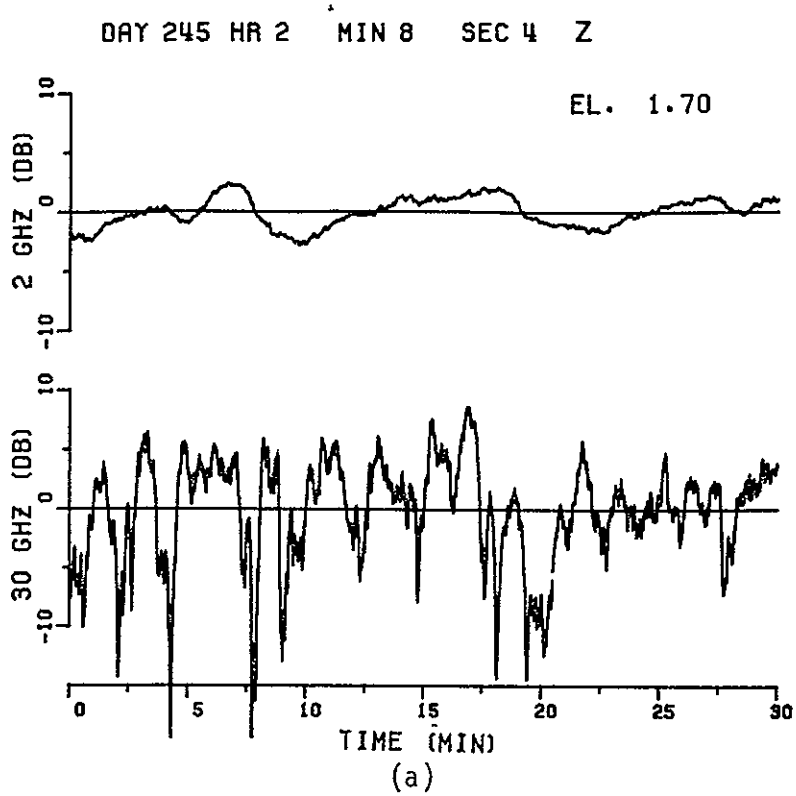

(a)

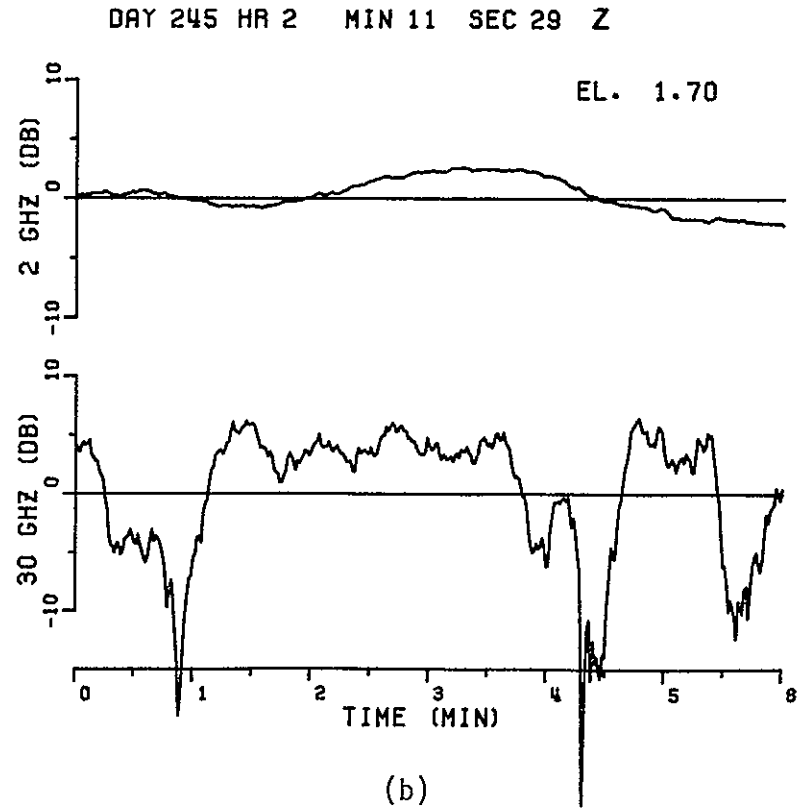

(b)

Figure 10. Received signals on day 245 Elevation angle 1.70°

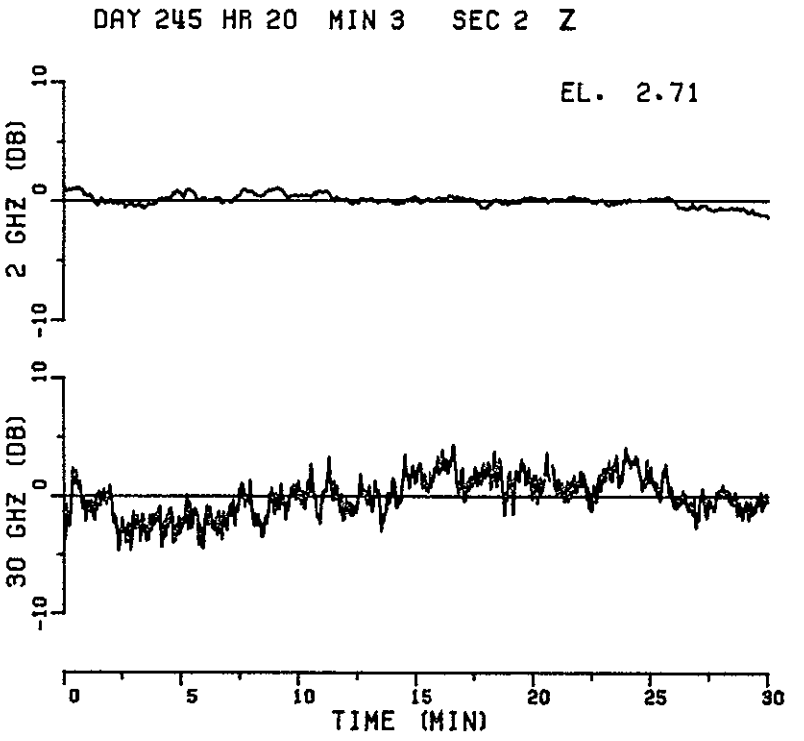

(a)

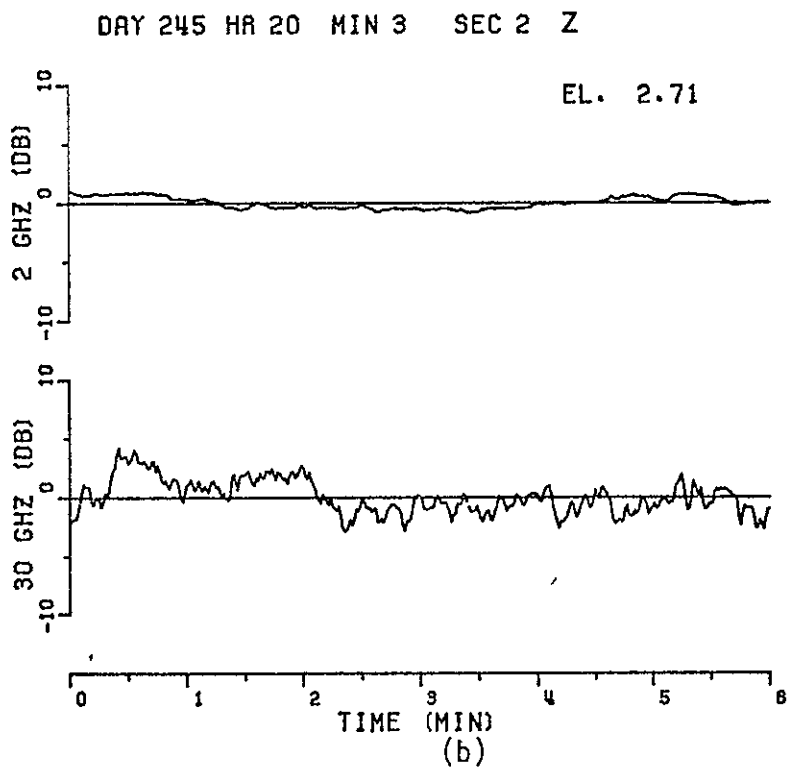

(b)

Figure 11 Received signals on day 245. Elevation angle 2.71°.

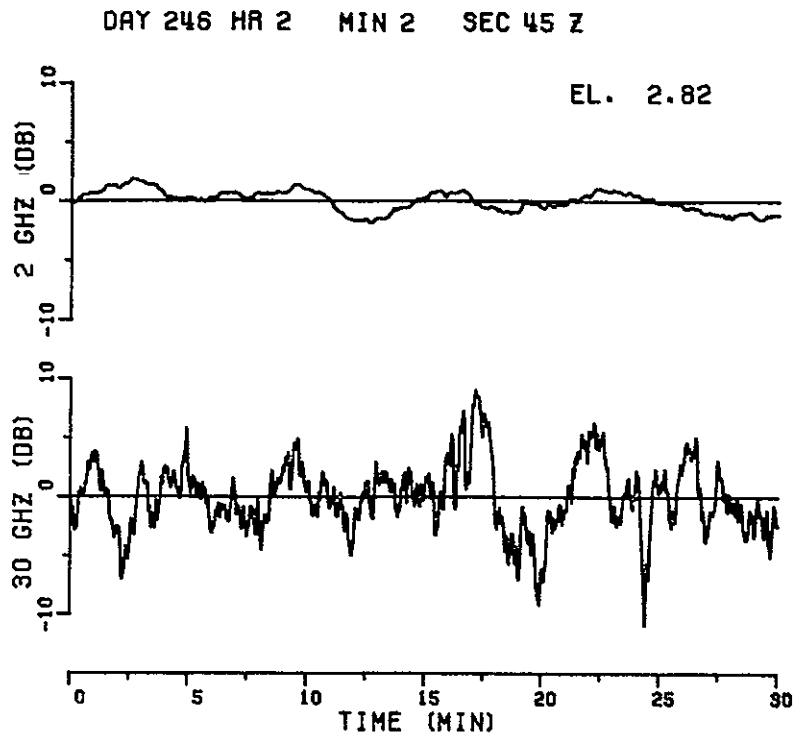

(a)

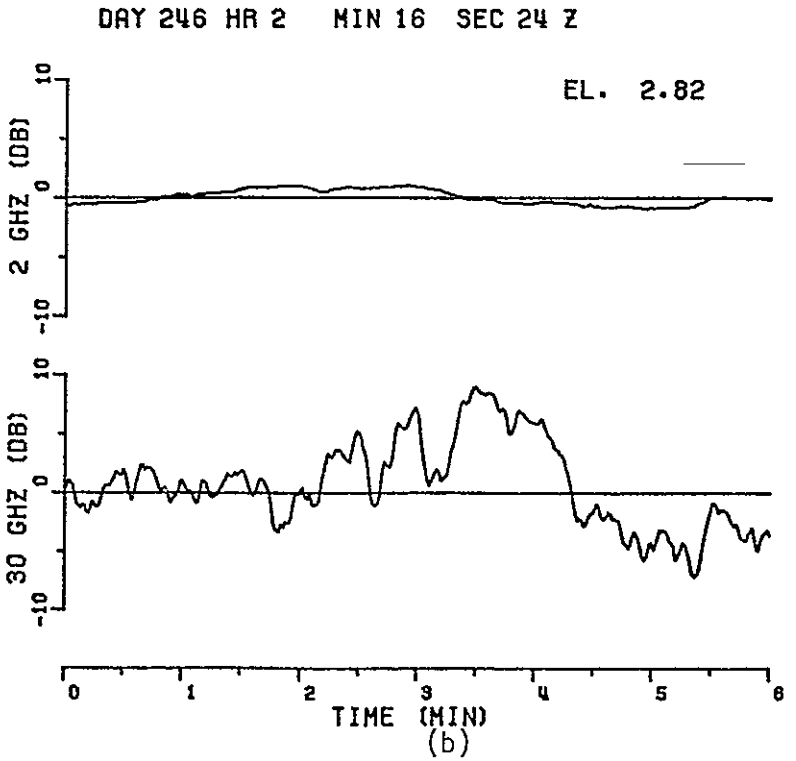

(b)

Figure 12 Received signals on day 246. Elevation angle 2.82°.

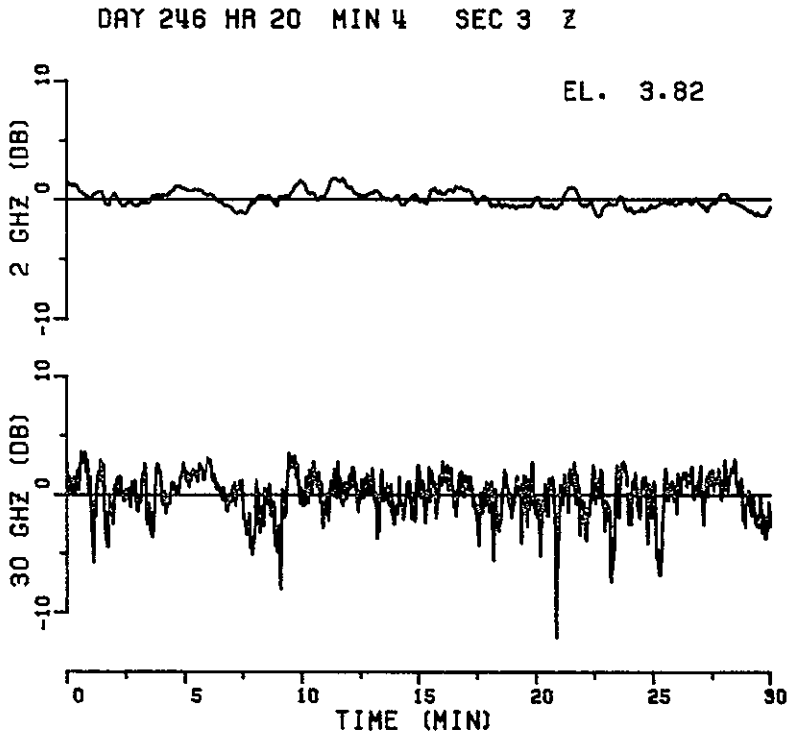

(a)

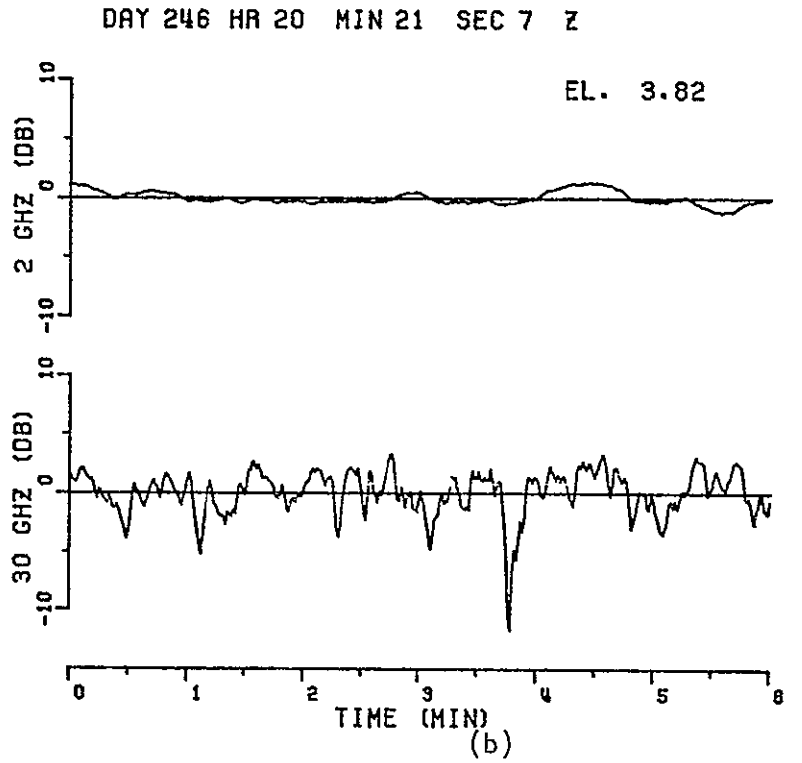

(b)

Figure 13 Received signals on day 246. Elevation angle 3.82°

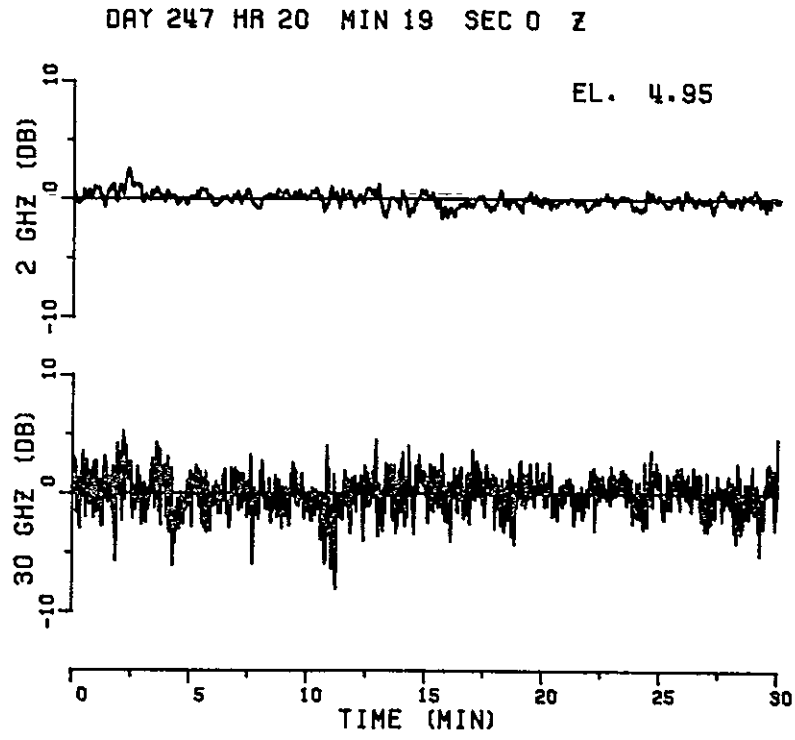

(a)

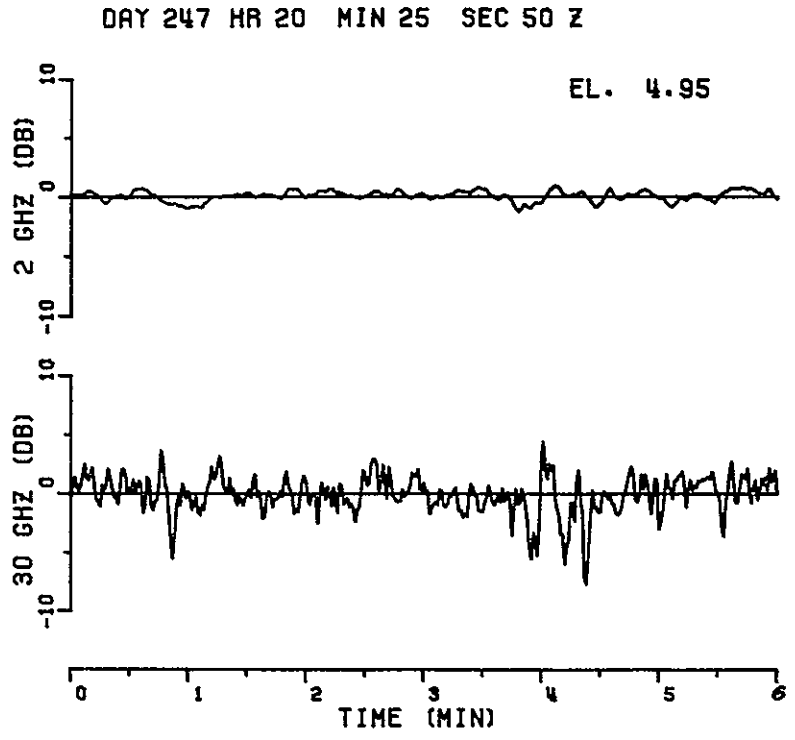

(b)

Figure 14. Received signals on day 247. Elevation angle 4.95°.

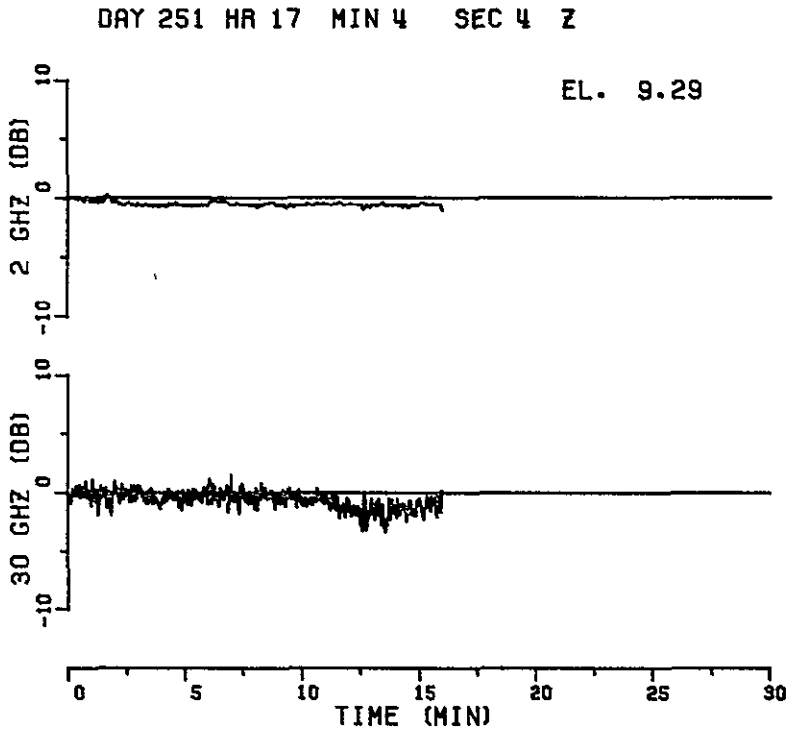

(a)

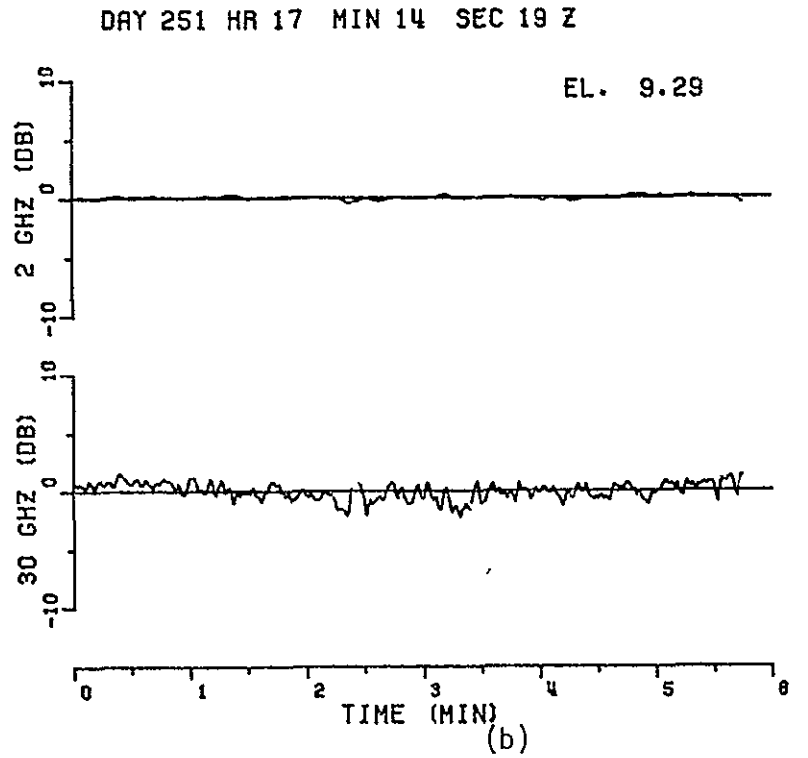

(b)

Figure 15. Received signals on day 251. Elevation angle 9.29°.

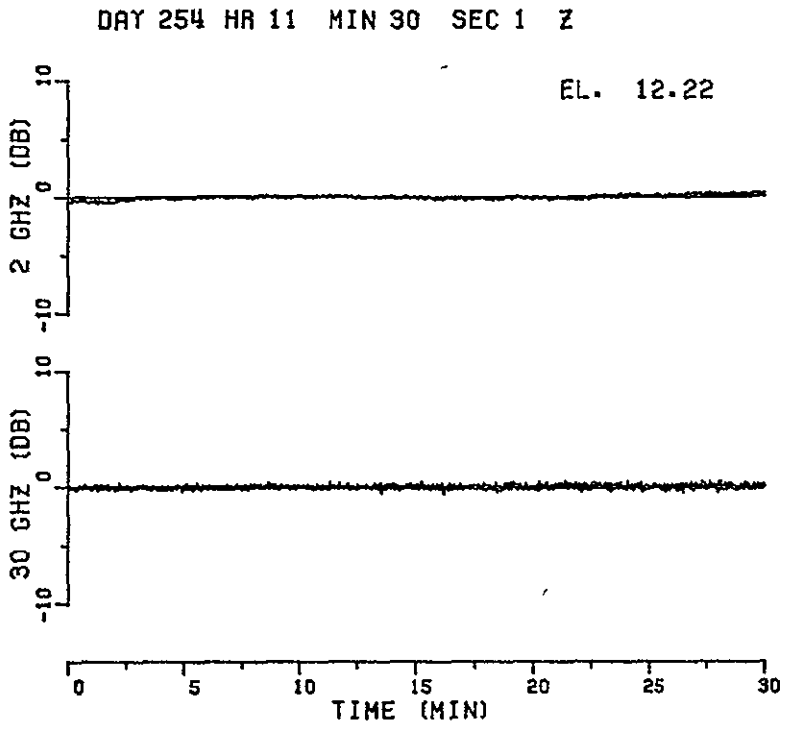

Figure 16. Received signals on day 254. Elevation angle 12.22°.

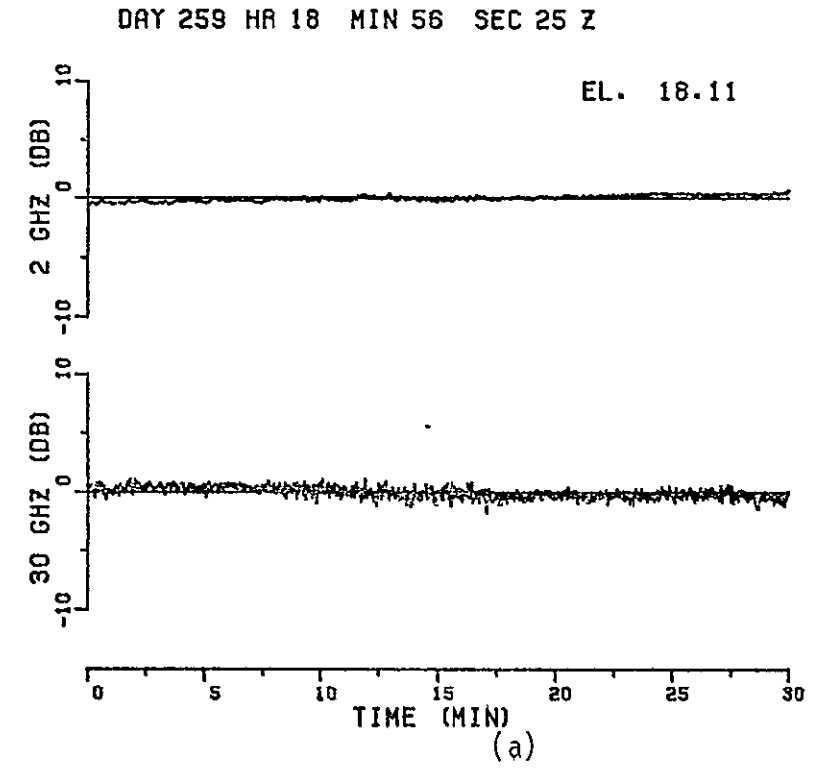

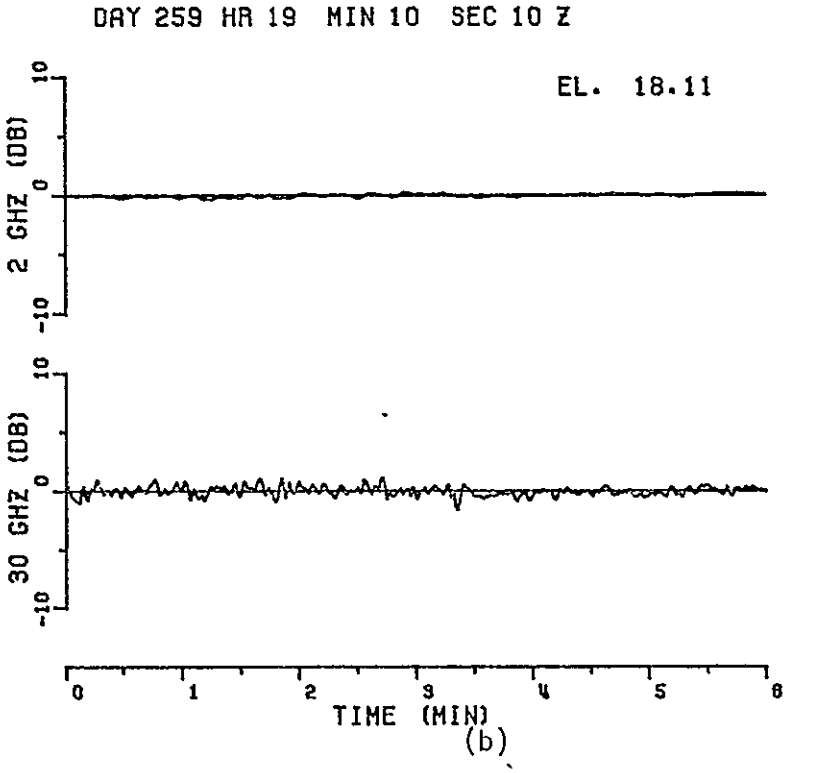

Figure 17. Received signals on day 259. Elevation angle 18.11°

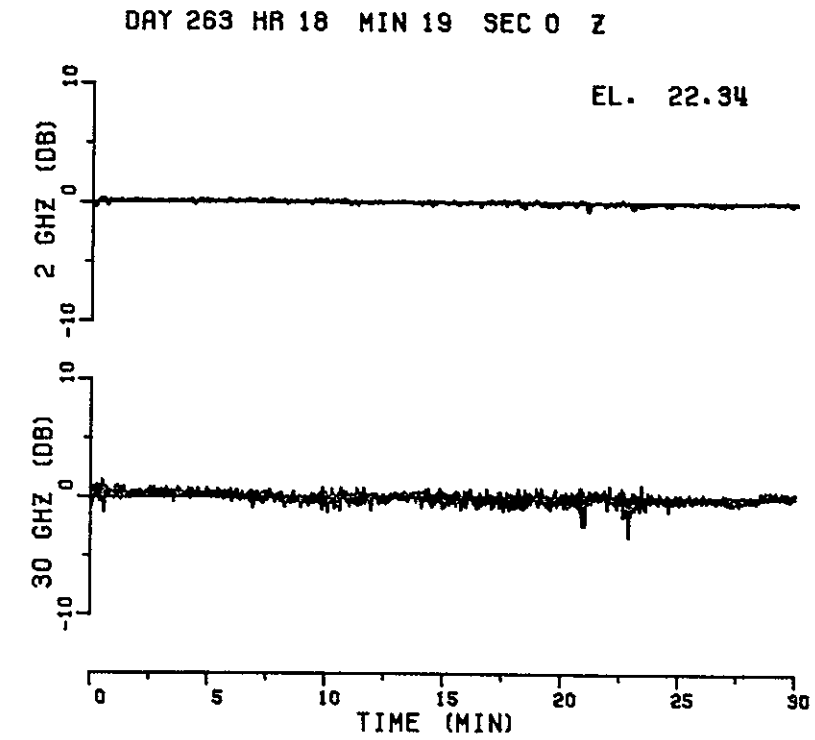

(a)

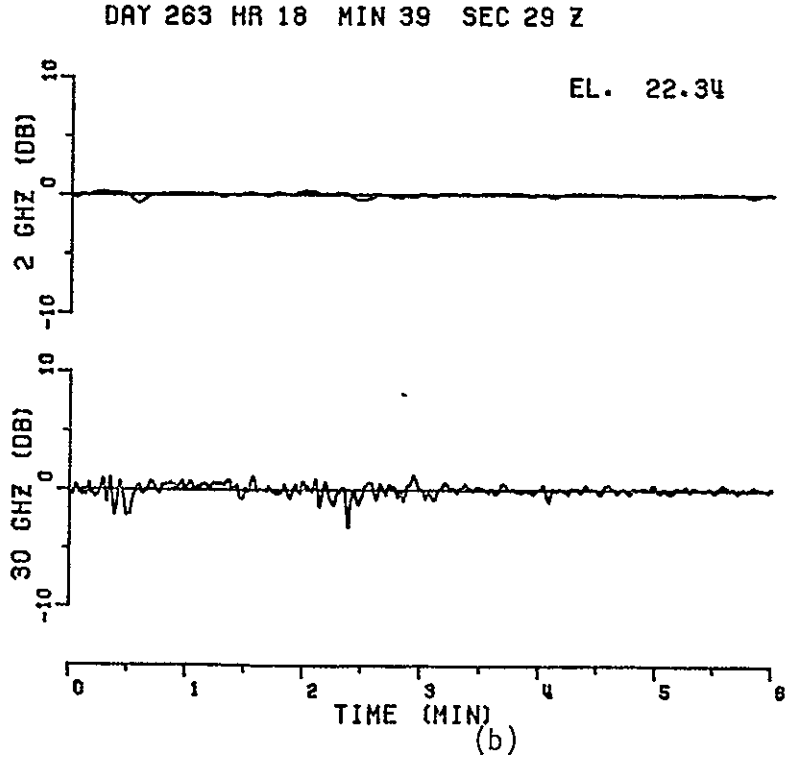

(b)

Figure 18. Received signals on day 263 Elevation angle 22 34°

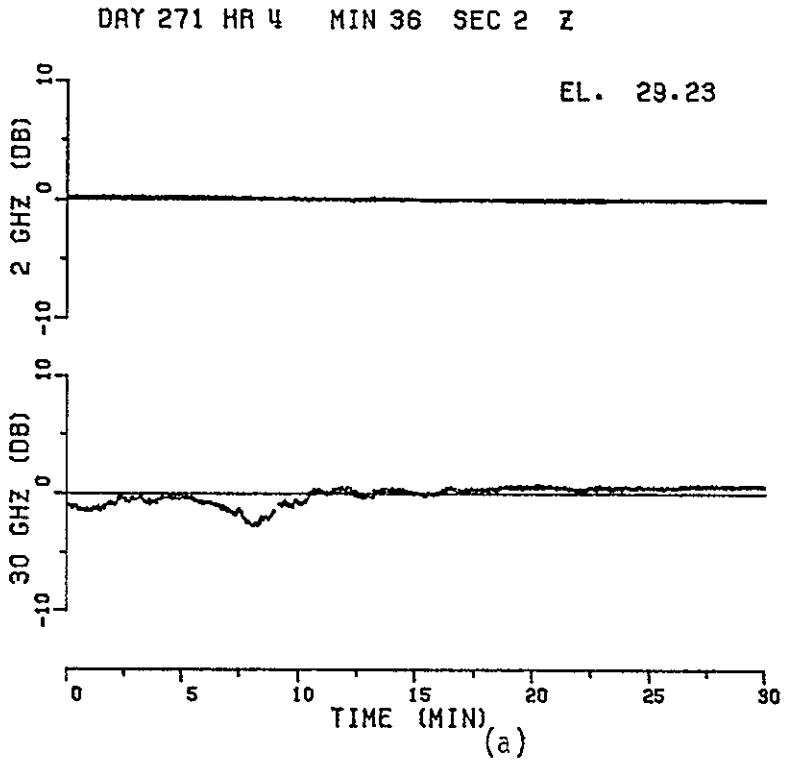

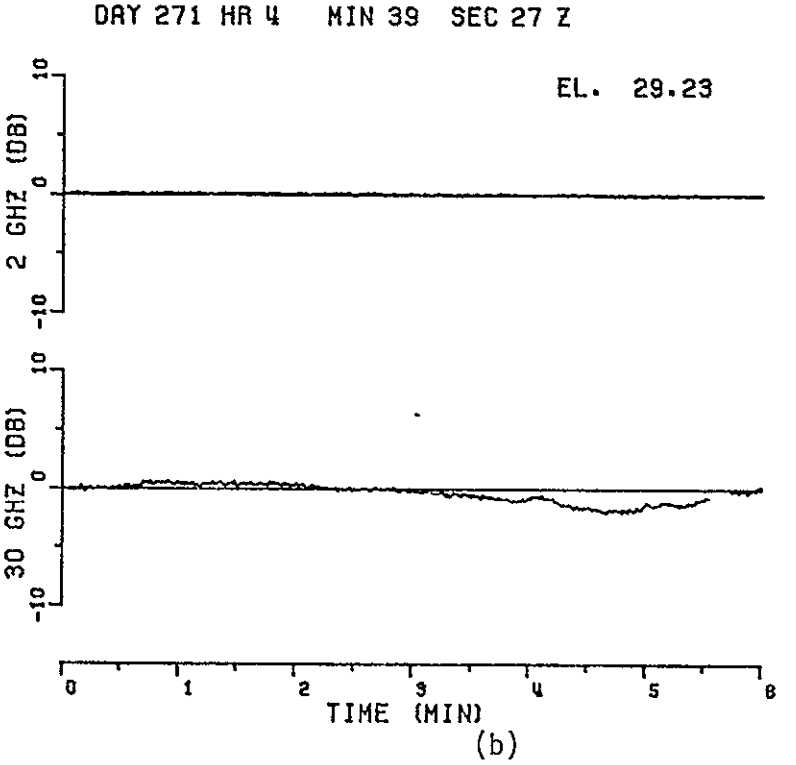

Figure 19 Received signals on day 271. Elevation angle 29 23°.

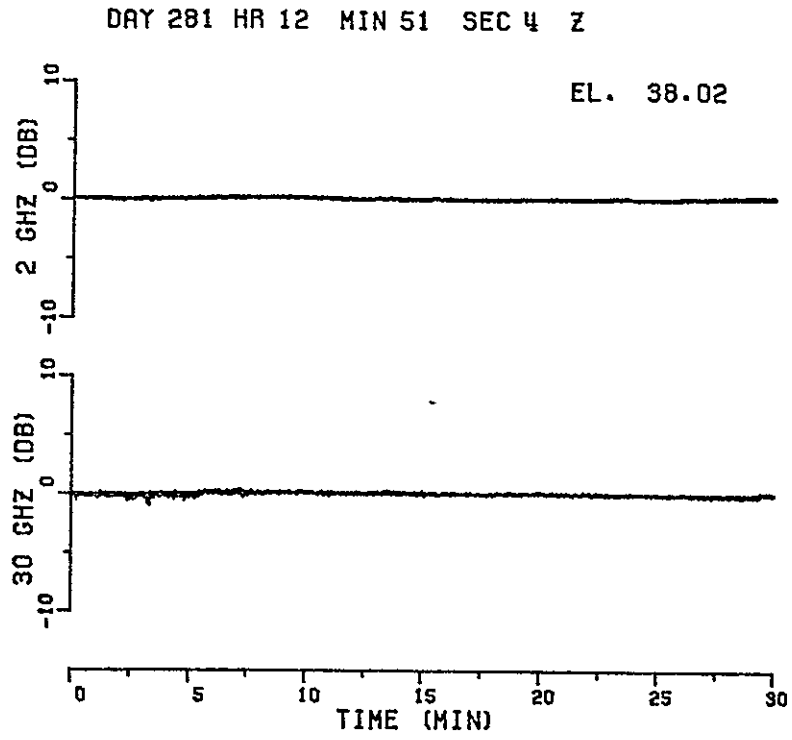

Figure 20 Received signals on day 281. Elevation angle 38.02°

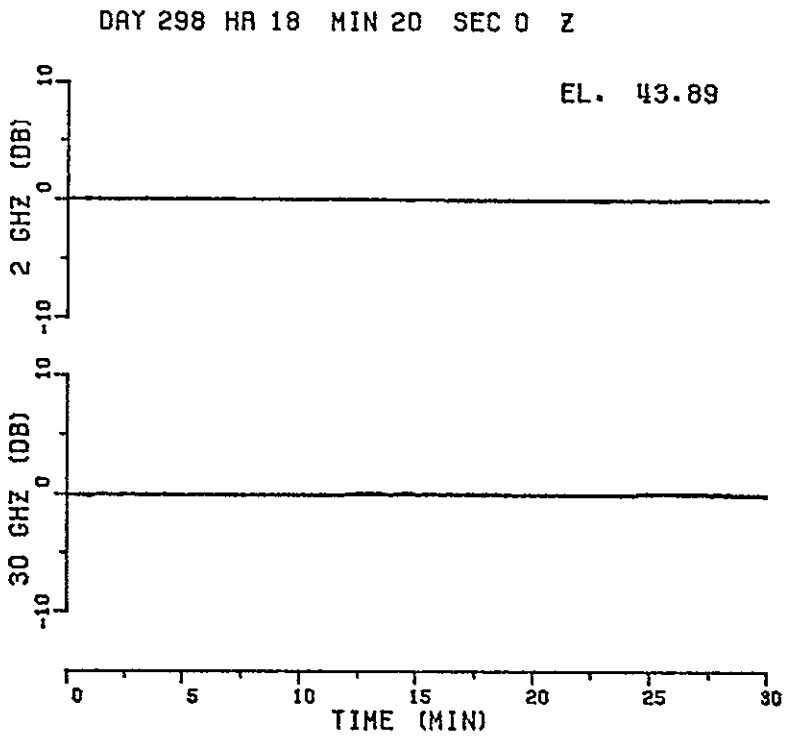

Figure 21. Received signals on day 298. Elevation angle 43 89°.

The following tabulation presents the typical characteristics of the received signal levels as a function of the propagation path elevation angle. All times noted on the figures are GMT; (GMT - 4 hours = Eastern Standard time).

a) Elevation = 0.38° - (Figure 7a,7b):

Signal swings up to about 30 dB within 2 minutes and sharp spikes are observed at 30 GHz. Rolling waveforms with flattened tops and sharp deep minima are found on the expanded plot.

Shifts of the "short term" mean level on the order of 15 dB are also seen over 10 minute intervals.

The behavior of the 2 GHz signal appears to be different. Though the signal varies by about 10 dB in 5 minutes and the "short term" mean level shifts approximately 3 dB, it is difficult to see the same type of behavior as was evident in the 30 GHz signal. A detailed examination of the cross correlation and spectra is presented in Chapter IV.

The sky was very clear and free from clouds.

b) Elevation = 0.74° (Figure 8a,8b).

The rapid large fluctuations have been reduced significantly. However large scintillations are still present. The local time is around 2 A.M.

The sky was relatively clear with few scattered cirrus clouds.

c) Elevation = 1.60° (Figure 9a,9b):

The large scale excursions are more infrequent and the higher frequency scintillations are more prominent.

No clouds were observed along the propagation path.

d) Elevation = 1.70° (Figure 10a,10b)

The period presented is around 10 P.M. (local time). Once more, large excursions exceeding 30 dB are seen at 30 GHz. The 2 GHz also shows enhanced activity.

The sky was overcast with few breaks in the clouds.

e) Elevation = 2.71° (Figure 11a,11b)

Compare these with the signals observed at an elevation angle of 1.60° (Figure 9a,9b) recorded at about the same time of day. Although the sky was still overcast, both signals have quieted down remarkably compared to the clear sky signals of Figure (9a,9b).

High frequency components are clearly seen.

f) Elevation = 2.82° (Figure 12a,12b):

This segment, too, is around 10 P.M. local time and should be compared with Figure (10a,10b). Once again an increase in large scale scintillation events can be seen.

The cloud conditions were solid overcast.

g) Elevation = 3.82° and 4.95° (Figures 13a to 14b):

Both of these were around 4 P.M. local time and should be compared with Figures 9a,9b and 11a,11b, (elevation angles 1.60° and 2.71°) which were also observed around this time. Higher scintillation frequencies are still present. However scattered clouds were seen during the data period of Figure 13 while the sky is relatively clear during that of Figure 14. The signals at 4.95° are particularly interesting because rapid fluctuations have increased and are present in the 2 GHz data also.

h) Elevation = 9.29°, 12.22°, 18.11°, 22.34°, 29.23° (Figures 15a to 19b).

The signals from the higher elevation angles are quieter except for isolated scintillation events. However it still appears that peak to peak scintillations are larger around the mid afternoon hours. Photographs taken at elevation 9.29° (around 1 P.M. local time) show a very clear day with some haze in the horizon. The period of Figure 16 (12.2°) shortly after local sunrise, on a cloudy morning is comparatively quiet. Day 263 was overcast. Precipitation is a possible cause for the fade events on Day 271.

Unfortunately, satellite scheduling did not permit sunrise measurement at these higher elevation angles.

i) Elevation = 38.02°, 43.89° (Figures 20 and 21)

Signal scintillations are too small to make any comments based on signal level plots alone. Isolated scintillation events are still present, sometimes up to about 10 minutes in duration; these appear to be related to cloud activity on the path In general, the levels appear to be very stable.

C. Comments

a) Several types of signal fluctuations can be seen in the data.

(i) - Slow variations of tens of dB over periods of tens of minutes at low elevation angles.

(ii) - Faster fluctuations or scintillations with durations of a few minutes or less. These may be continuous at low elevation angles or occur in isolated 'events' at high elevation angles.

(iii) - Continuous small rapid scintillation of a dB or less are found at all elevation angles.

b) At very low elevation angles, it is possible that angle-of-arrival scintillation plays a significant role in the amplitude perceived by the receiver, especially at 30 GHz. This is due to the very narrow beamwidth of the antenna (0.2°). The antenna was observed to have sharp nulls on either side of the main beam. Consequently the system was very sensitive to pointing errors. Therefore, slight changes in angle-of-arrival due to phase-front perturbations or ripple could cause sharp drops in received signal level.

The 2 GHz antenna on the other hand has a much wider beamwidth (1.3°) and was not as sensitive to pointing errors. This, coupled with reduced sensitivity to atmospheric inhomogeneities at 2 GHz may account for the smoother waveform, even at low elevation angles.

c) The terrain in front of the antennas is a well plowed, dry field. This, together with the elimination of very low angle data, ensures that the data considered is reasonably free from ground effects.

d) It was not possible to directly attribute scintillations to cloud cover. Scintillations were always observed and cloudy days were sometimes very quiet. It can only be said that the presence of clouds sometimes contributed to signal scintillations, particularly at the higher elevation angles.

CHAPTER III
RESULTS. VARIANCE

The characteristics of the amplitude and log-amplitude variance of the received signals are examined in this chapter. The dependence of the variance on path length is found to agree well with predictions based on the Kolmogorov turbulence theory. Equivalent heights are deduced for a homogeneous spherical troposphere.

A. Preliminaries

The relative received power is defined to be

$$p(t) = 10 \log_{10} \frac{P(t)}{P_o}$$

$$= 20 \log_{10} \frac{a(t)}{a_o} \quad \text{decibels} \tag{3-1}$$

where P_o is an arbitrary power level established during the calibration procedure (see Section II-A) and $P(t)$ is the received signal power level as determined from the receiver calibration characteristics. $a(t)$ and a_o are the corresponding amplitude quantities. Consequently, the relative amplitude of the signal is

$$A(t) = \frac{a(t)}{a_o}$$

$$= 10^{\frac{p(t)}{20}} \quad . \tag{3-2}$$

This will be called the 'amplitude' of the received signal in the following. All of the following statistical analysis will be based on statistical parameters normalized in such a manner that the choice of a_o is unimportant.

The relative log amplitude, called the 'log amplitude' hereafter is defined to be

$$\chi(t) = p(t) \quad . \tag{3-3}$$

Here again, the choice of the constant P_o will be of no consequence.

B. Variance

The variances and the means of received signal are defined for an interval T as follows:

a) Amplitude variance

$$\sigma_A^2 = \frac{1}{T} \frac{\int (A(t) - \overline{A})^2 \, dt}{\overline{A}^2} \tag{3-4a}$$

$$\sigma_{A_{dB}}^2 = 10 \log_{10} \left[\frac{1}{N\overline{A}^2} \sum_{t=1}^{N} (A_1 - \overline{A})^2 \right] \text{dB} \quad , \tag{3-4b}$$

where A_1 is the sampled value of A(t) as defined in Equation (3-2), N is the number of samples in T, and

b) Mean amplitude

$$\overline{A} = \frac{1}{T} \int A(t) \, dt \tag{3-5a}$$

$$\overline{A} = \frac{1}{N} \sum_{t=1}^{N} A_1 \quad . \tag{3-5b}$$

It should be noted that

$$\sigma_A^2 = S_2^2$$

where S_2 is the second scintillation index defined by Briggs and Parkin [22], so that

$$S_{2_{dB}} = \frac{1}{2} \sigma_{A_{dB}}^2$$

c) Log amplitude variance

$$\sigma^2_{\ell} = \frac{1}{K_1^2}\,\frac{1}{T}\int (\ell(t) - \overline{\ell})^2\, dt \qquad (3\text{-}6a)$$

$$\sigma^2_{\ell_{dB}} = 10 \log_{10}\left[\frac{1}{K_1^2 N}\sum_{t=1}^{N} (\ell_1 - \overline{\ell})^2\right] dB \quad . \qquad (3\text{-}6b)$$

ℓ_1 is the sampled value of $\ell(t)$ as defined in Equation (3-3) and

$$K_1 = 20 \log_{10} e \qquad (3\text{-}7)$$

is a constant required to satisfy the condition that $\sigma^2_A \approx \sigma^2_{\ell}$ for small signal variations.

d) Mean log amplitude

$$\overline{\ell} = \frac{1}{T}\int \ell(t)\, dt \qquad (3\text{-}8a)$$

$$\overline{\ell} = \frac{1}{N}\sum_{1=1}^{N} \ell_1 \quad . \qquad (3\text{-}8b)$$

Clearly, the amplitude variance represents the ratio of the power contained in the non zero frequency component to the power in the zero frequency component (dc power) of the signal.

The samples are taken at a rate of 10 samples per second and σ^2 is determined for N = 2048, i.e., a time interval of about 205 sec. or 3.4 minutes.

The maxima and minima of the amplitude and log variances of the 2 GHz and 30 GHz received signals are shown as functions of elevation angle in Figures 22 through 25 The range of the variances is seen to exceed 20 dB at certain times. The maxima and minima of both the amplitude and log amplitude variances are virtually identical, except at very low elevation angles, when they differ by a few dB. The data periods used for these calculations are shown in Appendix B, Section 2.

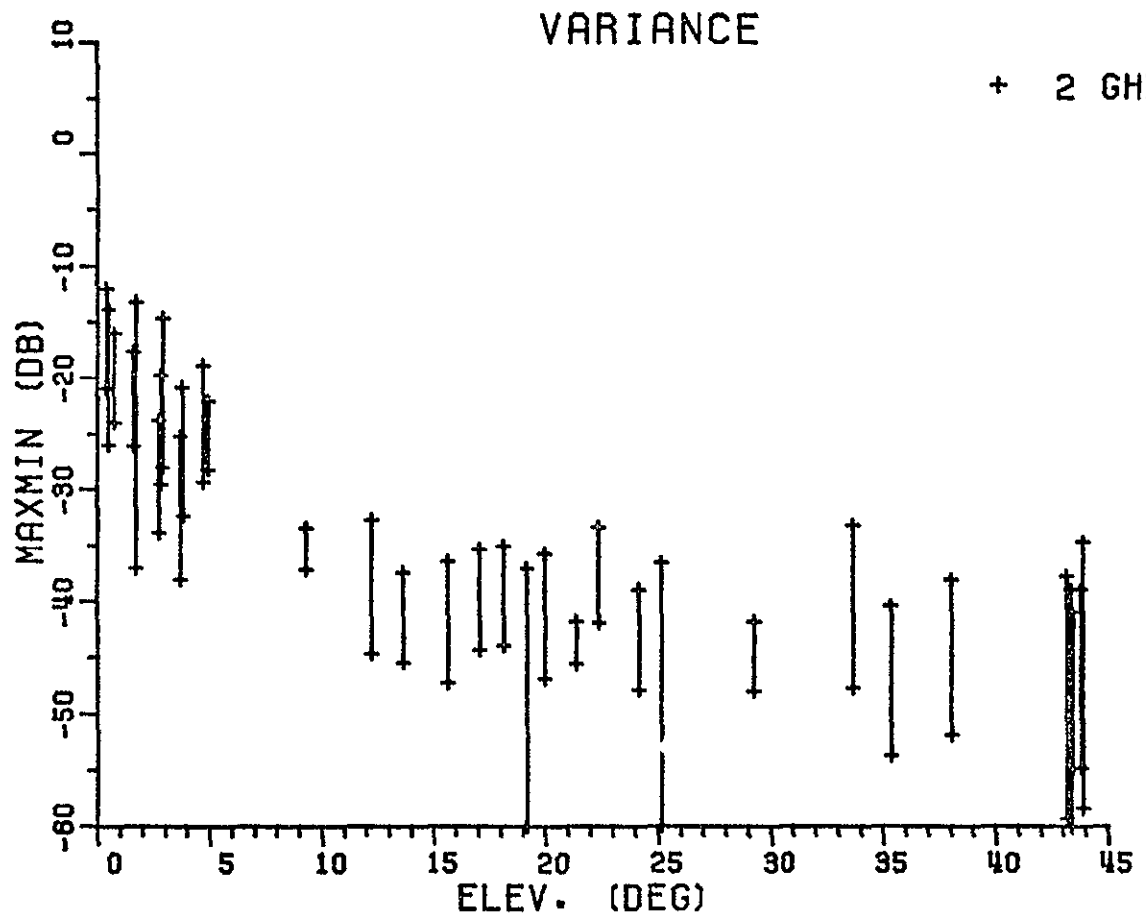

Figure 22. Amplitude variance. Maxmin, 2 GHz, with elevation angle

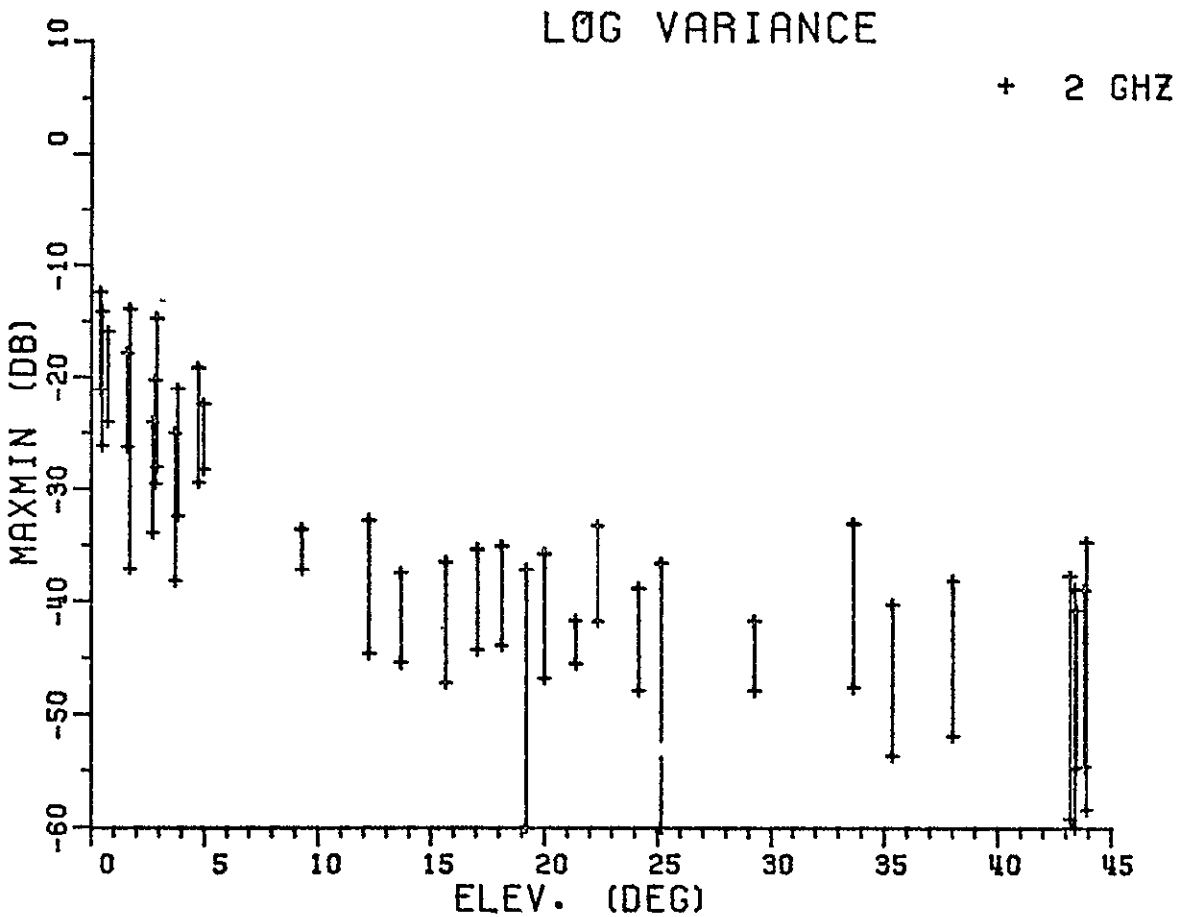

Figure 23. Log amplitude variance. Maxmin, 2 GHz, with elevation angle.

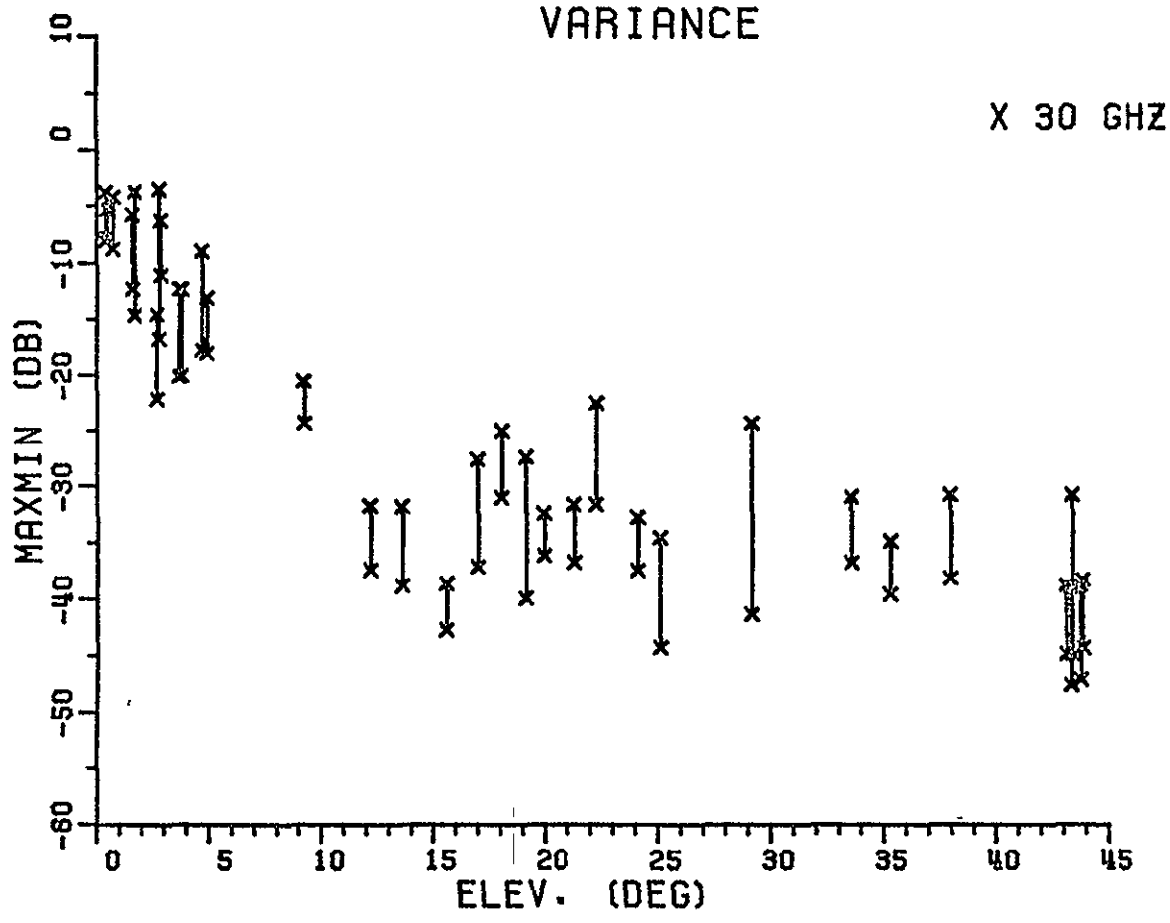

Figure 24 Amplitude variance. Maxmin, 30 GHz, with elevation angle

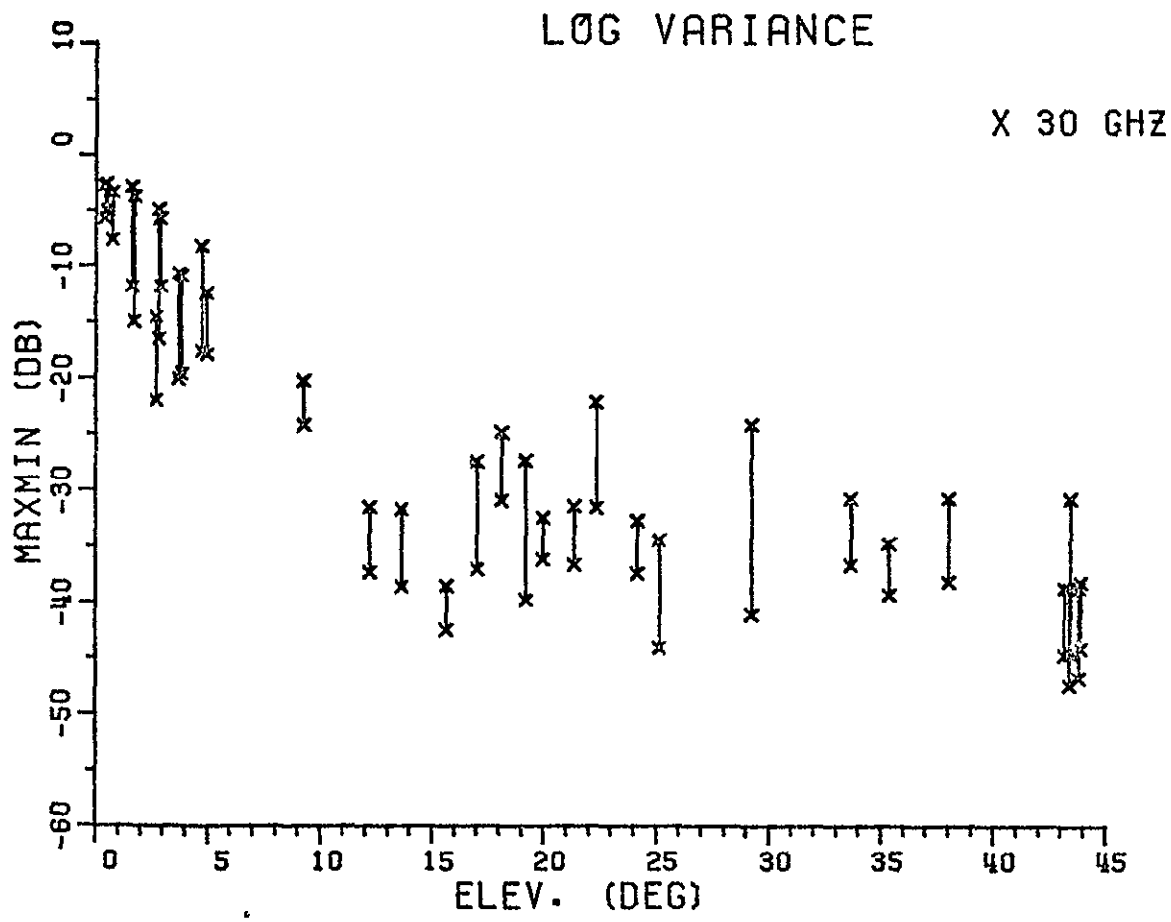

Figure 25. Log amplitude variance Maxmin, 30 GHz, with elevation angle

Next it was assumed that the variances followed the law,

$$\sigma^2 = A L^B \quad , \tag{3-9}$$

where L is the path length of the received signal through the atmosphere and A and B are constants. If the elevation angle is denoted by θ, then, for a plane earth with an atmosphere of finite thickness,

$$L \propto CSC(\theta) \quad . \tag{3-10}$$

A minimum-mean-square-error curve fit to $\sigma^2 = A\,[CSC(\theta)]^B$ was performed for all the variance values obtained in this experiment. The results were:

Amplitude variances

$$\sigma^2_{A_2} = 10^{-4.9}\,[CSC(\theta)]^{1.62 \pm .2} \tag{3-11}$$

$$\sigma^2_{A_{30}} = 10^{-4.3}\,[CSC(\theta)]^{2.14 \pm .3} \tag{3-12}$$

Log amplitude variances

$$\sigma^2_{\ell_2} = 10^{-4.9}\,[CSC(\theta)]^{1.62 \pm .2} \tag{3-13}$$

$$\sigma^2_{\ell_{30}} = 10^{-4.3}\,[CSC(\theta)]^{2.20 \pm .3} \quad . \tag{3-14}$$

The subscript on the variance denotes the frequency.

Kolmogorov turbulence would give a relationship of the form [23]:

$$\sigma^2_{\ell} = a\,L^{11/6} = a\,L^{1.833} \quad . \tag{3-15}$$

These results appear to be in fair agreement, with the 2 GHz results somewhat below and the 30 GHz results above the theoretical value.

The average amplitude and log amplitude variances at each elevation angle together with the fitted cosecant law curves are shown in Figures 26 and 27. As is to be expected this law breaks down at very small elevation angles, due to the plane earth assumption.

In order to improve the fit, a spherical earth with a uniform atmosphere of height h was next assumed (Figure 28). The effective radius R of the earth was taken to be 4/3 the actual radius, or 8479 km, in order to compensate for standard refraction. The radio waves may then be assumed to propagate in straight lines. The path length L within this equivalent atmosphere is then·

$$L = \sqrt{h^2+2hR+R^2\sin^2\theta} - R\sin\theta \quad . \tag{3-16}$$

Equation (3-9) was again fitted to all the variance values in the minimum mean-square-error sense, but with the path length L given by Equation (3-16) above. The equivalent height parameter h was also a variable and was adjusted to minimize the error. The computation was continued until successive values of h converged to within 0.01 km for best fit.

The results are·

Amplitude variance

$$\sigma^2_{A_2} = 10^{-6.5} L^{1.87 \pm .2} \tag{3-17}$$

$$h = 6.2 \pm 1 \text{ km} \tag{3-18}$$

$$\sigma^2_{A_{30}} = 10^{-6.4} L^{2.48 \pm .3} \tag{3-19}$$

$$h = 6.0 \pm 1 \text{ km} \tag{3-20}$$

Log variance

$$\sigma^2_{\ell_2} = 10^{-6.4} L^{1.87 \pm .2} \tag{3-21}$$

$$h = 6.1 \pm 1 \text{ km} \tag{3-22}$$

$$\sigma^2_{\ell_{30}} = 10^{-6.1} L^{2.49 \pm .3} \tag{3-23}$$

$$h = 4.5 \pm 1 \text{ km} \quad . \tag{3-24}$$

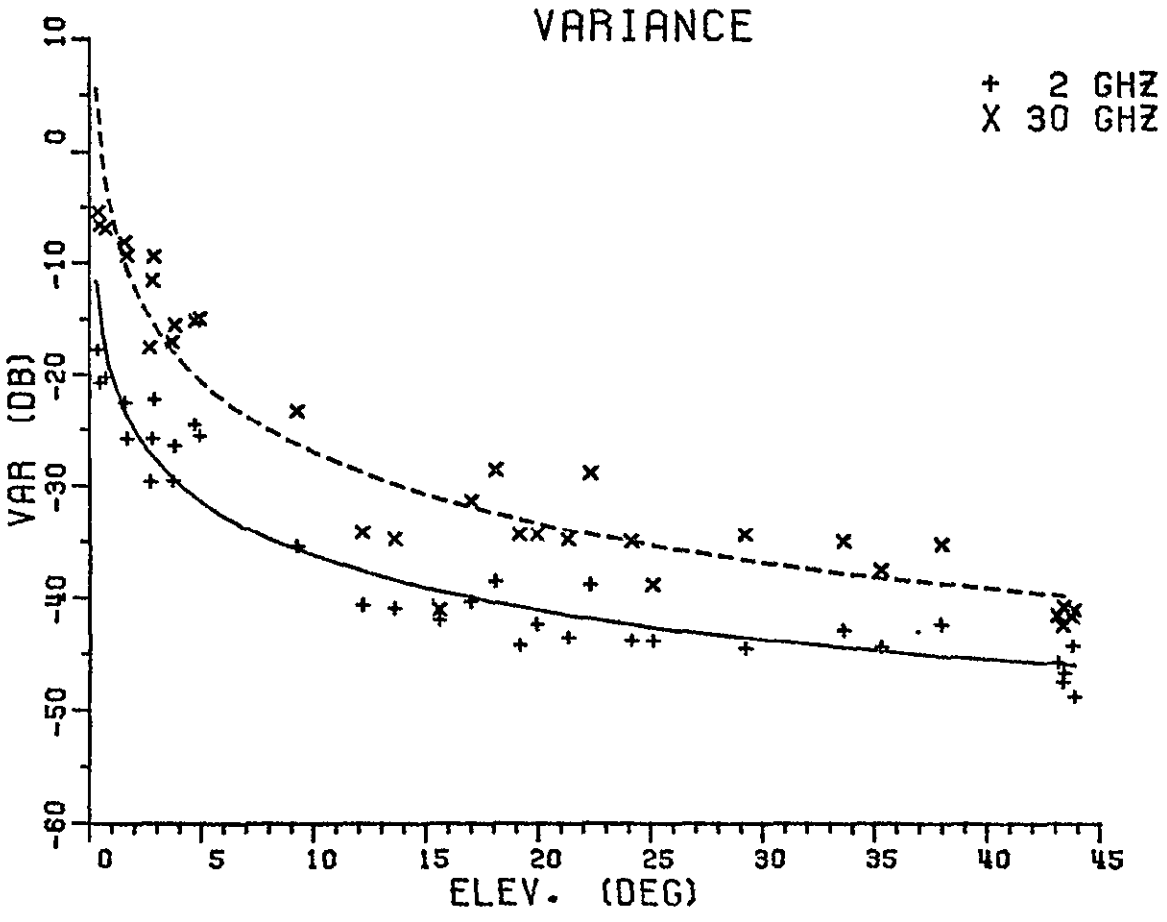

Figure 26. Mean amplitude variance with elevation angle. Cosecant law.

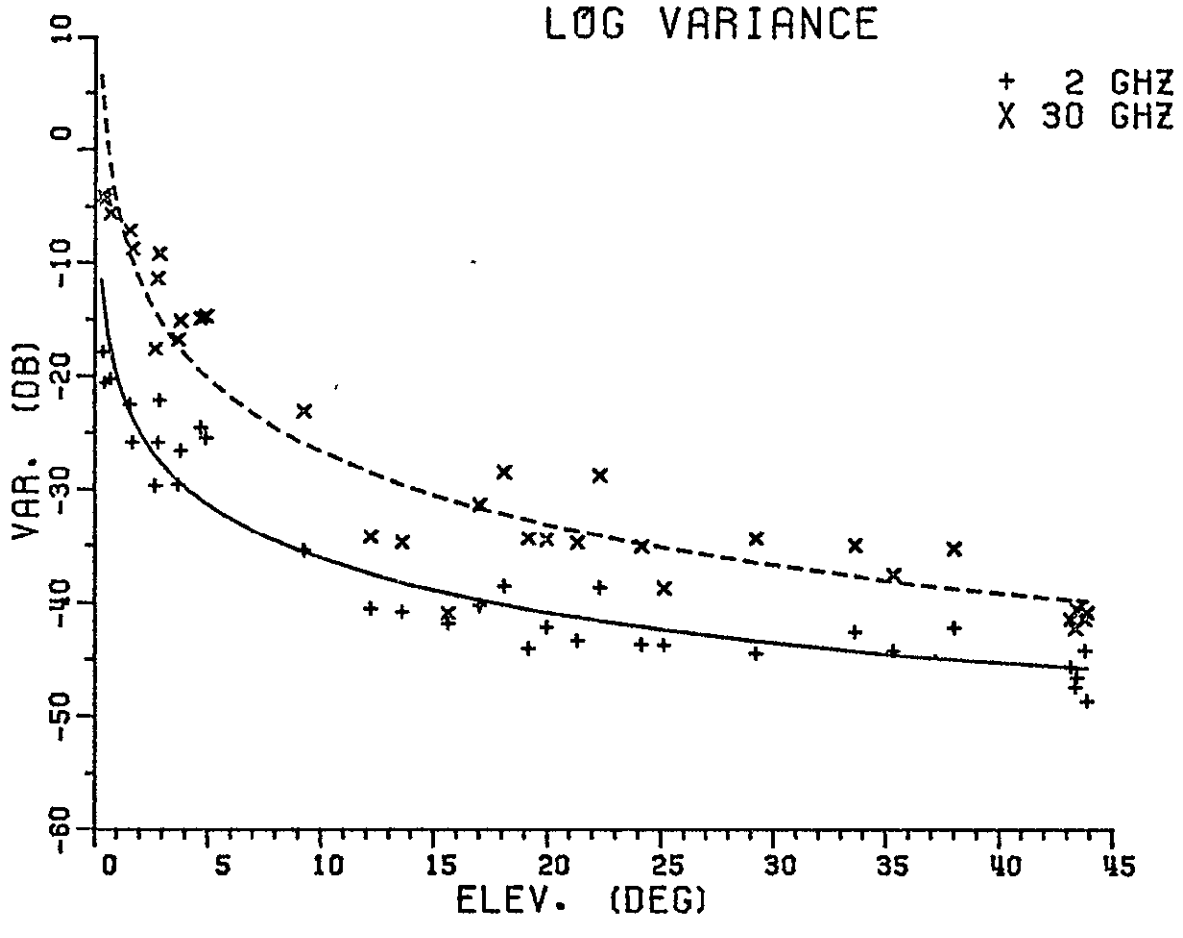

Figure 27. Mean log amplitude variance with elevation angle Cosecant law

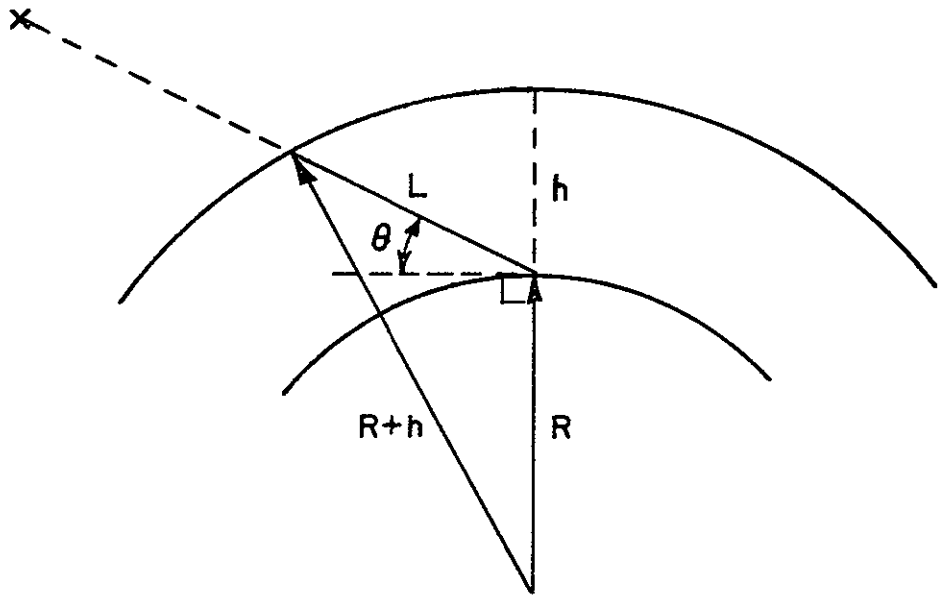

Figure 28. Ray geometry for a $\frac{4}{3}$ spherical earth.

The average amplitude and log amplitude variances at each elevation angle together with the fitted spherical earth law curves are shown in Figures 29 and 30. The amplitude and log amplitude variance curves are almost identical except at the very lowest elevation angles.

The reduction in mean square error using the spherical earth model ranged from 5% to 15%.

The value of the equivalent height parameter h is strongly dependent on low elevation angle data.

Figure 31 also shows the average amplitude variances together with the 30 GHz variance data derived from the earlier set of measurements made in 1975 during the departure of the ATS-6 [17].

The 1975 results agree well with the recent values. The cosecant law relationship found for the earlier data was [17],

$$\sigma^2_{A_{30}}(1975) = 10^{-3.6}\,[\mathrm{CSC}(\theta)]^{1.90}, \qquad (3\text{-}25)$$

which agrees fairly well with that shown in Equation (3-12).

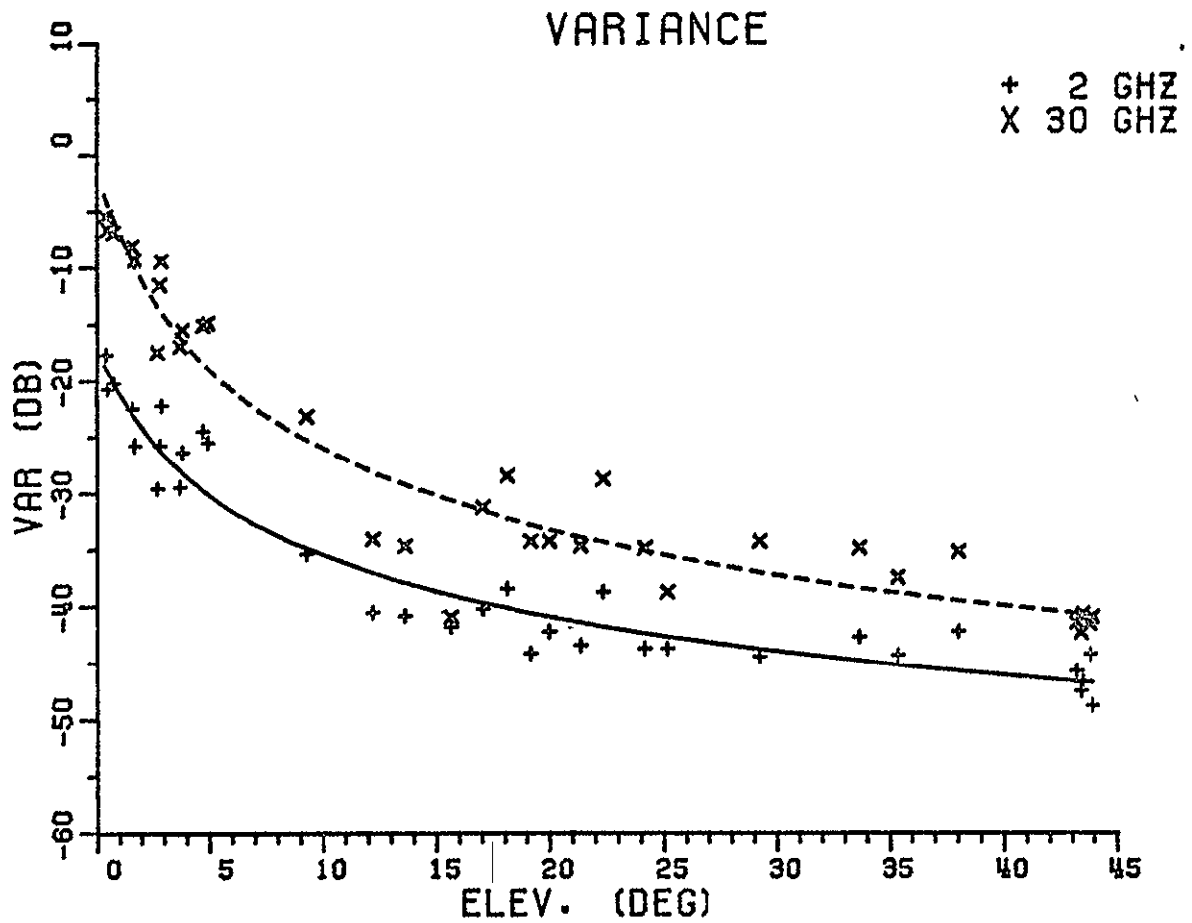

Figure 29. Mean amplitude variance with elevation angle Spherical earth model.

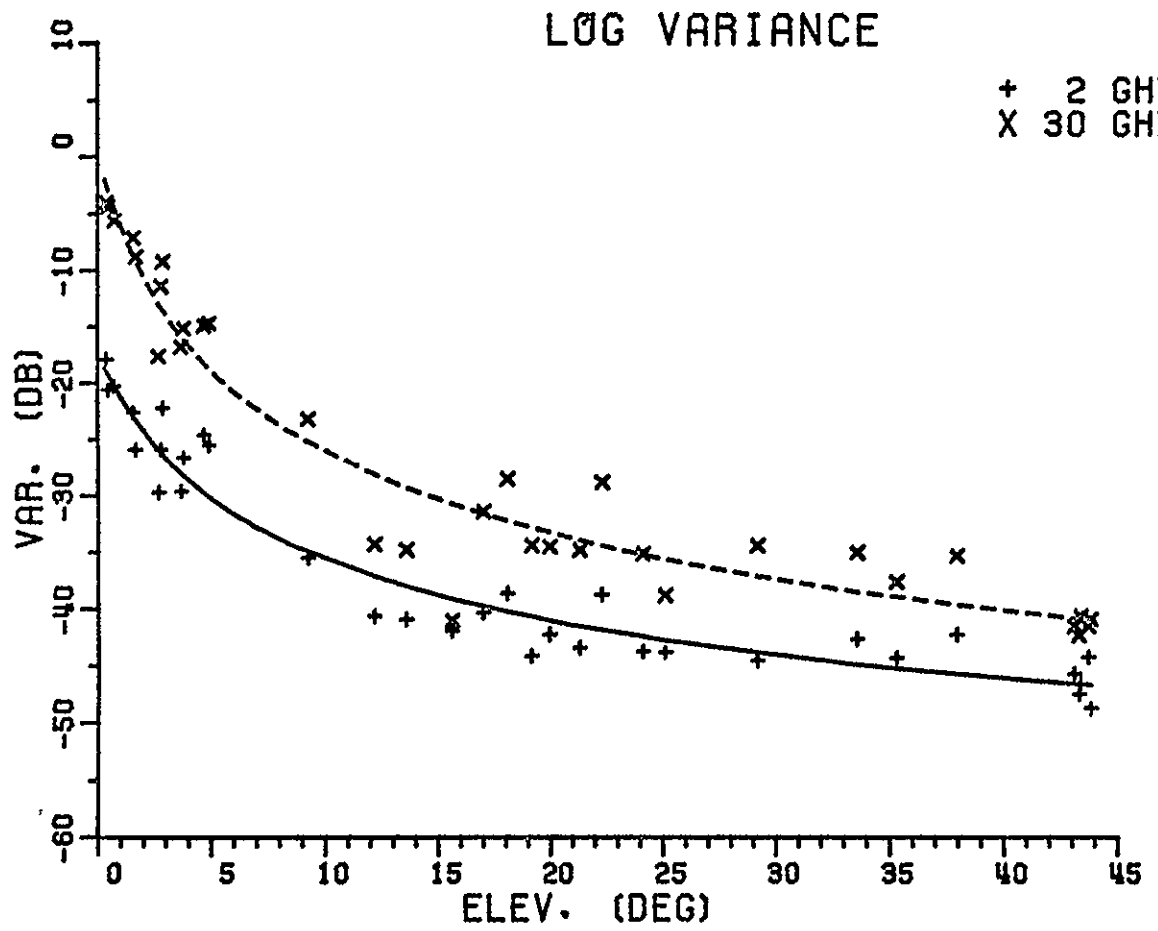

Figure 30. Mean log amplitude variance with elevation angle. Spherical earth model

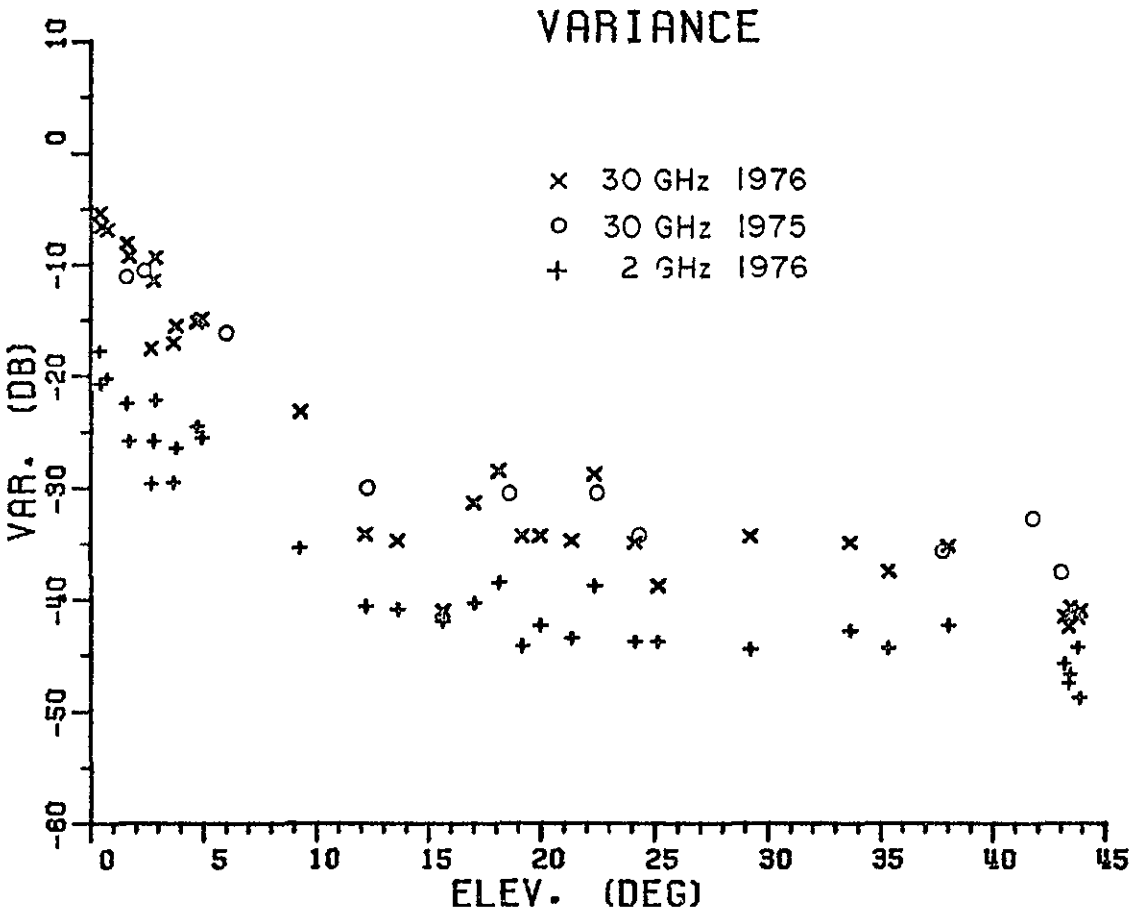

Figure 31. Mean amplitude variance with elevation angle. 1975 and 1976 results

Also at 20 GHz,

$$\sigma^2_{A_{20}}(1975) = 10^{-4.0}\,[\mathrm{CSC}(\theta)]^{1.87} \qquad (3\text{-}26)$$

The fairly large error bounds have been introduced in the present results, not to indicate uncertainty in the data itself, but to take into account the limited duration of the data and the correcting effect that observations over extended periods of time under different weather conditions would have on the results.

The ratio of the amplitude variances of the 30 and 2 GHz received signals ($\sigma^2_{A_{30}}/\sigma^2_{A_2}$) is shown in Figure 32. While it is difficult to draw any reliable conclusions from this, it is observed that the average value over all the elevation angles is 9.2 dB. Similarly a value of 4.4 dB was obtained for $\sigma^2_{A_{30}}/\sigma^2_{A_{20}}$ (i.e., for 30 and 20 GHz) during the departure of ATS-6 [17]. However, in this case there appears to be a tendency for this ratio to decrease as the elevation angle increases.

An example of the behavior of amplitude variance with time is illustrated in Figure 33. The corresponding received signals are shown in Figures 14a and 14b. This figure illustrates more clearly the manner in which the variances are affected by short periods of enhanced scintillations observed in Figure 14 and also shows how closely the 2 and 30 GHz variances track each other at this elevation angle. It suggests that the cross-correlation of the signals be examined. This is done in the next chapter.

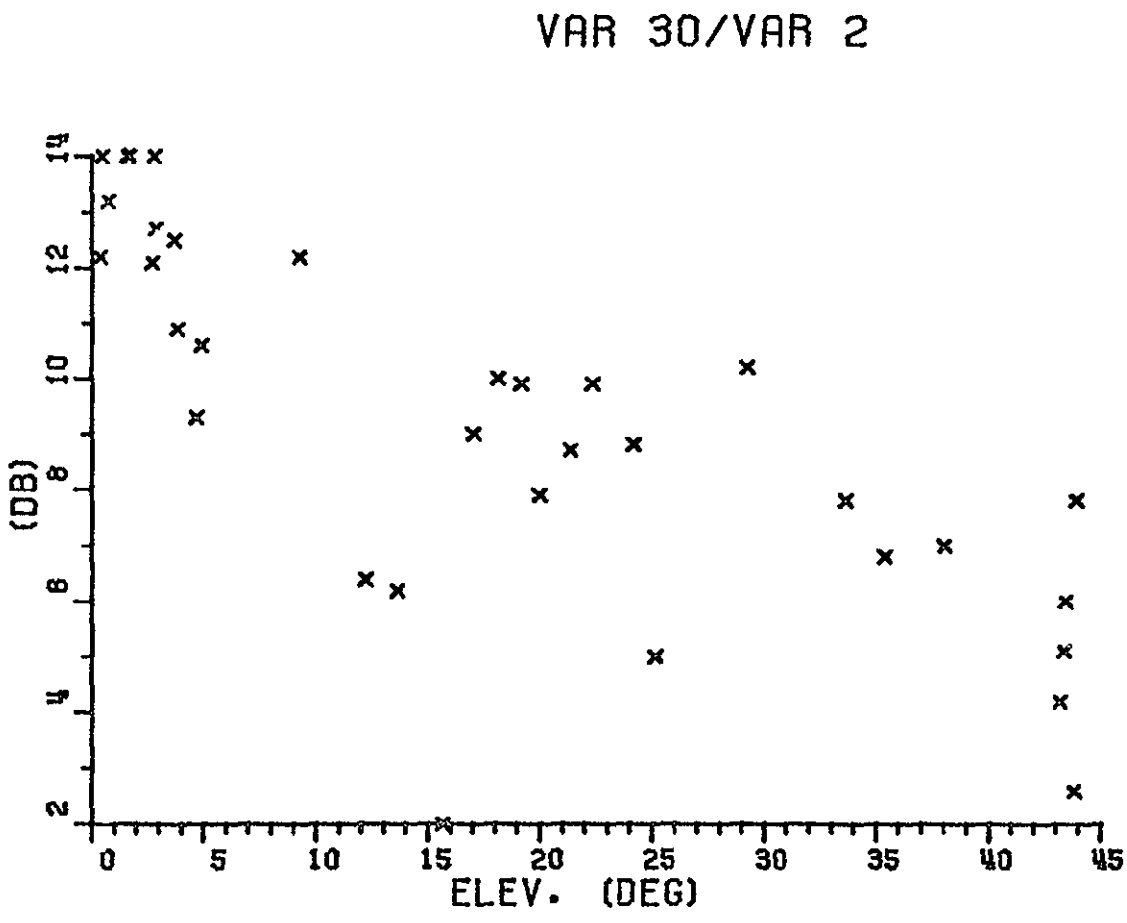

Figure 32 Ratio of variances $\sigma^2_{A_{30}}/\sigma^2_{A_2}$ with elevation angle

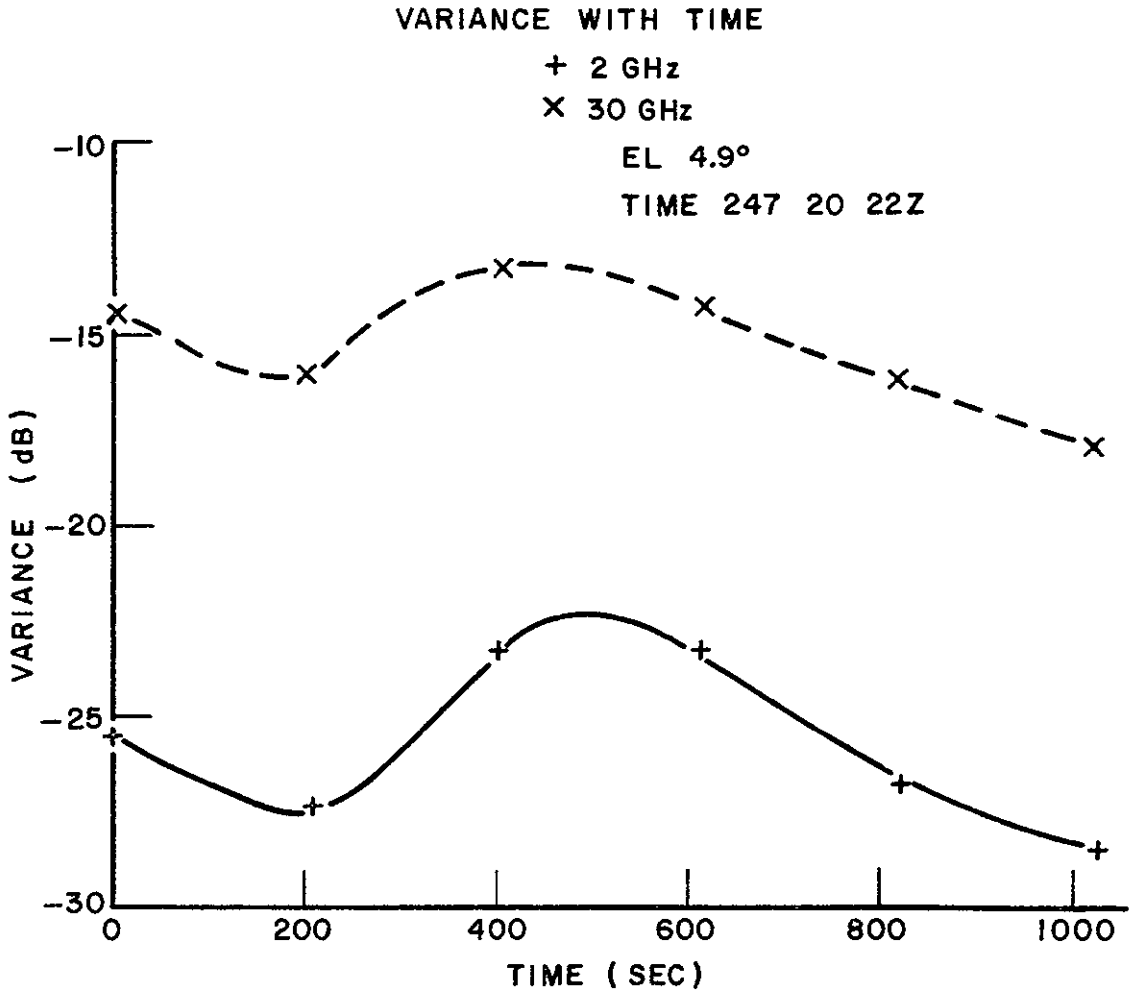

Figure 33. Amplitude variance with time, day 247.

CHAPTER IV
RESULTS· SIGNAL LEVELS, CORRELATION, SPECTRA AND FADE DISTRIBUTIONS

In this chapter, the average received signal levels are shown. The correlation between the signals is discussed in detail. The correlation results are compared with those predicted by the Lee and Harp model and good agreement is found. Some representative samples of correlation as a function of time lag are shown. Lags are in the range of 0 - 10 seconds with most of the values being around 0 - 5 seconds.

The power spectra are considered next. A characteristic decay is found in the 0.1 to 1 Hz range. This decay follows the $f^{-8/3}$ law.

Fade distributions are also shown. These are, in general, Gaussian except for anomalous cases which appear to point to some other mechanism. Standard deviations calculated from the Gaussian models agree reasonably well with those calculated directly in Chapter III.

A. Received Signal Levels

The mean relative power in the signal is defined as

$$\text{Mean Power} = \frac{1}{T}\int A^2(t)\,dt \qquad (4\text{-}1a)$$

$$= 10\log_{10}\left[\frac{1}{N}\sum_{i=1}^{N} A_i^{\,2}\right] \text{ dB} \qquad (4\text{-}1b)$$

with T = 205 seconds as before. The mean power averaged over each elevation angle is shown in Figure 34. As expected, the mean log amplitude (Figure 35) and mean power are virtually identical. The sharp reduction in signal level at an elevation of 9.3° is due to the fact that the spacecraft antennas were directed toward Texas for another experiment on that day.

A substantial reduction in the received power level below that predicted by simple atmospheric path loss calculations [24] at the lower elevation angles is also noted; this behavior has been observed earlier by McCormick and Maynard [25].

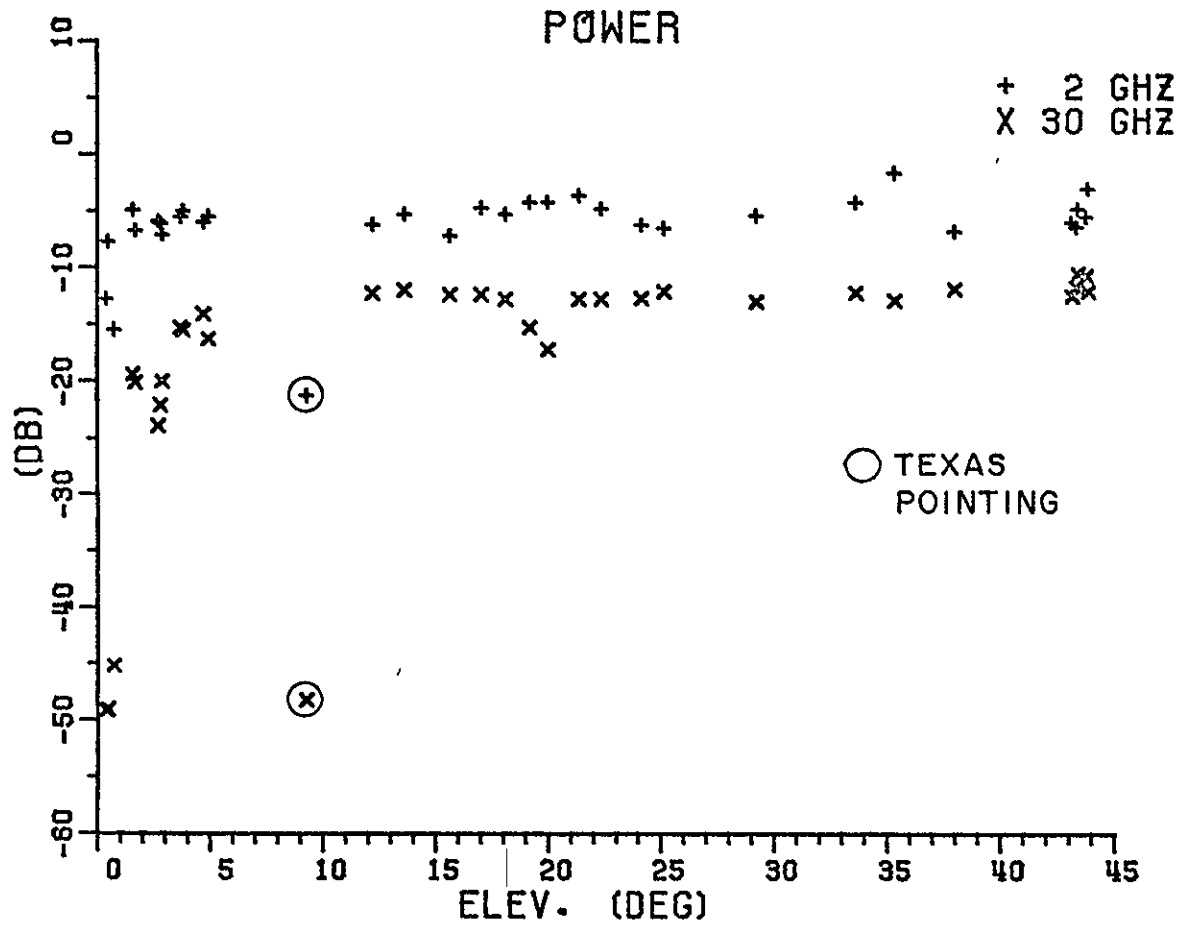

Figure 34. Mean relative power in the signal, with elevation angle.

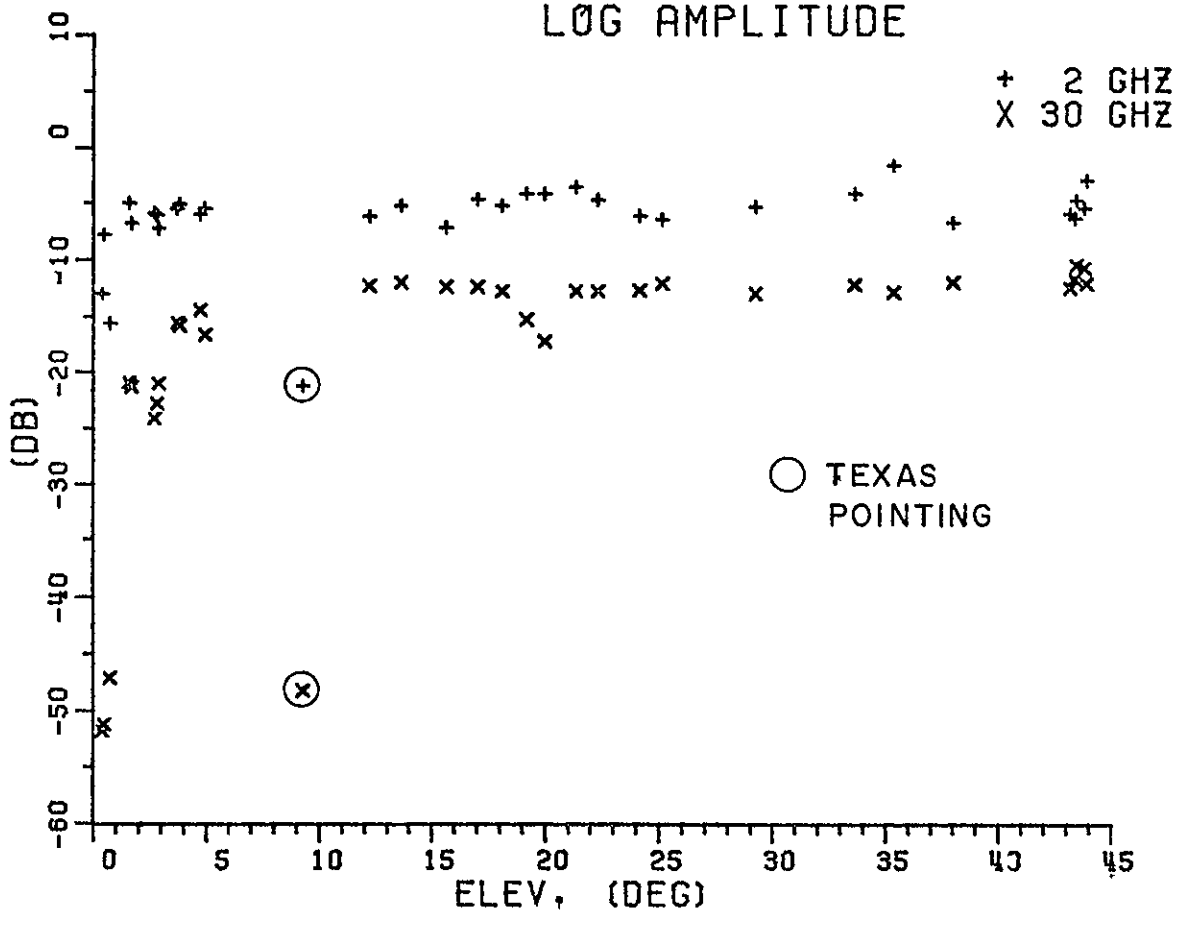

Figure 35. Mean relative log amplitude of the signal, with elevation angle.

The more pronounced variations in the 2 GHz mean power at the higher elevation angles is believed to be due to equipment problems.

B. Correlation (Covariance)

The terms Correlation and Covariance are used interchangeably in this report and both denote the correlation functions defined for lag, τ, by

$$\rho_{\psi_{12}}(\tau) = \frac{1}{T} \frac{\int (\psi_1(t)-\bar{\psi}_1)\ (\psi_2(t+\tau)-\bar{\psi}_2)\ dt}{\left[\frac{1}{T}\int (\psi_1(t)-\bar{\psi})^2 dt\right]^{1/2} \left[\frac{1}{T}\int (\psi_2(t)-\bar{\psi}_2)^2 dt\right]^{1/2}} \tag{4-3}$$

where ψ denotes either the log amplitude, χ, or the amplitude, A, and T is 205 seconds. Therefore,

$$\rho_{A_{2,30}} = \frac{1}{N\bar{A}_2\bar{A}_{30}} \frac{\sum_{i=1}^{N} (A_{2_i} - \bar{A}_2)(A_{30_{i+J}} - \bar{A}_{30})}{\sigma_{A_2}\sigma_{A_{30}}} \tag{4-4}$$

$$\rho_{\chi_{2,30}} = \frac{1}{K_1^2 N} \frac{\sum_{i=1}^{N} (\chi_{2_i} - \bar{\chi}_2)(\chi_{i+J_{30}} - \bar{\chi}_{30})}{\sigma_{\chi_2}\sigma_{\chi_{30}}} \tag{4-5}$$

$$\tau = J\frac{T}{N} \quad .$$

These correlation functions are equal for small scintillations.

The log amplitude and amplitude peak correlation coefficients are averaged at each elevation angle and plotted in Figure 36. Although some divergence is found at the lowest elevation angles, they are found to agree well at higher elevation angles.

It should be noted that the effective separation between the antennas varied from 10.2 meters at 0.4° to 7.3 m at 43.8°. This separation tends to reduce the observed correlation values.

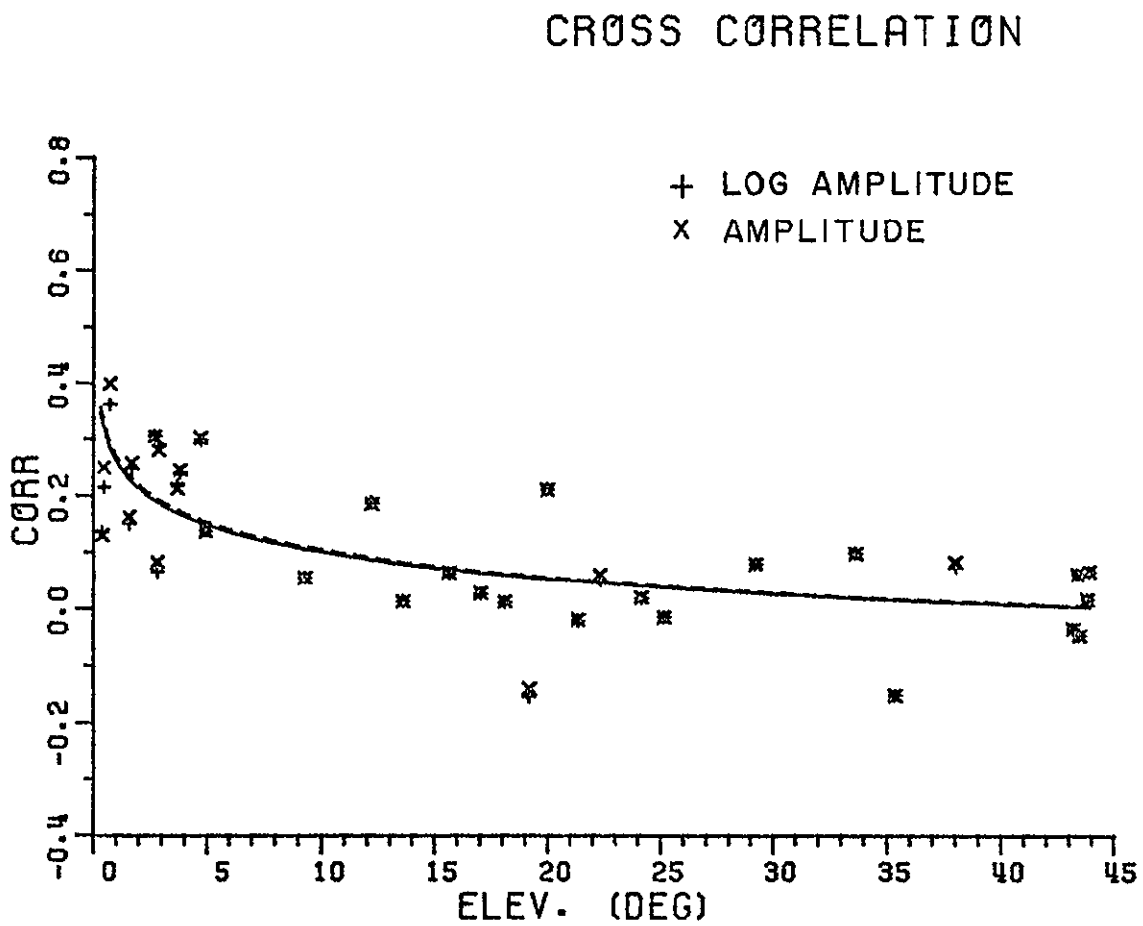

Figure 36 Cross correlation with elevation angle

Although there appears to be no theoretical justification, the curves are again suggestive of a cosecant law. A minimum-mean-square error curve fit was made to test this and the results were:

Amplitude Correlation

$$\rho_{A_{2,30}} = 0.59\ [CSC(\theta)]^{1.62 \pm .3} \tag{4-6}$$

Log Amplitude Correlation

$$\rho_{\ell_{2,30}} = 0.59\ [CSC(\theta)]^{1.66 \pm .2} \tag{4-7}$$

These are also plotted in Figure 42.

It is interesting to note that these exponents also lie in the range of the values calculated earlier for the CSC(θ) exponent in the case of variance.

Next, the Amplitude Correlation Coefficient obtained was compared with the theoretical value predicted by Lee and Harp [26] for this frequency ratio of 14.46. The covariance between the 2.075 and 30 GHz signals is shown in Figure 37 together with the theoretical curve of Lee and Harp. Although the spread of the covariance is large, the average over the entire data base agrees well with the theoretical prediction. Also included are the results for the 20 and 30 GHz data obtained earlier [17].

As the cosecant law suggested by Figure 36 appeared to be a good approximation, the covariance was also plotted against CSC(θ). However Figures 36 and 37 show a wide range of values for the correlation coefficient, but do not show its behavior over ranges of elevation angles of interest. Therefore, the correlation coefficient was next averaged over selected elevation angles and shown in Figure 38, together with the Lee and Harp value. The agreement is now seen to be very good for elevation angles up to about 5°, i.e., in the region where the signals are being affected the most. Somewhat surprisingly, the correlation is seen to fall off to nearly zero at the higher elevation angles, i.e., the region of weaker turbulence effects.

It should be noted that the path length was constantly changing during the experiment, while the Lee and Harp curve was calculated for a fixed path length. This and the change in the effective separation between the antennas should be considered in evaluating the agreement with the theoretical value.

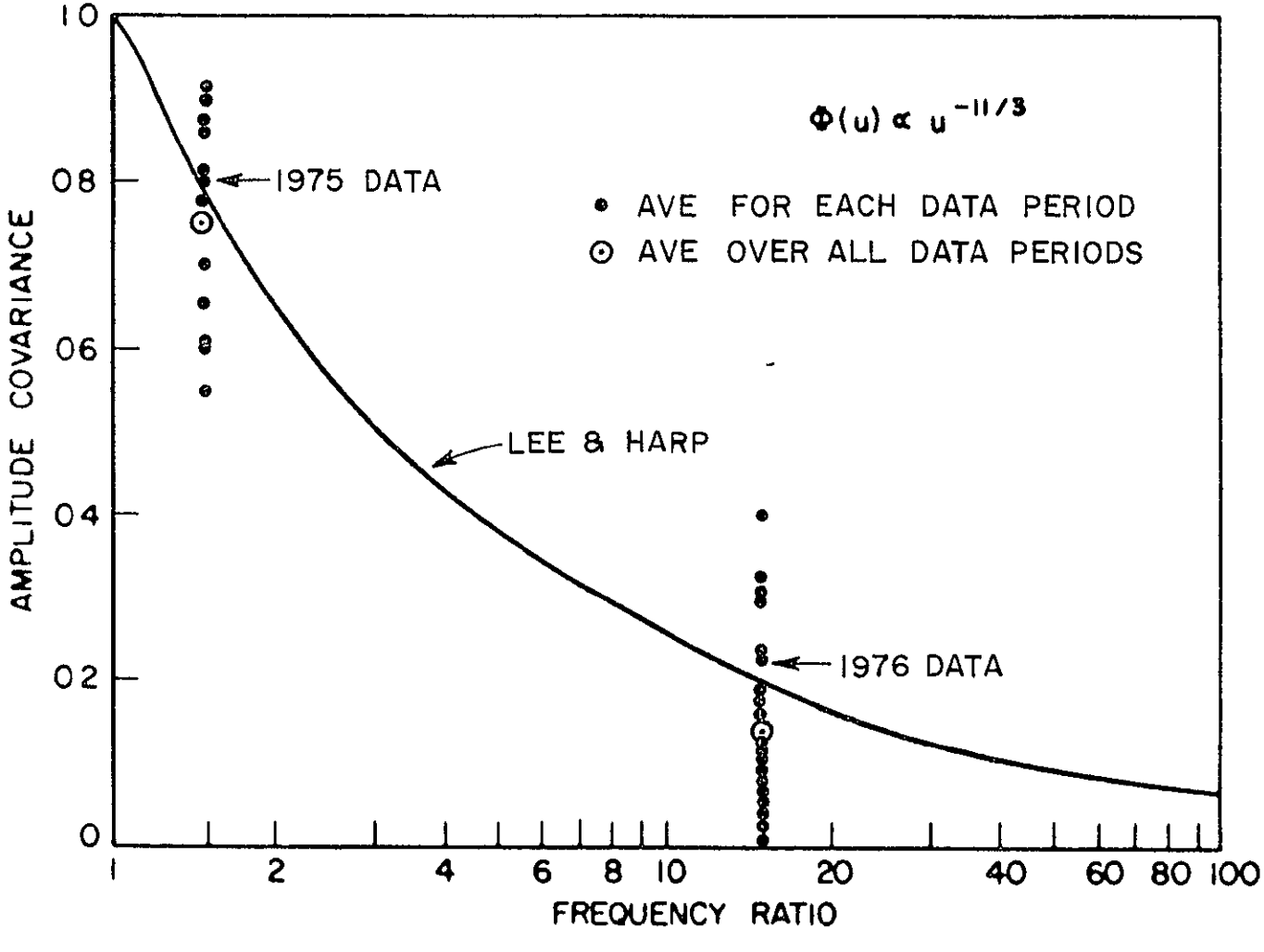

Figure 37 Cross correlation with frequency ratio

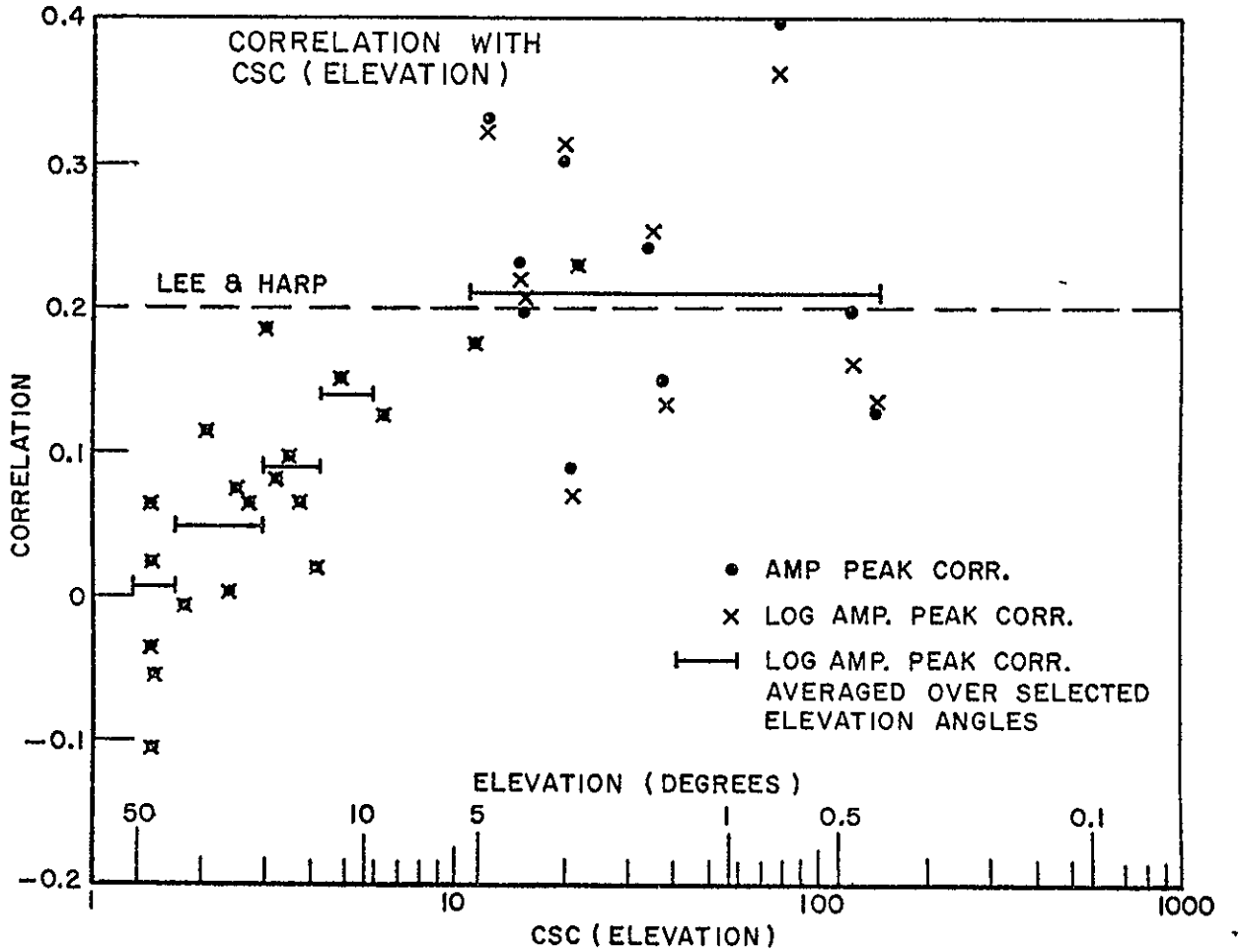

Figure 38. Cross correlation averaged over selected elevation angles, with cosecant (elevation).

Some examples of cross-correlation and auto-correlation functions of the received signals are presented in Figures 39 through 46. It was observed that over a period of a record (i.e., 205 seconds), significant shifts of the mean level occurred. This would tend to make the process non-stationary. Consequently, a correction was applied to the record being analyzed by assuming that the mean-shift was linear with time over the interval of the record. This correction narrows the peak of the correlation functions, i.e., reduces the interval of high correlation values, which would otherwise be obtained.

The lags associated with the maximum values of the cross correlation were in the range of 0 - 10 seconds with most of the values in the region of 0 - 5 seconds. It also appeared that significant correlation was lost for lags exceeding about 15 seconds.

The effects of various wind fields on the correlation function have been studied in [26]. The lag of the peak correlation is shown to depend on the wind velocity across the propagation path and the shape of the curve on the wind distribution. The double hump in Figure 41, for example, may be attributed to non-uniform wind fields.

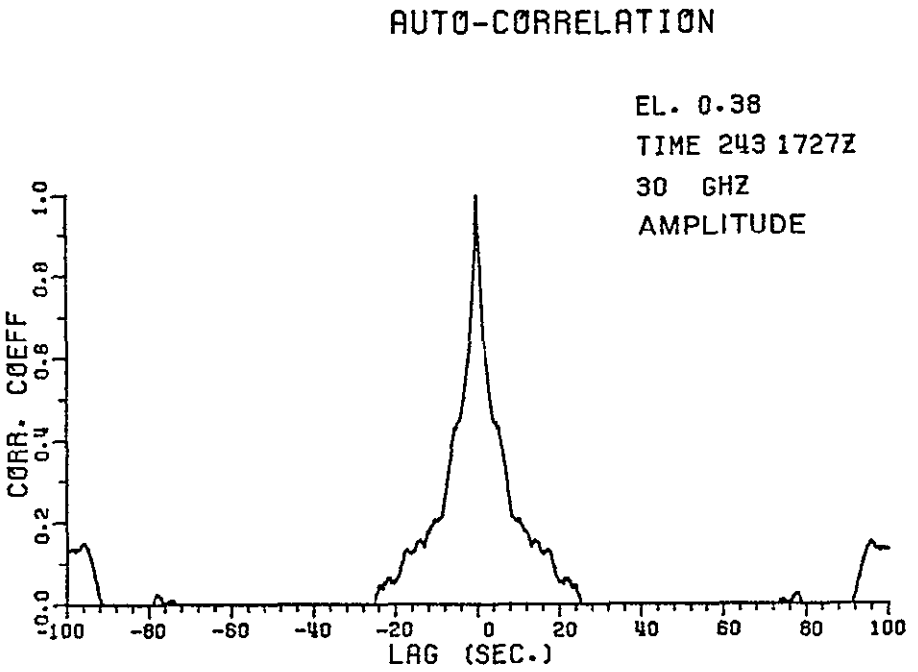

Figure 39. 30 GHz amplitude autocorrelation function at elevation angle 0.38°

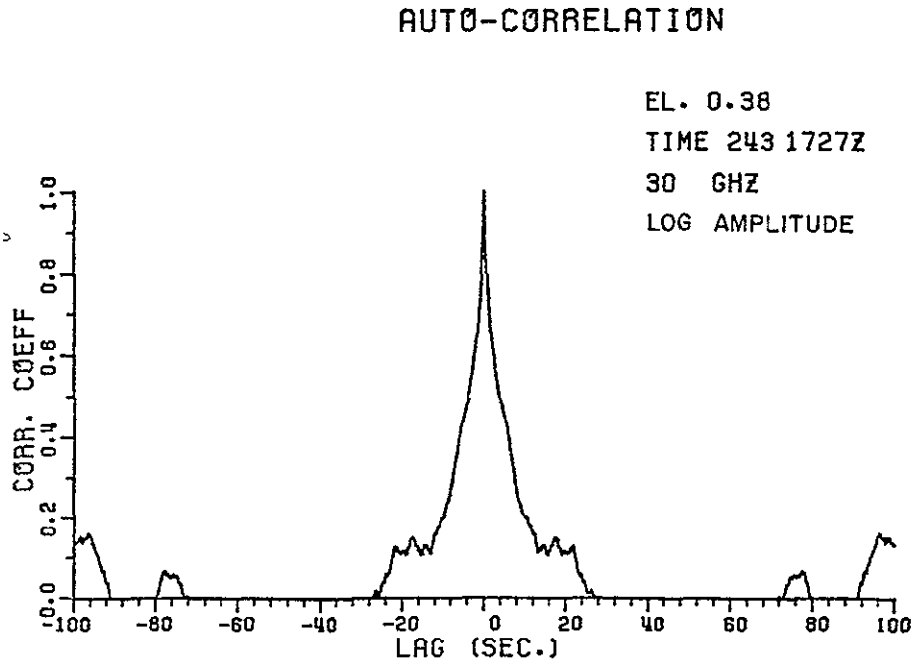

Figure 40. 30 GHz log amplitude autocorrelation function at 0 38°.

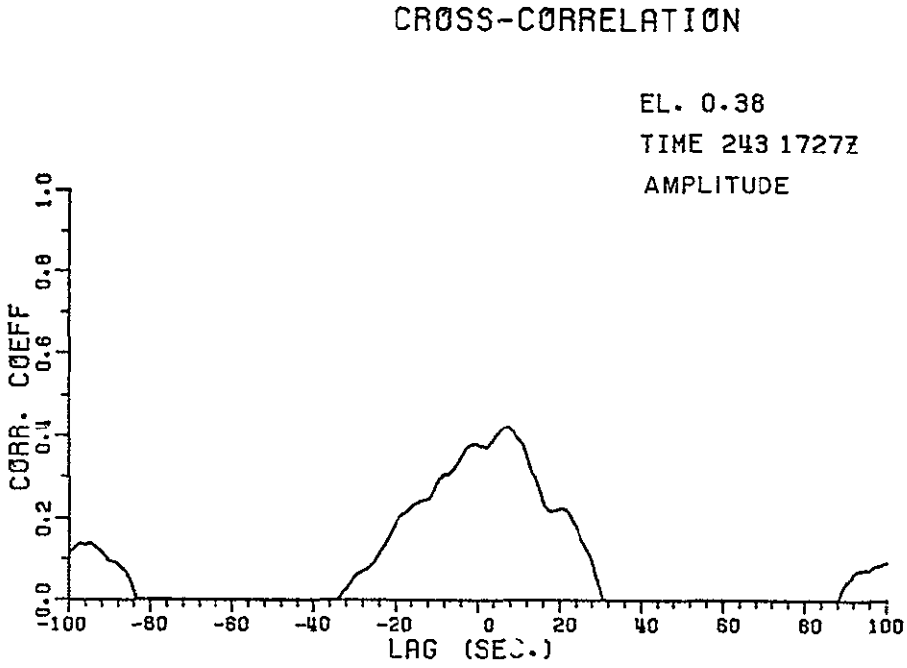

Figure 41 Amplitude cross correlation function at 0.38°

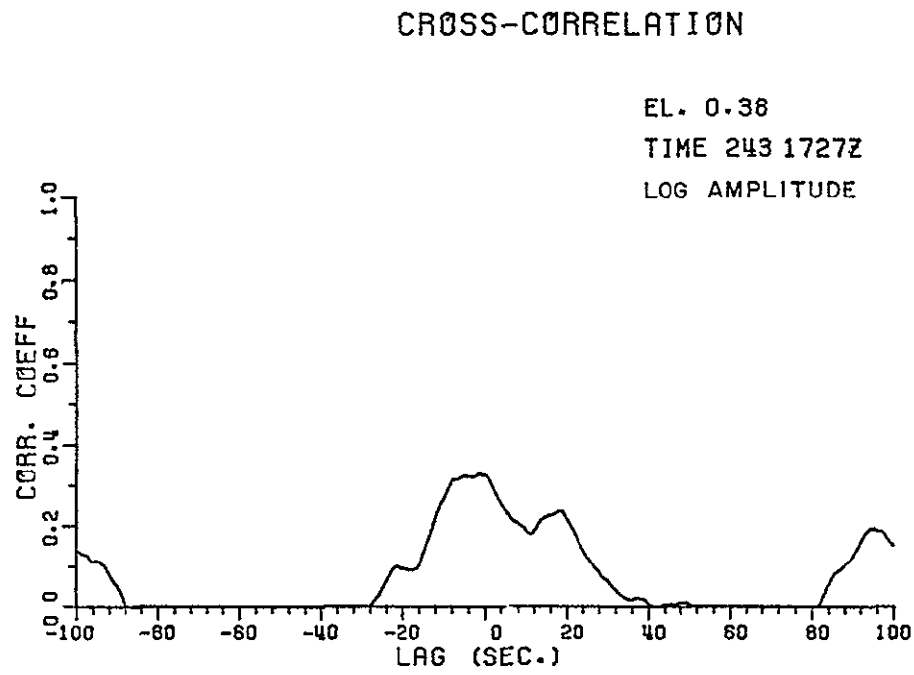

Figure 42 Log amplitude cross correlation function at 0 38°.

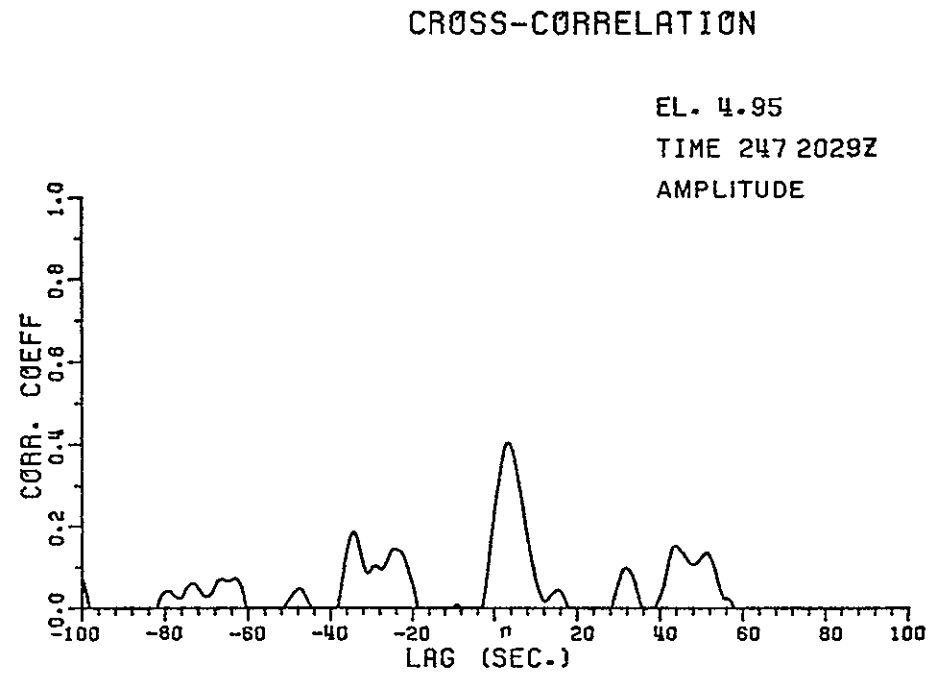

Figure 43. Amplitude cross correlation function at 4.95°

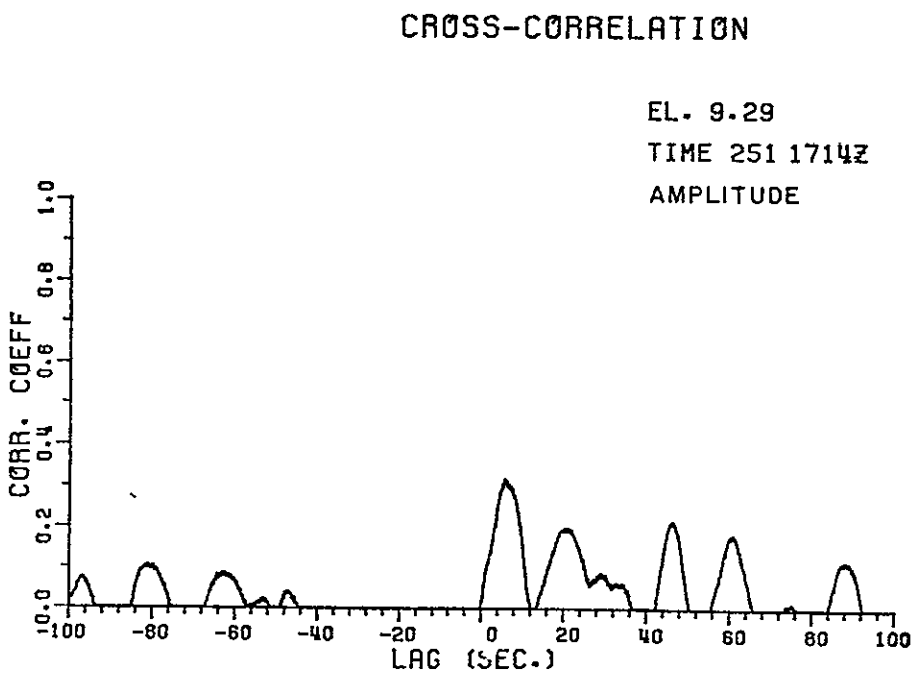

Figure 44. Amplitude cross correlation function at 9 29°.

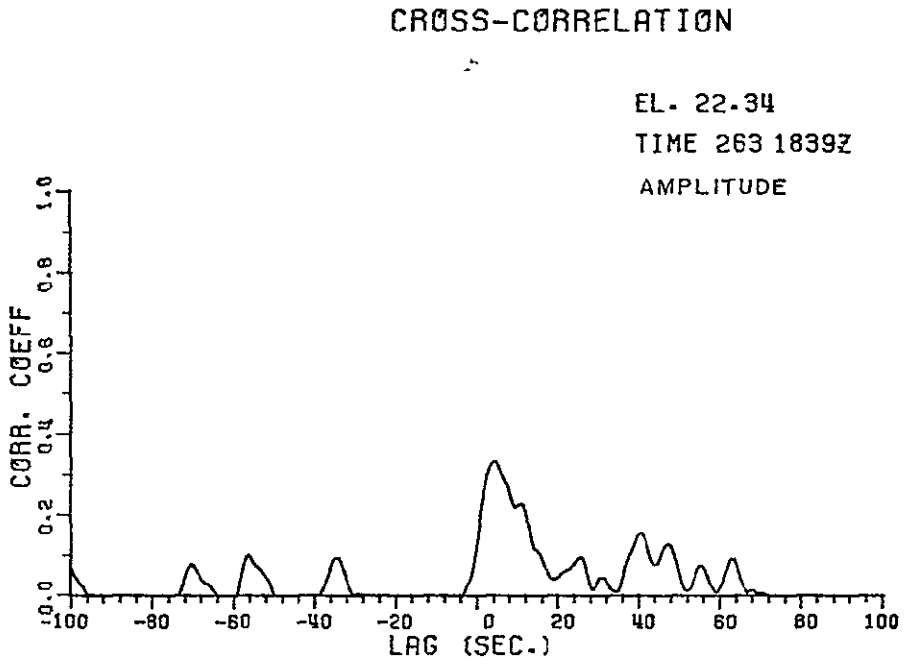

Figure 45. Amplitude cross correlation function at 22.34°

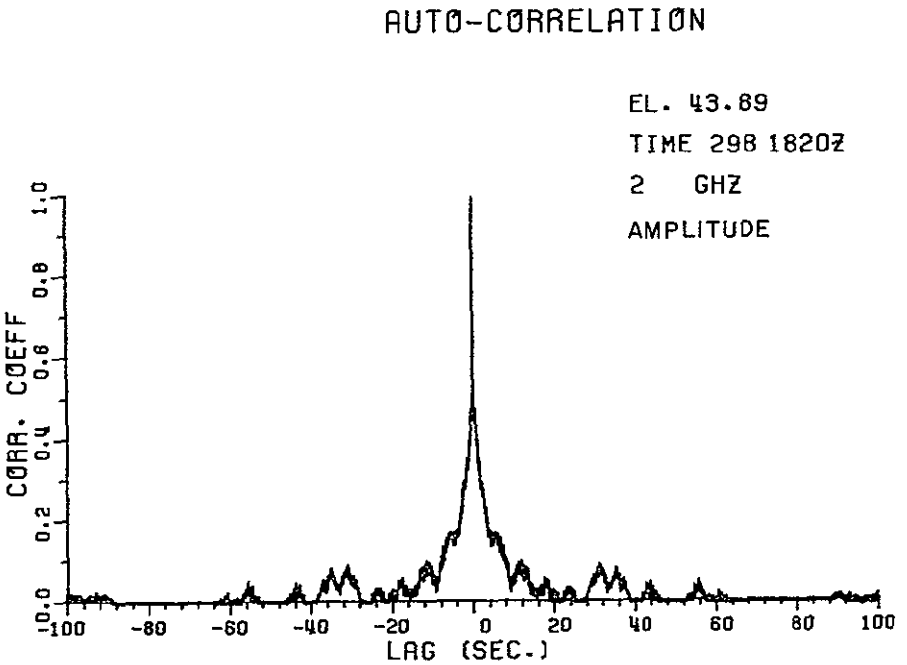

Figure 46 2 GHz amplitude auto correlation function at 43.89°

C. Spectra

Sample spectra of the received signal are shown in Figures 47 through 53. Corresponding records of received signal will be found in Figures 7 through 28. These spectra all show a characteristic decay with frequency in the range from approximately 0.1 Hz to 1.0 Hz. The spectra tend to be relatively flat outside that range.

The slope of the spectra in the decaying region was measured manually for several samples. The results of 12 samples each at 2 GHz and 30 GHz are shown in Table 3.

Table 3

SLOPE OF SIGNAL SPECTRA

	2 GHz dB/decade	30 GHz dB/decade
MAXIMUM	30.6	31.2
MINIMUM	23.5	20.0
MEAN	25.5	26.8

These results agree closely with a power roll-off relationship of the form $f^{-8/3}$, or 26.7 dB/decade. This result also agrees with the assumption that a tropospheric turbulence mechanism is producing the observed scintillations [27].

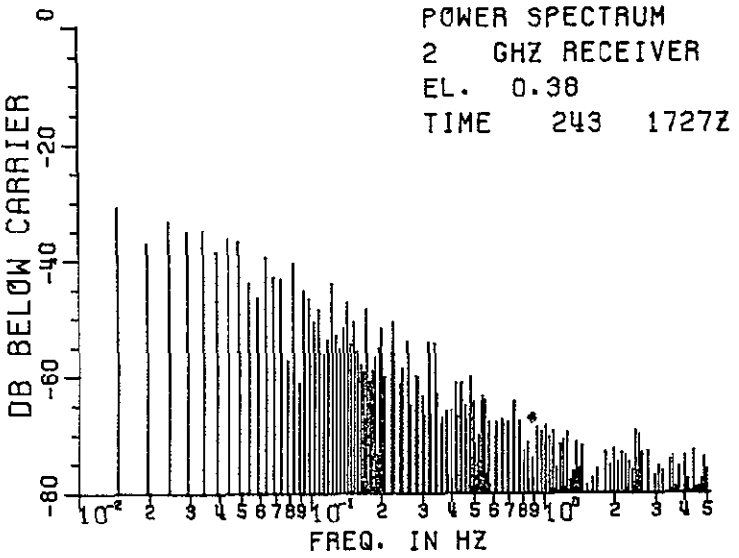

(a)

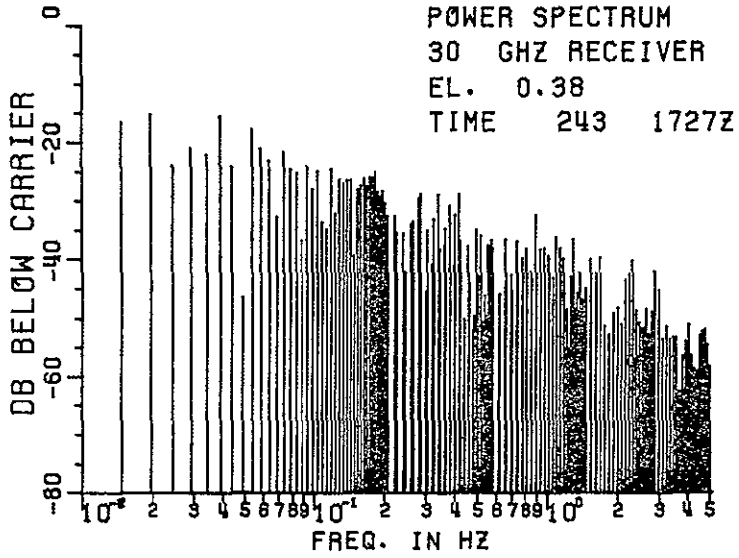

(b)

Figure 47 Power spectra at 0 38°

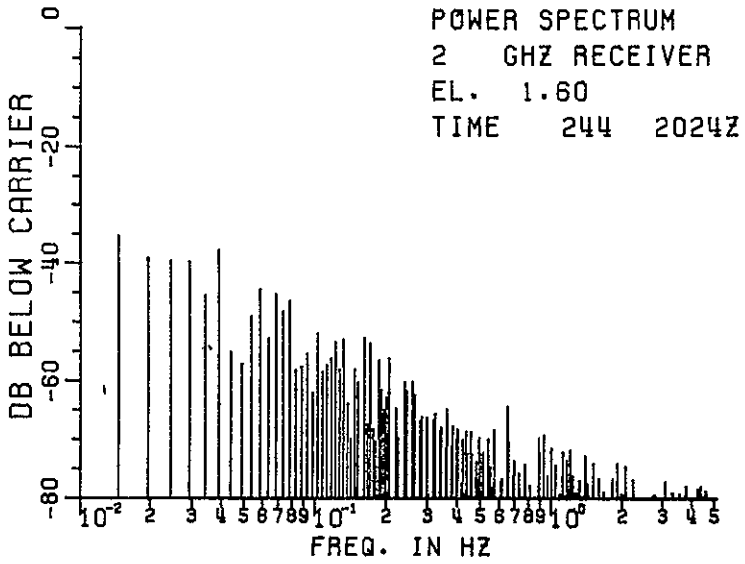

(a)

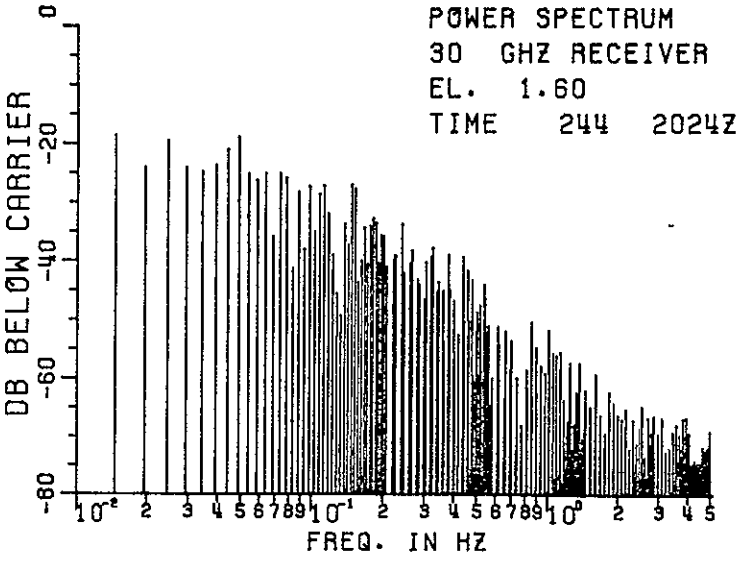

(b)

Figure 48. Power spectra at 1.60°.

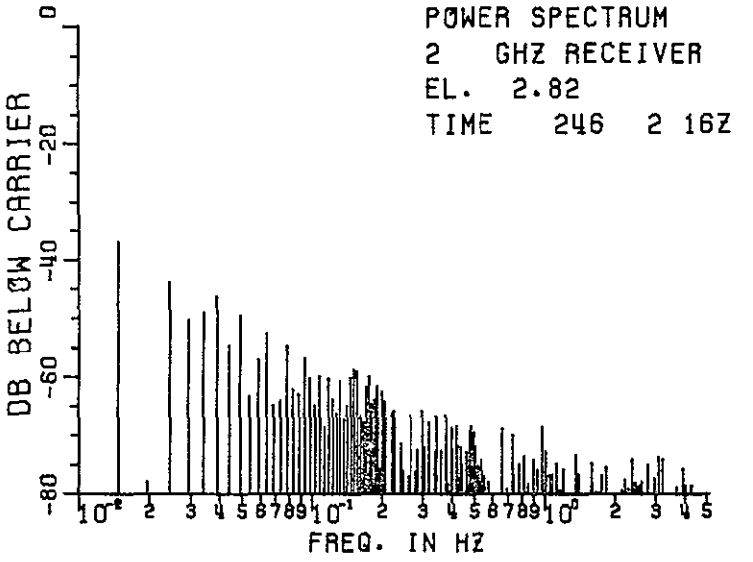

(a)

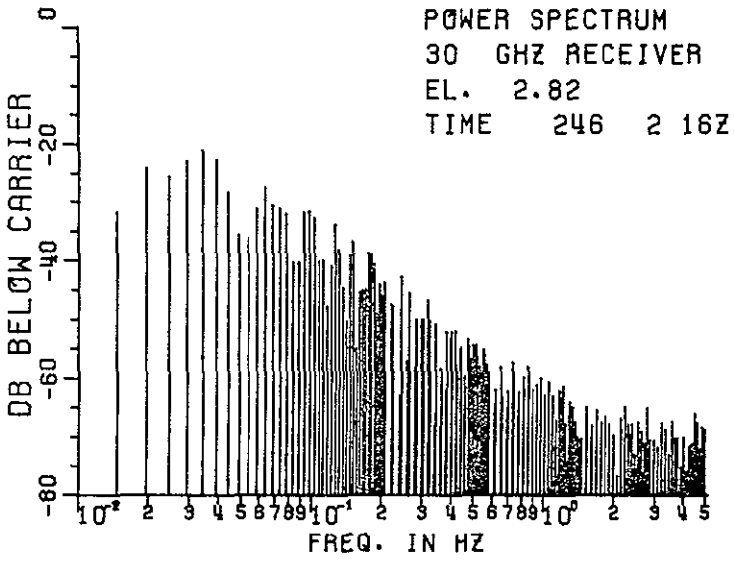

(b)

Figure 49. Power spectra at 2.82°.

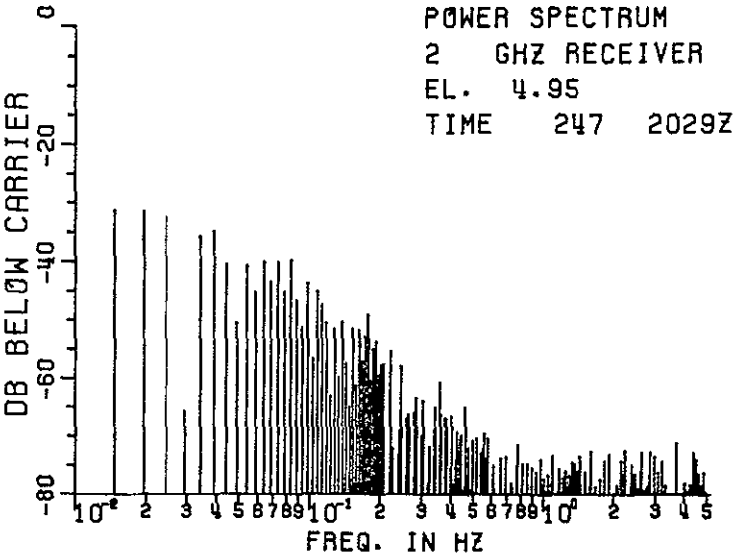

(a)

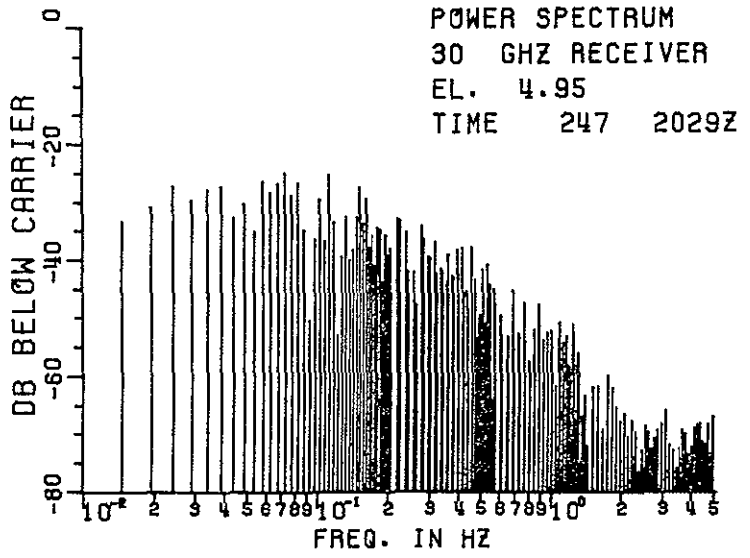

(b)

Figure 50. Power spectra at 4.95°

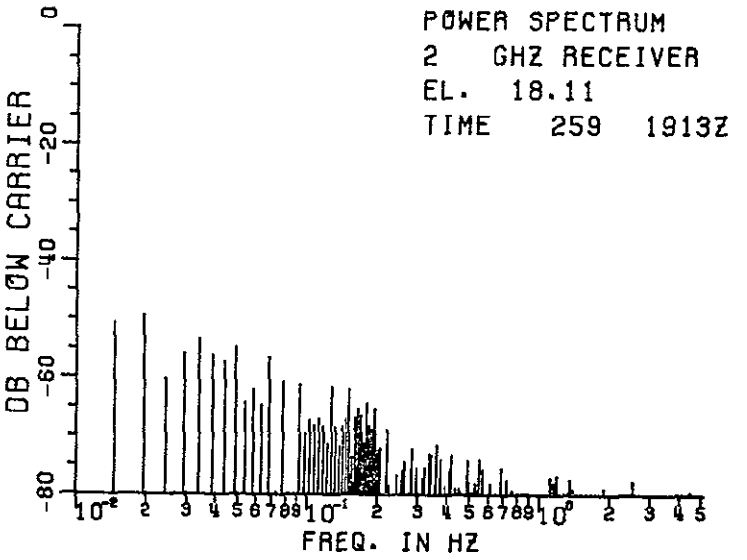

(a)

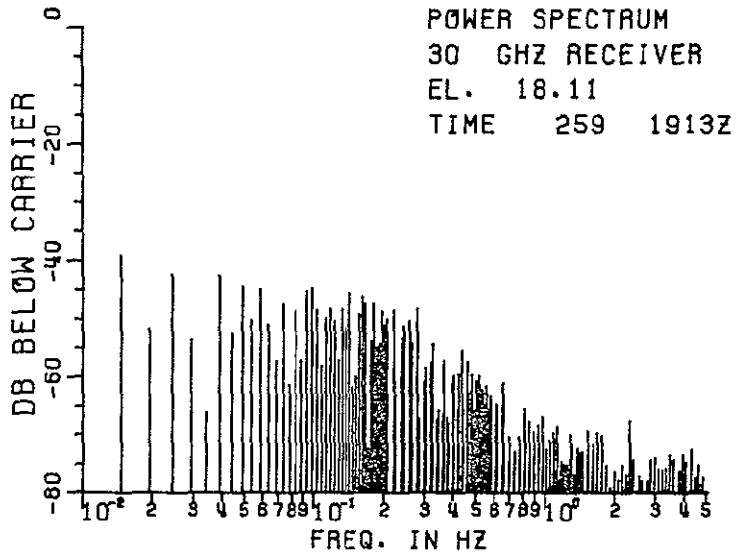

(b)

Figure 51. Power spectra at 18.11°.

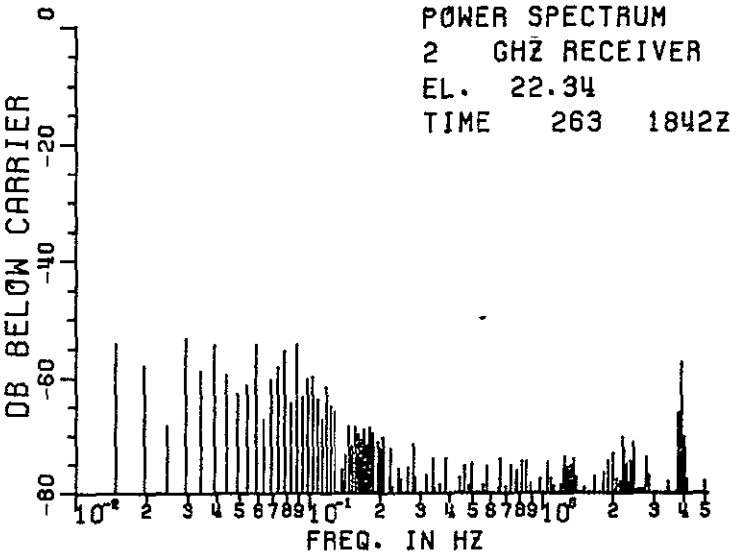

(a)

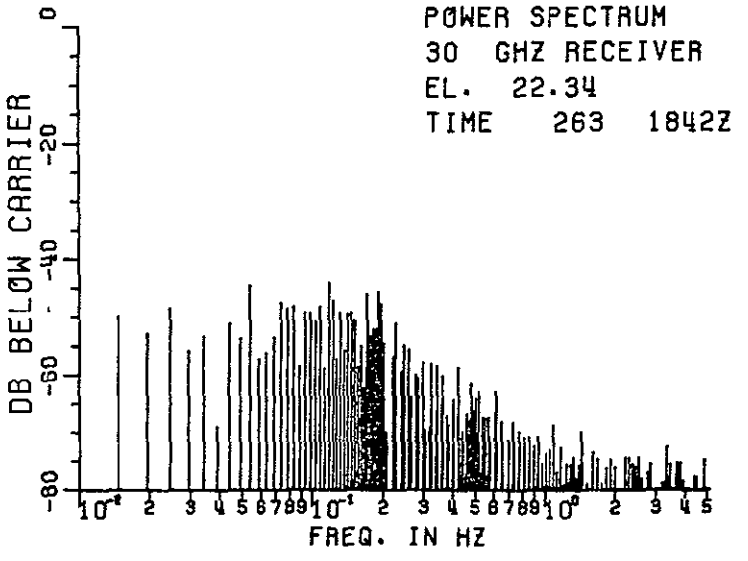

(b)

Figure 52. Power spectra at 22.34°.

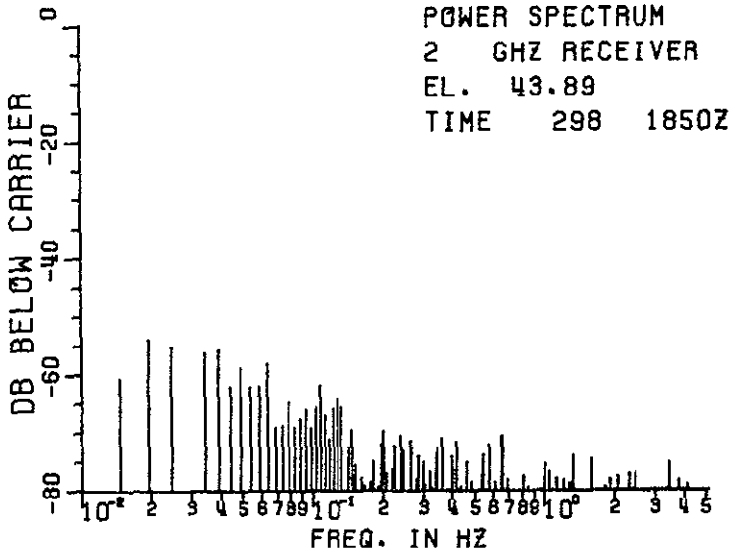

Figure 53. Power spectrum at 43.89°.

D. Fade Distributions

Fade distributions were also studied at several elevation angles, averaging about 30,000 samples, i.e., 50 minutes each. Figures 54 and 55 show the percentage of time a given fade depth was exceeded, plotted on a log-normal scale.

The curves appear to fit fairly well within each other with increasing elevation. However exceptions are clearly seen at 0.38° and 1.60° for both 2 and 30 GHz and at 4.95° for the 2 GHz signal. The reason for the behavior at 4.95° is not clear at present. It should be noted that the 30 GHz fade distribution at this elevation angle does not behave in the same way.

The distributions at 2.82° are taken to be a representative sample for the higher elevation angle cases and show good fit to straight line approximations, indicating that they are Gaussian. Even the anomalous distributions show a Gaussian nature over a large portion of their ranges.

The fade distributions could, in fact, be a combination of more than one type of statistic. Deviations from the Gaussian curve are prominent for large scintillations. Furthermore, since the sampling rate is high (10/sec.), it is possible that the effects of rapid short term scintillations, which are believed to be Rayleigh distributed, are also being displayed in these distribution curves [28].

Assuming that the dominant long-term statistics at the higher elevation angles are Gaussian, a check was performed at 2.82° as follows. Let the un-normalized variance be s^2. For a log-normal distribution, the interval between the 50 and 99.9 percentile values of the cumulative distribution function, - i.e., 50 and 0.1 percentile values of the fade distribution function - is 3.1 s [29]. For 30 GHz, from Figure 55

$$3.1\, s_{30} = 8.6$$

$$s_{30} = 2.7.$$

Now, from the definition of σ^2_{ℓ} (Equation (3-6)) we can write that

$$\sigma^2_{\ell_{dB}} = 10 \log_{10} \frac{s^2}{K_1^2}$$

$$s = K_1 . 10^{\frac{\sigma^2_{\ell_{dB}}}{20}}$$

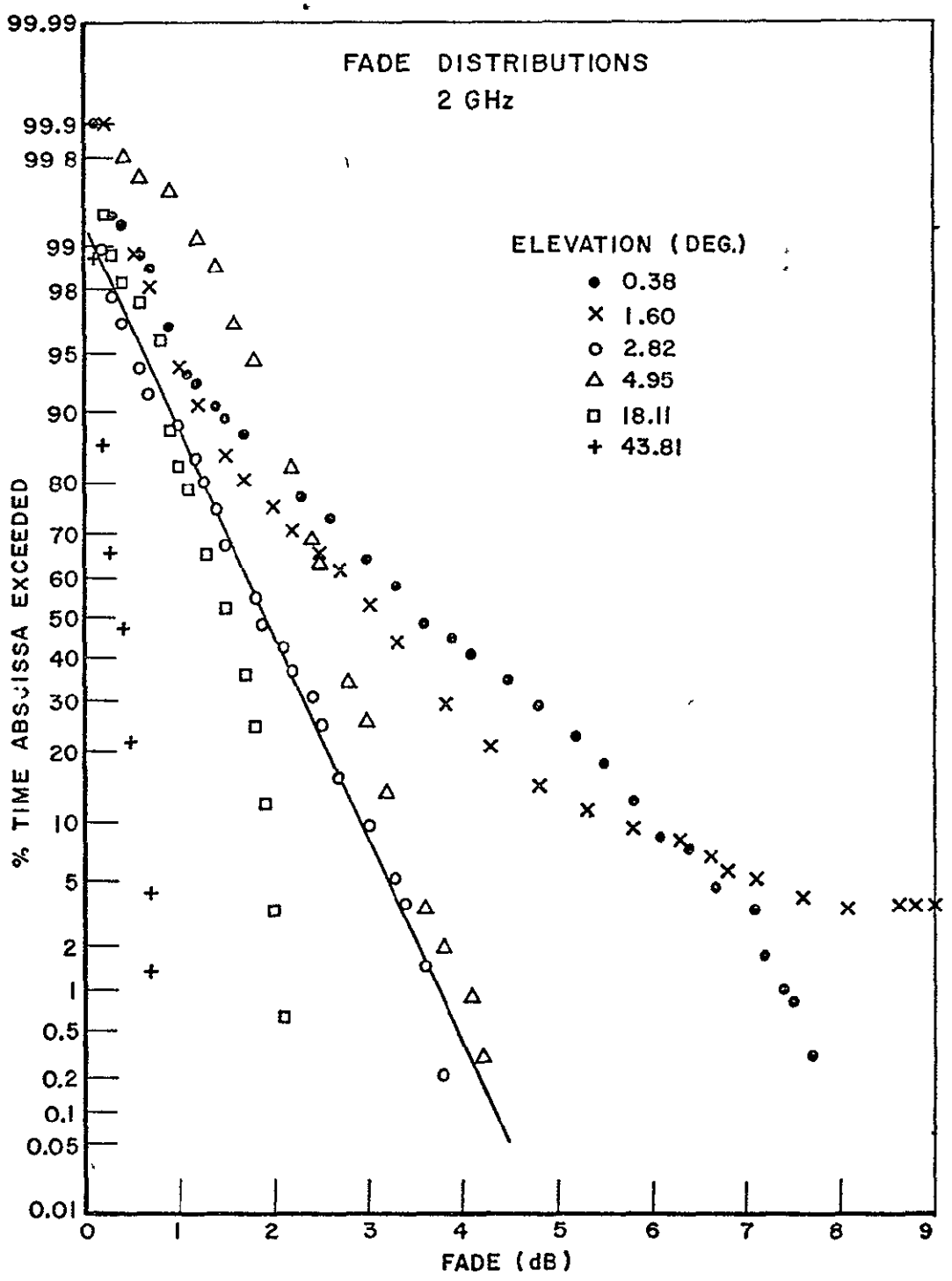

Figure 54. Fade distributions at 2 GHz

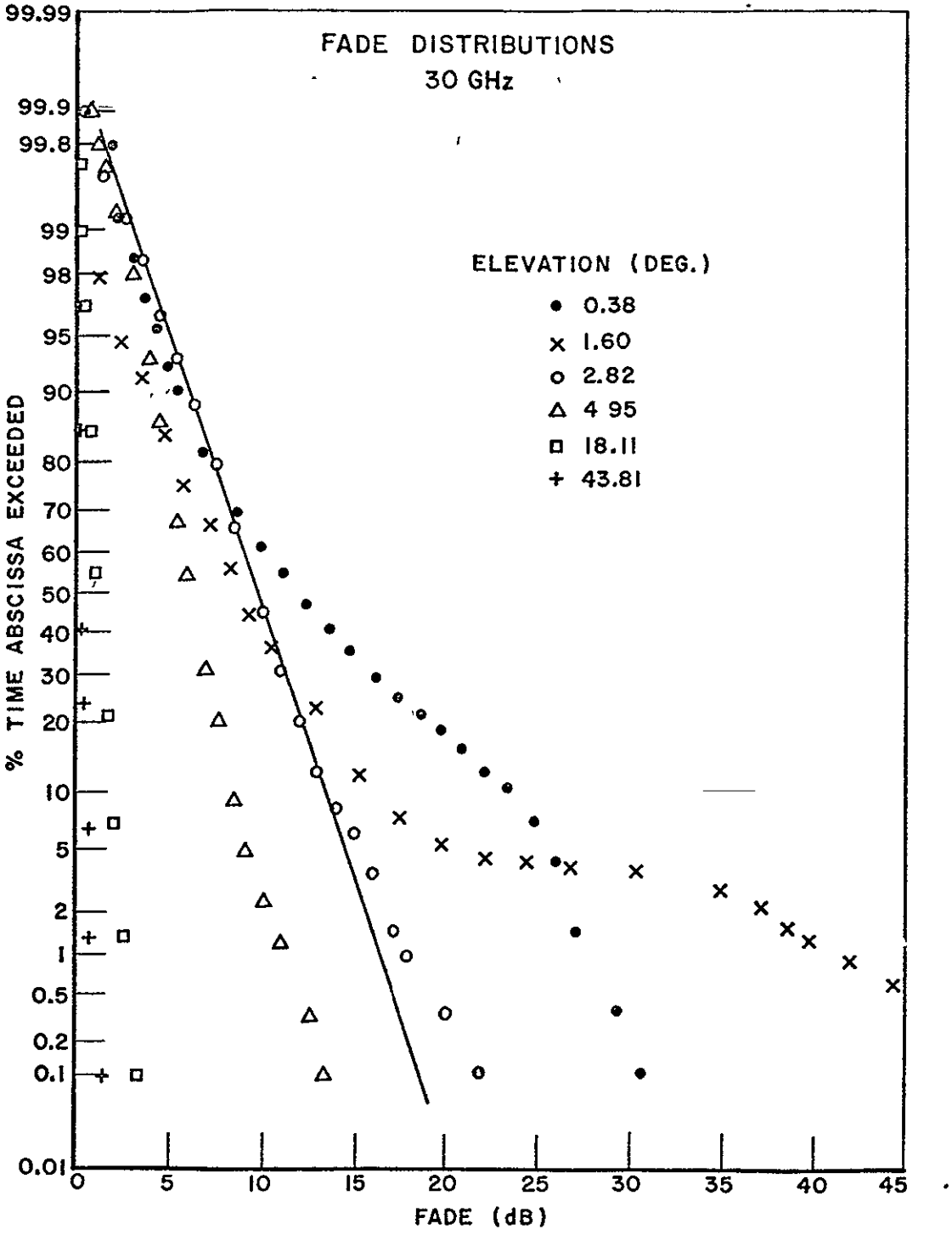

Figure 55. Fade distributions at 30 GHz.

From Figure 27, average log amplitude variance at 2.82°

$$\sigma^2_{\ell_{dB\ 30}} = -11.5\ dB \quad ,$$

$$s_{30} = (20 \log_{10} e) \cdot 10^{\frac{-11.5}{20}}$$

$$s_{30} = 2.34 \ .$$

This compares favorably with s as calculated from Figure 55.

Similarly for 2 GHz at 2.82°, from Figure 54

$$3.1\ s_2 = 2.3$$

$$s_2 = 0.74$$

from Figure 27, and following the same procedure as above,

$$s_2 = 0.45 \ .$$

The discrepancies could be partly due to the fact that the values shown in Figure 27 are calculated for 205 second intervals only and then averaged over each elevation angle. These are therefore short-term statistics and would tend to be Rayleigh distributed, whereas the distributions in Figures 54 and 55 were calculated over the whole elevation angle directly, these tend to be Gaussian. Further, the deviations from the log-normal curve for strong scintillations would also affect the result.

CHAPTER V
CONCLUSIONS

The results of the experiment are summarized in this chapter.

A. The Received Signals

The received signals show several types of fluctuations.

a) Very low elevation angles, (less than 4°):

(i) Slow rises and fades of tens of dB over periods of tens of minutes.

(ii) Faster fluctuations or scintillations with durations of a few minutes or less, occurring continuously.

(iii) Continuous rapid scintillations of a dB or less.

(iv) Slow roller-type fading is also seen. However, the high signal correlation found rules out ground reflection effects (Appendix D).

b) Low elevation angles (4° to 10°):

(i) Very slow changes in mean level of a few dB, over 30 minutes or more.

(ii) Faster scintillations of several dB with periods of a few tens of seconds.

(iii) Continuous rapid scintillations.

c) Medium elevation angles (10 - 44°):

(i) Virtually no change in mean level except during precipitation events.

(ii) Enhanced scintillations of a few dB for a few minutes are now visible.

(iii) Continuous rapid scintillations.

Scintillations were observed at all times in clear air and also in the presence of non-precipitating clouds. At the highest elevation angles there appears to be a tendency for the scintillations to be enhanced in the presence of non-precipitating cumulus clouds.

In the following discussion, the symbols A and ℓ are used to denote amplitude and log amplitude quantities respectively. The symbol ψ is used to denote either one in general.

B. Variances

Amplitude and log variances are defined in Equations (3-4) and (3-6).

The range of the variances at any elevation angle exceeded 20 dB at times. However the average variances followed a cosecant power law with elevation angle fairly well.

Table 4

$$\sigma^2_{\psi} = A\,[CSC(EL.)]^B$$

	2 GHz		30 GHz	
	A	B	A	B
σ^2_A	$10^{-4.9}$	1.62 ±.2	$10^{-4.3}$	2.14 ±.3
σ^2_ℓ	$10^{-4.9}$	1.62 ±.2	$10^{-4.3}$	2.20 ±.3

The fairly large error bounds have been introduced to account for the limited data. Observations over extended periods under widely varying weather conditions would give a closer estimate. The exponents, B, compare well in their range of error with the theoretical value B = 1.833 for Kolmogorov type turbulence.

As a refinement, a spherical earth model was assumed with a uniform, homogeneous atmosphere of effective height h km. When this was fitted to the data the results were as follows:

Table 5

$$\sigma^2_{\psi} = A\, L^B$$

$$L = \sqrt{h^2 + 2hR + R^2 \sin^2\theta} - R\sin\theta$$

$R = 8479$ km. θ = elevation angle.

	2 GHz			30 GHz		
	A	B	h_{km}	A	B	h_{km}
σ^2_A	$10^{-6.5}$	$1.87 \pm .2$	6.2 ± 1	$10^{-6.4}$	$2.48 \pm .3$	6.1 ± 1
σ^2_{ℓ}	$10^{-6.4}$	$1.87 \pm .2$	6.1 ± 1	$10^{-6.1}$	$2.49 \pm .3$	4.5 ± 1

A reduction in mean square error of between 5% to 15% is obtained. However, in general, the much simpler cosecant law

$$\sigma^2_{\psi} = A\,[CSC(\theta)]^B$$

appears to be quite adequate for elevation angles above 4°.

The 30 GHz data obtained during the departure of ATS-6 in 1975 agree well with the present data.

The ratio of variances, $\sigma^2_{\psi_{30}}/\sigma^2_{\psi_2}$, has a mean value of 9.2 dB. A value of 4.4 dB was obtained for $\sigma^2_{A_{30}}/\sigma^2_{A_{20}}$, in the 1975 measurements.

C. Received Signal Levels

The relative received signal levels show a strong dependence on elevation angle for elevations less than 5°. They are relatively independent of elevation thereafter. The drop in signal levels at low elevation angles are much greater than simple path-loss calculations predict.

D. Cross Correlations

Cross correlation was evaluated as a function of elevation angle. Both the amplitude and log amplitude cross correlations are identical for elevations above 5°. Below this angle, they diverge slightly. The cross correlations appear to follow a cosecant law with an exponent of 1.61 to 1.66.

The average amplitude correlation was found to agree well with that predicted by Lee and Harp for the frequency ratio of 14.46. The 1975 data also show good agreement with the predicted value for a frequency ratio of 1.5.

Representative samples of auto and cross correlation functions with time lag were also shown. Cross correlation lag ranged from 0 to about 10 seconds with most of the values in the region of 0 to 5 seconds. Significant correlation was not found for lags exceeding 15 seconds.

E. Power Spectra

The power spectra of the 2 and 30 GHz signals show a characteristic decay with frequency in the region of 0.1 to 1 Hz. The roll-off follows the $f^{-8/3}$ law, agreeing with the assumption of tropospheric turbulence as a dominant mechanism in the samples analyzed.

F. Fade Distributions

Fade distributions were calculated for selected elevation angles. The results suggest dominant Gaussian distributions. However there is significant deviation from the normal curve for strong scintillations at low elevation angles.

Fades in excess of 30 dB at 30 GHz and 7 dB at 2 GHz were observed for 5% of the time at low elevation angles. These dropped to 1 dB and 0.6 dB respectively at 41°.

G. Summary

Microwave signal amplitude scintillation characteristics were studied on earth-space paths for elevation angles varying from 0.4° to 43.9° using the ATS-6 satellite. Beacon signals at two frequencies, 2 GHz and 30 GHz, were monitored simultaneously. The results are consistent with similar measurements made earlier at 20 and 30 GHz.

Variances are modeled well by the cosecant law and by a homogeneous spherical earth model with an equivalent height of 6 km. Agreement with the Kolmogorov turbulence model is found. The mean ratio of the variances is 9.4 dB.

The correlation between the two signals was as high as 0.4 at low elevation angles and follows a cosecant law. The average value is close to that predicted by Lee and Harp for the ratio of these frequencies. Correlation lags were in the 0 - 5 second range, and significant correlation was not found for lags exceeding 15 seconds. The lags may be attributed to wind fields as modeled by Lee and Harp.

The power spectra at both 2 and 30 GHz show an $f^{-8/3}$ roll-off in the 0.1 to 1 Hz range. This agrees with the assumption of tropospheric turbulence as the dominant mechanism.

Mean signal levels dropped sharply below predicted values at elevation angles below about 4°. Fades exceeded 30 dB and 7 dB at 30 and 2 GHz respectively for 5% of the time at low elevation angles. These reduced to less than 1 dB at an elevation of 41°.

The long term statistics are Gaussian, except for strong scintillations when significant divergence from the Gaussian distribution was found.

APPENDIX A
EDITED TAPE FORMAT

The format of the final edited working digital magnetic tape, corrected for receiver calibration characteristics, is shown.

Packed Tape #48 File Format

File No.	Day (1976)	No. of Records
1	243, 244	38
2	245	40
3	246, 247	100
4	251, 254, 255	47
5	257 - 263, 265, 266	165
6	271	18
7	275, 277, 281	54
8	291, 292, 294, 296, 298	70

Packed Tape #48 Record Format

Record Length = 2555 Integer words

Words 1-10 = Header

- W1 = No. of words in Record
- W2 = Day
- W3 = Hour
- W4 = Minute
- W5 = Second
- W6 = millisecond
- W7 = Azimuth (milli degrees)
- W8 = Elevation (milli degrees)
- W9 = Record Type (10 ≡ 1/10 sec. rate samples)
- W10 = Data Status

  Bit ϕ = -
  Bit 1 = 2 GHz Rec.
  Bit 2 = 30 GHz Rec.

  If receiver is on and data is usable the corresponding bit = 1

Words 11 - 2555

W11 - W2058 max = Packed data words in 0.1 dB below reference

- Bits 0 - 11 2 GHz
- Bits 12 - 23 30 GHz

Remaining words are unused.

APPENDIX B
TABLE OF USEFUL DATA PERIODS

The data recorded during the experiment were edited by eliminating periods of equipment adjustment, antenna peaking or adjustment and data corrupted by ground reflections at elevation angles below 0.38°.

B-1. This section of the Appendix shows the periods during which the data was considered usable after editing.

a) Column 1

Entry number

b) Column 2,3,4

Time of day (Days, Hours, Minutes), Greenwich Mean Time.

c) Column 5,6

Nominal Azimuth and Elevation angles in degrees.

d) Column 7,8

These give the external additional attenuators in the receivers which were not directly recorded by the data recording system.

e) Column 9

The status of the data is given in this column as an octal number as shown below

Bit no.	2	1	0
Status			
Receiver	30 GHz	2 GHz	360 MHz

An acceptable data period is indicated by the corresponding bit being set to 1.

NO.	DAY	HOUR	MIN.	AZIM. (DEG)	ELEV. (DEG)	30 GHZ (DB)	2 GHZ (DB)	STAT.
1	243	3	10	97.10	-.49	0	1	4
2	243	4	0	97.10	-.49	1	1	0
3	243	17	24	97.48	.38	6	6	6
4	243	17	56	97.48	.38	6	6	0
5	243	18	22	97.48	.38	0	6	4
6	243	19	12	97.48	.38	1	6	0
7	243	19	18	97.57	.45	0	6	4
8	243	20	3	97.61	.47	0	8	7
9	243	20	15	97.61	.47	0	8	5
10	243	20	17	97.61	.47	0	0	7
11	243	20	30	97.61	.47	1	1	0
12	244	5	40	98.19	.74	2	0	7
13	244	6	0	98.19	.74	0	0	5
14	244	9	30	98.30	.99	3	0	5
15	244	10	8	98.30	.99	3	0	1
16	244	10	9	98.30	.99	5	1	4
17	244	10	36	98.30	.99	5	0	4
18	244	10	57	98.31	1.08	10	0	5
19	244	14	30	98.37	1.35	10	1	4
20	244	18	50	98.50	1.54	10	1	4
21	244	20	14	98.59	1.60	10	2	6
22	244	21	0	98.59	1.60	10	2	0
23	245	1	54	98.95	1.70	10	2	2
24	245	2	8	98.95	1.70	10	2	7
25	245	3	19	98.95	1.70	10	2	5

NO.	DAY	HOUR	MIN.	AZIM. (DEG)	ELEV. (DEG)	30 GHZ (DB)	2 GHZ (DB)	STAT.
26	245	4	56	99.13	1.81	10	2	4
27	245	4	58	99.13	1.81	10	2	5
28	245	7	30	99.22	1.96	10	2	5
29	245	9	20	99.22	1.96	10	2	4
30	245	9	40	99.27	2.11	10	2	5
31	245	11	30	99.27	2.11	10	2	0
32	245	12	50	99.31	2.33	10	2	5
33	245	13	15	99.31	2.33	10	2	4
34	245	13	30	99.31	2.33	10	2	4
35	245	14	30	99.34	2.47	10	2	4
36	245	16	30	99.39	2.57	10	2	4
37	245	18	50	99.47	2.66	10	2	4
38	245	20	5	99.56	2.71	10	2	6
39	245	21	0	99.56	2.71	10	2	0
40	246	1	54	99.94	2.82	10	2	7
41	246	3	0	99.94	2.82	10	2	5
42	246	4	0	100.06	2.89	10	2	5
43	246	5	5	100.06	2.89	10	2	7
44	246	6	0	100.06	2.89	10	2	0
45	246	17	4	100.40	3.72	10	2	6
46	246	18	4	100.40	3.72	10	2	4
47	246	19	0	100.49	3.79	10	2	4
48	246	20	4	100.54	3.82	10	2	6
49	246	21	0	100.54	3.82	10	2	4
50	246	21	30	100.54	3.82	10	2	0

NO.	DAY	HOUR	MIN.	AZIM. (DEG)	ELEV. (DEG)	30 GHZ (DB)	2 GHZ (DB)	STAT.
51	247	15	9	101.33	4.74	22	2	6
52	247	16	1	101.33	4.74	22	2	4
53	247	17	0	101.39	4.83	22	2	4
54	247	18	54	101.47	4.91	22	2	5
55	247	20	19	101.55	4.95	22	2	7
56	247	21	2	101.55	4.95	22	2	0
57	248	16	55	102.38	5.94	22	2	5
58	248	19	0	102.47	6.02	22	2	0
59	251	17	4	105.45	9.29	2	0	7
60	251	17	20	105.45	9.29	2	0	0
61	254	11	6	108.50	12.22	22	0	7
62	254	11	55	108.50	12.22	22	0	6
63	254	12	5	108.50	12.22	22	0	7
64	254	12	30	108.50	12.22	22	0	0
65	255	15	34	109.67	13.63	22	0	7
66	255	16	28	109.67	13.63	22	0	0
67	257	13	5	111.85	15.65	22	0	7
68	257	14	0	111.85	15.65	22	0	0
69	258	18	36	113.16	17.04	22	0	6
70	258	19	30	113.16	17.04	22	0	0
71	259	18	31	114.32	18.11	22	0	6
72	259	19	30	114.32	18.11	22	0	0
73	260	18	29	115.50	19.18	22	0	6
74	260	19	26	115.50	19.18	22	0	4
75	260	19	27	115.50	19.18	22	2	6

NO.	DAY	HOUR	MIN.	AZIM. (DEG)	ELEV. (DEG)	40 GHZ (DB)	2 GHZ (DB)	STAT.
76	260	19	51	115.50	19.18	22	2	0
77	261	13	31	116.53	19.98	22	2	6
78	261	14	31	116.53	19.98	22	2	0
79	262	20	2	118.03	21.35	22	2	6
80	262	20	59	118.03	21.35	22	2	0
81	263	15	19	119.17	22.34	22	2	6
82	263	19	20	119.17	22.34	22	2	0
83	265	13	49	121.58	24.16	22	2	6
84	265	14	30	121.58	24.16	22	2	0
85	266	13	15	122.89	25.14	22	2	6
86	266	13	37	122.89	25.14	22	2	0
87	266	14	1	122.89	25.14	22	2	6
88	266	14	30	122.89	25.14	22	2	0
89	271	4	32	129.22	29.23	22	0	6
90	271	4	34	129.22	29.23	22	0	0
91	271	4	66	129.22	29.23	22	2	6
92	271	5	31	129.22	29.23	22	2	0
93	275	17	33	136.10	33.65	22	2	6
94	275	18	30	136.10	33.65	22	2	0
95	277	20	52	139.72	35.36	22	2	6
96	277	21	53	139.72	35.36	22	2	0
97	281	12	51	146.41	38.02	22	2	6
98	281	13	47	146.41	38.02	22	2	0
99	291	20	8	167.64	43.19	22	2	6
100	291	21	0	167.64	43.19	22	2	0

NO.	DAY	HOUR	MIN.	AZIM. (DEG)	ELEV. (DEG)	30 GHZ (DB)	2 GHZ (DB)	STAT.
101	292	18	38	169.76	43.44	22	2	6
102	292	19	15	169.76	43.44	22	2	0
103	294	2	55	172.78	43.38	22	2	6
104	294	3	30	172.78	43.38	22	2	0
105	296	14	54	178.44	43.81	22	2	6
106	296	15	0	178.44	43.81	22	2	0
107	298	18	20	183.42	43.89	22	2	6
108	298	19	0	183.42	43.89	22	2	0

B-2. The durations of the data periods used in the calculations in this report are given below.

Elevation (degrees)	Duration (minutes)	Elevation (degrees)	Duration (minutes)
0.38	32	17.04	54
0.48	19	18.11	59
0.74	20	19.18	81
1.60	46	19.98	59
1.70	71	21.35	57
2.71	57	22.34	71
2.82	61	24.16	41
2.89	57	25.14	50
3.72	60	29.23	57
3.82	56	33.65	57
4.74	52	35.36	57
4.95	42	38.02	56
9.29	16	43.19	52
12.22	84	43.44	57
13.63	54	43.58	35
15.65	57	43.81	66
		43.89	40

APPENDIX C
COMMENTS ON LOG AND AMPLITUDE VARIANCE

Expanding the definition of log variance, (Equation (3-6)):

$$\sigma^2_{\ell} = \frac{1}{K_1^2 N} \sum_{I=1}^{N} \left(\ell_I - \frac{1}{N} \sum_{J=1}^{N} \ell_J \right)^2$$

$$= \frac{1}{K_1^2 N} \sum_{I=1}^{N} \left(20 \log_{10} \frac{a_I}{a_o} - \frac{1}{N} \sum_{J=1}^{N} 20 \log_{10} \frac{a_J}{a_o} \right)^2 \qquad \text{(C-1)}$$

but

$$\log_{10} \frac{a_I}{a_o} = \log_{10} \frac{a_I}{\bar{a}} + \log_{10} \frac{\bar{a}}{a_o}$$

$$\sigma^2_{\ell} = \frac{20^2}{K_1^2 N} \sum_{I=1}^{N} \left(\log_{10} \frac{a_I}{\bar{a}} + \log_{10} \frac{\bar{a}}{a_o} - \frac{1}{N} \sum_{J=1}^{N} \log_{10} \frac{a_J}{\bar{a}} + \log_{10} \frac{\bar{a}}{a_J} \right)^2$$

$$= \frac{20^2}{K_1^2 N} \sum_{I=1}^{N} \left(\log_{10} \frac{a_I}{\bar{a}} - \frac{1}{N} \sum \log_{10} \frac{a_J}{\bar{a}} \right)^2$$

$$K_1 = 20 \log_{10} e$$

$$\log_{10} \frac{a_I}{\bar{a}} = \log_{10} e \log_e \frac{a_I}{\bar{a}}$$

$$\therefore \quad \sigma^2_{\ell} = \frac{(20 \log_{10} e)^2}{(20 \log_{10} e)^2} \sum_{I=1}^{N} \left(\log_e \frac{a_I}{\bar{a}} - \frac{1}{N} \sum_{J=1}^{N} \log_e \frac{a_J}{\bar{a}} \right)^2$$

For small scintillations $\frac{a_1}{\bar{a}} \approx 1$

$$\therefore \log_e \frac{a_1}{\bar{a}} \approx \frac{a_1}{\bar{a}} - 1$$

$$\therefore \quad \sigma^2_{\ell} = \frac{1}{N} \sum_{1=1}^{N} \left(\frac{a_1}{\bar{a}} - 1 - \frac{1}{N} \sum_{J=1}^{N} \frac{a_J}{\bar{a}} - 1 \right)^2$$

$$\sigma^2_{\ell} = \frac{1}{N_1} \sum_{1=1}^{N} \frac{(a_1 - \bar{a})^2}{\bar{a}^2} \qquad \text{(C-2)}$$

Also

$$\sigma^2_{A} = \frac{1}{N_1} \sum_{1=1}^{N} \frac{(A_1 - \bar{A})^2}{\bar{A}^2}$$

$$= \frac{1}{N_1} \sum_{1=1}^{N} \frac{\left(\frac{a_1}{a_o} - \frac{\bar{a}}{a_o} \right)^2}{\left(\frac{\bar{a}}{a_o} \right)^2}$$

$$\sigma^2_{A} = \frac{1}{N_1} \sum_{1=1}^{N} \frac{(a_1 - \bar{a})^2}{\bar{a}^2} \qquad \text{(C-3)}$$

$$\therefore \quad \sigma^2_{\ell} = \sigma^2_{A} \quad \text{for small scintillations.}$$

The computed results show excellent agreement even at low elevation angles (i.e., large scintillations).

Further, Fried has shown [30] from energy considerations that;

$$\sigma^2_{\ell} \propto - \bar{\ell} \quad . \qquad \text{(C-4)}$$

(This result has been adapted to be consistent with the definitions used in this study.)

Now, $\bar{\ell}$ shows a sharp drop at low elevation angles. It is seen in Figure 56, where the numerical values of $K_1^2\sigma^2_\ell$ (N.B. not $\sigma^2_{\ell_{dB}}$) are plotted, that this behavior is, in fact, reflected.

The observations are therefore consistent. However the reason for the sharp knee in the mean levels is yet to be determined.

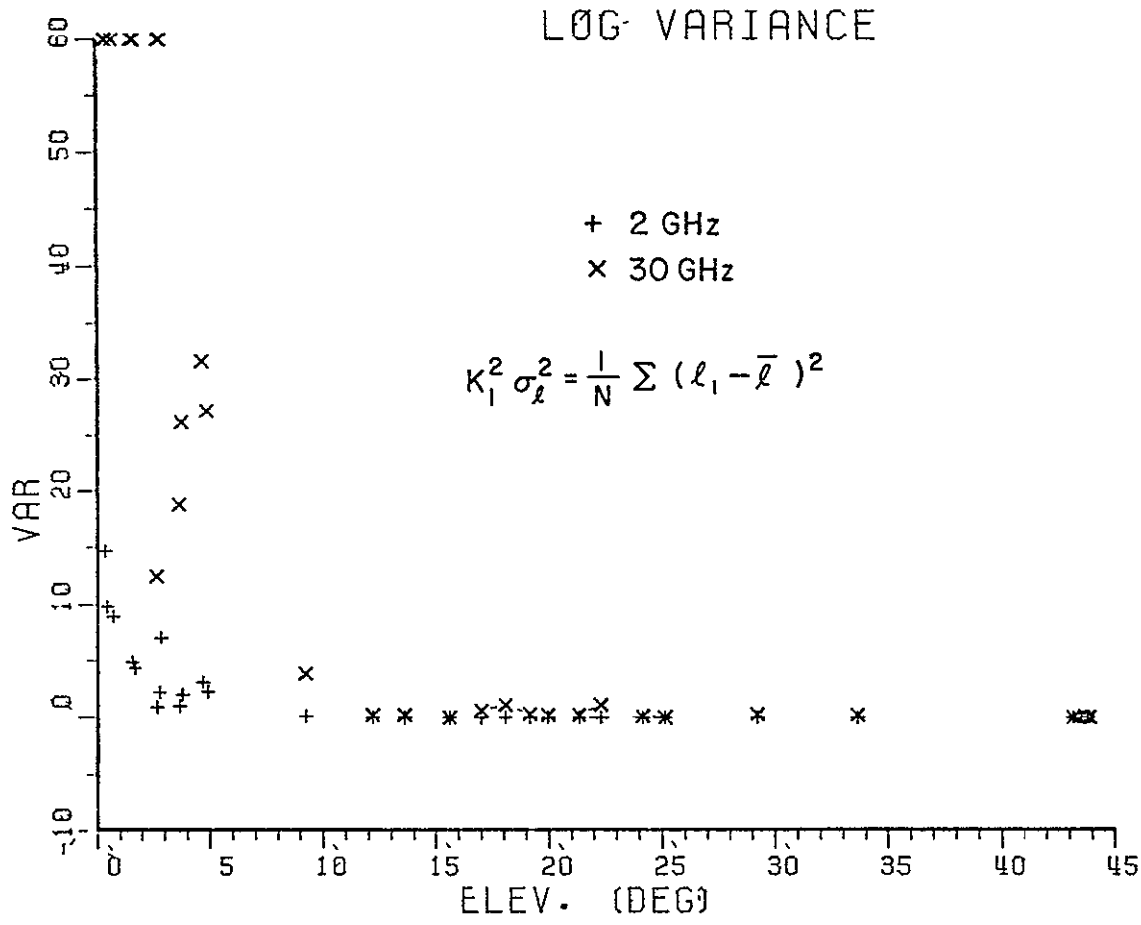

Figure 56. Log amplitude variance (numeric).

APPENDIX D
RECEIVED SIGNALS AT LOW ELEVATION ANGLES AND MULTIPATH EFFECTS

The mechanism which causes the amplitude scintillations may be regarded as being either refractive or multipath in nature. Low two-frequency correlation would be expected if multipath were the dominant factor, because an arbitrary differential path length cannot produce simultaneous subtractive or additive phasing at the two wavelengths employed, as shown below [17].

Subtractive multipath phasing will occur at a wavelength of λ_1 if the difference between the two path lengths satisfy,

$$\Delta L = (2n+1)\frac{\lambda_1}{2} \quad , \qquad n = 0, 1, 2 \ . \cdots$$

Similarly, at a second wavelength λ_2

$$\Delta L = (2m+1)\frac{\lambda_2}{2} \quad , \qquad m = 0, 1, 2 \ . \cdots$$

Therefore,

$$(2n+1)\lambda_1 = (2m+1)\lambda_2 \quad .$$

But in general

$$\lambda_1 = \mu\lambda_2 \quad \text{where } \mu \text{ is an arbitrary number.}$$

So that

$$\mu(2n+1) = 2m+1. \tag{D-1}$$

For example, the 1975 measurements were performed simultaneously at 20 and 30 GHz, therefore $\mu = 3/2$. Then

$$\frac{3}{2}(2n+1) = 2m+1,$$

or
$$3(2n+1) = 2(2m+1) \quad . \tag{D-2}$$

However the left side of Equation (D-2) is odd and the right side is even. Therefore, simultaneous fading due to simple multipath propagation cannot occur. This result contradicts the very high correlations observed between the 20 and 30 GHz signal fluctuations. Thus, one is forced to conclude that the observed fluctuations are not a result of a simple multipath mechanism.

APPENDIX E
SUMMARY OF DEFINITIONS

$a(t)$ is a positive real signal amplitude. a_1 are discrete samples of $a(t)$ at equal intervals over a time interval T. $a(t)$ has been corrected for receiver nonlinearities. The relative amplitude is defined to be

$$A_1 = \frac{a_1}{a_0} \quad ,$$

and the relative log amplitude as

$$\ell_1 = 20 \log_{10} \frac{a_1}{a_0}$$

where a_0 is an arbitrary constant.

	AMPLITUDE	LOG AMPLITUDE	RELATIONSHIP FOR SMALL SCINTILLATIONS
MEAN	$\overline{A} = \frac{1}{T}\int A(t)\,dt$ $= \frac{1}{N}\sum_{i=1}^{N} A_i$	$\overline{\ell} = \frac{1}{T}\int \ell(t)\,dt$ $= \frac{1}{N}\sum_{i=1}^{N} \ell_i$	$\overline{\ell} \approx 20 \log_{10} \overline{A}$
MEAN TOTAL POWER (MEAN SQUARE)	$\overline{A}^2 = \frac{1}{T}\int A^2(t)\,dt$ $= \frac{1}{N}\sum_{i=1}^{N} A_i^2$	-	$\overline{A^2}_{dB} \approx \overline{\ell}$
VARIANCE (NORMALIZED TO DC POWER)	$\sigma_A^2 = \frac{1}{T}\int \frac{(A(t)-\overline{A})^2}{\overline{A}^2}\,dt$ $= \frac{1}{N\overline{A}^2}\sum_{i=1}^{N} (A_i-\overline{A})^2$	$\sigma^2_{\ell} = \frac{1}{T}\int \frac{(\ell(t)-\overline{\ell})^2}{K_1^2}\,dt$ $= \frac{1}{K_1^2 N}\sum_{i=1}^{N} (\ell_i-\overline{\ell})^2$	$\sigma^2_A \approx \sigma^2_{\ell}$

	AMPLITUDE	LOG AMPLITUDE
CORRELATION COEFFICIENT	$\rho_{A_{1,2}}(t) = \frac{1}{T}\int \frac{(A_1(t)-\overline{A}_1)(A_2(t+\tau)-\overline{A}_2)dt}{\overline{A}_1\overline{A}_2\sigma_{A_1}\sigma_{A_2}}$ $= \frac{1}{N\overline{A}_1\overline{A}_2}\sum_{1=1}^{N}\frac{(A_{1_2}-\overline{A}_1)(A_{2_{1+J}}-\overline{A}_2)}{\sigma_{A_1}\sigma_{A_2}}$	$\rho_{\ell_{1,2}}(\tau) = \frac{1}{T}\int \frac{(\ell_1(t)-\overline{\ell}_1)(\ell_2(t+\tau)-\overline{\ell}_2)dt}{K_1^2\sigma_{\ell_1}\sigma_{\ell_2}}$ $= \frac{1}{K_1^2 N}\sum_{1=1}^{N}\frac{(\ell_{1_1}-\overline{\ell}_1)(\ell_{2_{1+J}}-\overline{\ell}_2)}{\sigma_{\ell_1}\sigma_{\ell_2}}$

RELATIONSHIP FOR SMALL SCINTILLATIONS

$$\rho_{A_{1,2}}(\tau) \approx \rho_{\ell_{1,2}}(\tau)$$

$$K_1 = 20 \log_{10} e \qquad \tau = J\frac{T}{N}$$

REFERENCES

[1] L. Cuccia, W. Quan and C. Hellman, "Above 10 GHz Satcom Bands Spur New Earth Terminal Development," Microwave System News, March 1977, p. 37,38.

[2] L. Cuccia et al, Op. Cit., p. 46-50.

[3] D. E. Kerr, Propagation of Short Radio Waves, McGraw Hill, 1964.

[4] B. R. Bean and E. J. Dutton, Radio Meteorology, Dover, 1968.

[5] D. C. Livingston, The Physics of Microwave Propagation, Prentice Hall, 1970.

[6] "Propagation Factors in Space Communications," AGARD Conference Proceedings, No. 3, W. J. Mackay and Co., 1967.

[7] P. David and J. Voge, Propagation of Radio Waves, Pergamon Press, 1969.

[8] Communications Satellite Corporation, "COMSAT Technical Review," Vol. 3, No. 1 to Vol. 5, No. 2.

[9] E. V. Appleton, URSI Proceedings, Washington, 1927.

[10] E. H. Whitney and S. Basu, "The Effect of Ionospherеic Scintillation on VHF/UHF satellite Communications," Radio Science, Vol. 12, No. 1, 1977, p. 123-133.

[11] Aarons et al, "Radio Astronomy Measurements at VHF and Microwaves," Proceedings IRE, January 1958, p. 325-333.

[12] L. A. Hoffman et al, "Propagation Observations at 3.2 Millimeters," Proceedings IEEE, Vol. 54, No. 4, April 1966.

[13] L. J. Ippolito, "Effects of Precipitation on 15.3 and 31.65 GHz Earth-Space Transmission With the ATS-V Satellite, Proceedings IEEE, Vol. 59, No. 2, 1971.

[14] L. J. Ippolito, "ATS-6 Millimeter WaVe Propagation and Communications Experiments at 20 and 30 GHz," IEEE Transactions, Vol. AES-11, No. 6, 1975.

[15] Goddard Space Flight Center, ATS-F and -G Data Book, September 1972, p. A39-A42.

[16] D. B Hodge and D. M. Theobold, "Scintillations Observed on the ATS-6 20 and 30 GHz Downlinks," URSI/USNC meeting, Boulder, Colorado, October 1975.

[17] D. B. Hodge, D. M. Theobold and R. C. Taylor, "ATS-6 Millimeter Wavelength Propagation Experiment," Report 3863-6, January 1976, The Ohio State University ElectroScience Laboratory, Department of Electrical Engineering, prepared under Contract NAS5-21983 For NASA Goddard.

[18] V. I. Tatarski, Wave Propagation in a Turbulent Medium, Israel Program for Scientific Translation, Jerusalem, 1971.

[19] R. F. Filipowski and E. I. Muehldorf, Space Communication Systems, Prentice Hall, 1965

[20] G. N. Krassner, Introduction to Space Communication Systems, Chapter 4, McGraw Hill, 1964.

[21] D. M. Theobold and D. B. Hodge, "ATS-6 Millimeter Wavelength Propagation Experiment," Report 3863-4, April 1975, The Ohio State University ElectroScience Laboratory, Department of Electrical Engineering, prepared under Contract NAS5-21983 for NASA Goddard.

[22] B. H. Briggs and I. A. Parkin, "On The Variation of Radio Star and Satellite Scintillations with Zenith Angle," J. Atmos. Terr. Phys., 25, p. 339-366.

[23] A. Kolmogorov, "Turbulence, Classic Papers on Statistical Theory," S. K. Friedlander and L. Topper, Eds., New York Interscience, 1961, p. 151.

[24] A. Benoit, "Signal Attenuation Due to Neutral Oxygen and Water Vapor, Rain and Clouds," The Microwave Journal, November 1968, p. 73-80.

[25] K. S. McCormick and L. A. Maynard, "Measurements of S.H.F. Tropospheric Fading Along Earth-Space Paths at Low Elevation Angles," Electronics Letters, Vol. 8, 1972, p. 274.

[26] R. W Lee and J. C. Harp, "Weak Scattering in Random Media with Applications to Remote Probing," Proc. IEEE, Vol. 57, 1969, p. 375-406.

[27] R. S. Lawrence and J. W. Strohbehn, "A Survey of Clear Air Propagation Effects Relevent to Optical Communications," Proc. IEEE, Vol. 58, No. 10, October 1970, pp. 1537,1538.

[28] P. F. Panter, Communication Systems Design, McGraw Hill, 1972, pp. 347-358.

[29] P. F. Panter, Op. Cit., p 355.

[30] D. L. Fried, "Optical Resolution Through a Randomly Inhomogeneous Medium for Very Long and Very Short Exposures," J. Opt. Soc. Am. 56, October 1966, pp. 1372-1379.